simplified form for the case when $r_A = r_B = 1$.

1.2.5. Fick's second Law

We have seen that the fluxes in a binary alloy have the form:

$$J_i = -D_i \nabla n_i \quad \text{or} \quad J_i = -D_i \nabla n_i + n_i < v >_i$$

By using the *conservation equation*:

$$\frac{\partial n_i}{\partial t} = -\mathrm{div} J_i$$

we obtain *Fick's second Law*; this partial differential equation can be solved for given initial and boundary conditions. D_i and $<v>_i$ can then be obtained from a comparison between the experimental and the calculated concentration curve C(x).

When D_i and $<v>_i$ are constant and the diffusion is along the x direction Fick's second Law has the form:

$$\frac{\partial n_i}{\partial t} = D_i \frac{\partial^2 n_i}{\partial x^2} \tag{18}$$

or

$$\frac{\partial n_i}{\partial t} = D_i \frac{\partial^2 n_i}{\partial x^2} - < v >_i \frac{\partial n_i}{\partial x} \tag{19}$$

The geometry which is most commonly used for measuring D_i is a thin layer deposited onto a "semi-infinite sample" (see fig. 4b and 4c); in this case the solution of eq. (18) has the well-known form:

$$n_i(x,t) = \frac{Q}{\sqrt{\pi D_i t}} \exp\left(-\frac{x^2}{4 D_i t}\right) \tag{20}$$

where Q is the quantity of the diffusing species deposited per unit surface, so that D_i is obtained from the slope of the straight line: log n_i versus x^2.

In the presence of an electric field, the equation to be solved is eq. (19); very often the geometry used is a thin layer sandwiched between two semi-infinite samples. The solution is then:

$$n_i(x,t) = \frac{Q}{2\sqrt{\pi D_i t}} \exp\left[-\frac{(x - < v >_i t)^2}{4 D_i t}\right] \tag{21}$$

$<v>_i$ is obtained from the displacement of the maximum of the curve $n_i(x)$ with respect to the origin (defined by the welding interface).

For chemical diffusion (see fig. 4a), $\tilde{D}$ is not constant, we have then to solve:

$$\frac{\partial n_i}{\partial t} = \frac{\partial}{\partial x}\left(\tilde{D}_i \frac{\partial n_i}{\partial x}\right) \tag{22}$$

References: p. 651.

MATANO [1933] has shown that, when $\tilde{D}_i$ depends on x through n_i:

$$\tilde{D}_i(n_i) = -\frac{1}{2t}\frac{\int_0^{n_i} x \, d \, n_i}{(dn_i/dx)} \tag{23}$$

the x origin must be chosen so that:

$$\int_0^{n_{i,\max}} x \, d \, n_i = 0 \tag{24}$$

This origin defines the *Matano plane*. In fig. 5 the different terms of eqs. (23) and (24) are illustrated.

Numerous solutions of the diffusion equation can be found in CRANK [1956] and CARSLAW and JAEGER [1959]. We will see that in some cases Fick's first law is not valid; the first restriction is related to the discontinuous nature of crystals (lattice effect) and will be discussed in § 1.3.5. The second restriction is met in chemical diffusion (spinodal decomposition: CAHN [1967]; ch. 15, § 3.1). In both cases the discrepancy with Fick's law becomes noticeable only for harmonics of concentration with short wavelengths.

1.3. The random walk theory of diffusion

The aim of the random walk theory is to describe the observed macroscopic effects from the atomic jumps which are the elementary processes in diffusion.

1.3.1. Einstein relation and flux expression

For a *random walk motion*, EINSTEIN [1905] has shown that the diffusion coefficient of species i along the x direction is given by:

$$D_i = \frac{\overline{X^2}}{2\tau} \tag{25}$$

where $\overline{X^2}$ is the mean square displacement along the x direction for the duration τ. If X_k is the displacement of the k^{th} atom along the x direction during τ, we have:

$$\overline{X^2} = \frac{1}{N}\sum_{k=1}^{N} X_k^2 \tag{26}$$

where N is the number of diffusing atoms of species i.

In many cases the motion is not random but the expression (25) still holds provided that $\tau \to 0$.

According to LE CLAIRE [1958] and MANNING [1968], the flux J_i measured with respect to the lattice reference frame is equal to:

$$J_i = < v >_i \, n_i - D_i \frac{\partial n_i}{\partial x} - n_i \frac{\partial D_i}{\partial x} \tag{27}$$

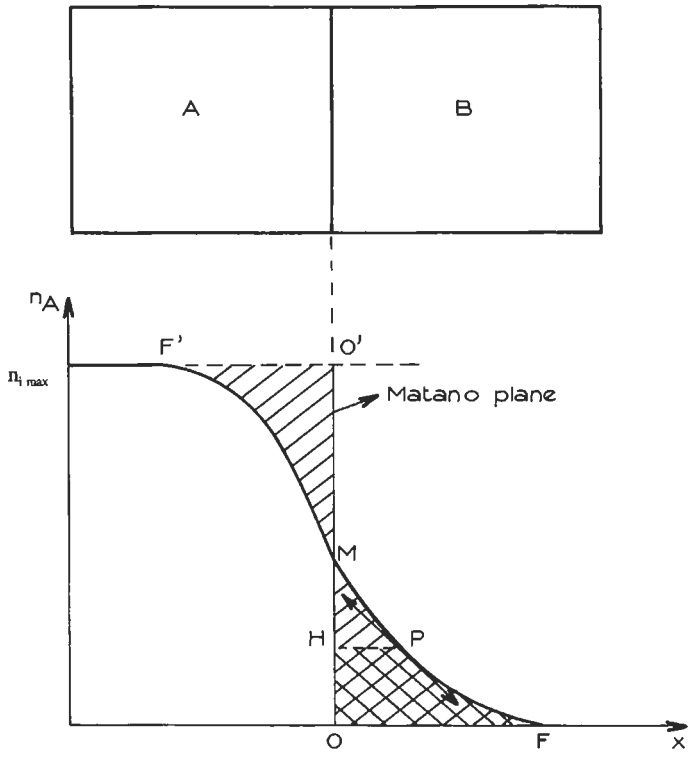

Fig. 5. Matano method for the calculation of $\tilde{D}$. The Matano plane is defined by the equality of the two areas F'O'M and FOM (hatched surfaces). $\int_0^{n_i} x\, dn_i$ is equal to the area HPFO (doubly hatched surface), dn_i/dx is the slope of the tangent to the concentration curve at P.

where:

$$< v >_i = \lim_{\tau \to 0} \frac{\overline{X}}{\tau} \tag{28}$$

D_i is given by eq. (25) when $\tau \to 0$, $\overline{X^2}$ is the mean displacement during τ for species i.

These relations, (25), (27) and (28), are valid for anisotropic media but to save space we have omitted the more precise notation D_{ix}, $<v>_{ix}$ etc...

1.3.2. Calculation of $\overline{X}$ and $\overline{X^2}$ in terms of jump frequencies

It is easy to show that:

$$\overline{X} = \sum_{i=1}^{n} \overline{x_i} \tag{29}$$

$$\overline{X^2} = \sum_{i=1}^{n} \overline{x_i^2} + 2 \sum_{1=1}^{n-1} \sum_{j=i+1}^{n} \overline{x_i x_j} \tag{30}$$

where x_i is the i th displacement along x and n is the mean number of atomic jumps during τ. The overbar denotes an average over a large number of atoms.

1.3.2.1. Expression for $\overline{X^2}$. For a truly random walk motion the last term in eq. (30), $P = 2 \sum\sum \overline{x_i x_j}$, *vanishes*. When $\overline{X}$ differs from zero (chemical diffusion, electro and thermal diffusion, etc.) this term P is also different from zero but is has been shown that the $\overline{X}$ contribution to P is of the order to τ^2 whereas the $\sum \overline{x_i^2}$ term, eq. (30), is of the order of τ; as a consequence the $\overline{X}$ contribution to P is negligible when $\tau \to 0$.

But even if $\overline{X} = 0$, the P term is not necessarily equal to zero, owing to the mechanism of diffusion. We will see later that for most diffusion mechanisms the successive atomic jumps are not independent of each other, and *that the motion is not a truly random walk*. This can be easily understood for the vacancy mechanism: the vacancy concentration is so low ($\sim 10^{-4}$ to the melting point) that two consecutive atomic jumps are likely due to the same vacancy and it is obvious that after one jump an atom has a greater than random probability of making a reverse jump; there is *correlation*. This correlation between the directions of two successive jumps initiated by the same vacancy reduces the efficiency of the walk with respect to a truly random walk. Correlation occurs for all defect-assisted diffusion mechanisms except for the purely interstitial and exchange mechanisms; it is related to the low concentration of point defects (vacancies, divacancies, interstitials, etc.) and decreases when this concentration increases (WOLF [1980]).

How to take this effect into account will be reported in § 1.3.4. *To summarize, we can always calculate $\overline{X^2}$ by assuming $\overline{X} = 0$, because when $\tau \to 0$, $\overline{X^2}$* does not depend on $\overline{X}$.

For a truly random walk motion, $P = 0$ and we have:

$$\overline{X^2} = \tau \sum_{k=1}^{z} \Gamma_k x_k^2 \tag{31}$$

where z is the number of jump directions, Γ_k the mean atomic jump frequency for the k direction and x_k the displacement along x for a k-jump. Hence:

$$D_{random} = \tfrac{1}{2} \sum_{k=1}^{z} \Gamma_k x_k^2. \tag{32}$$

For cubic lattices all the frequencies Γ_k are equal, and:

$$D_{random} = \frac{\Gamma l^2}{6} \tag{33}$$

where $\Gamma = \sum_k \Gamma_k$ is the total jump frequency and l is the jump distance ($\frac{1}{2} a\sqrt{2}$ for fcc, $\frac{1}{2} a\sqrt{3}$ for bcc).

1.3.2.2. Expression for $\overline{\overline{X}}$. With the same notation as for $\overline{X^2}$ we have:

$$\overline{X} = \tau \sum_{k=1}^{z} \Gamma_k x_k = < v > \tau \tag{34}$$

For the case where $\overline{X}$ is not zero, the potential energy of the atoms versus their position is schematized in fig. 6 (for simplicity we have shown regular energy barriers which correspond to a mean displacement $\overline{X}$ independent of x). The shape of this energy diagram is due to a force F_i acting on the atoms such that (see fig. 6):

$$\Delta W = \frac{F_i x_j}{2}$$

The atom jumps are easier towards the right than towards the left (in fig. 6) and if $\Delta W \ll kT$ we have for thermally activated jumps:

$$\Gamma(\rightarrow) = \Gamma_0\left(1 + \frac{F_i x_j}{2kT}\right) \quad \Gamma(\leftarrow) = \Gamma_0\left(1 - \frac{F_i x_j}{2kT}\right) \tag{35}$$

where Γ_0 is the jump frequency when $F_i = 0$; $\rightarrow$ denotes jumps towards the right and $\leftarrow$ jumps towards the left.

We then obtain, with eqs. (34) and (35):

$$< v >_i = \frac{\overline{X}}{\tau} = \frac{F_i D_i}{kT} \tag{36}$$

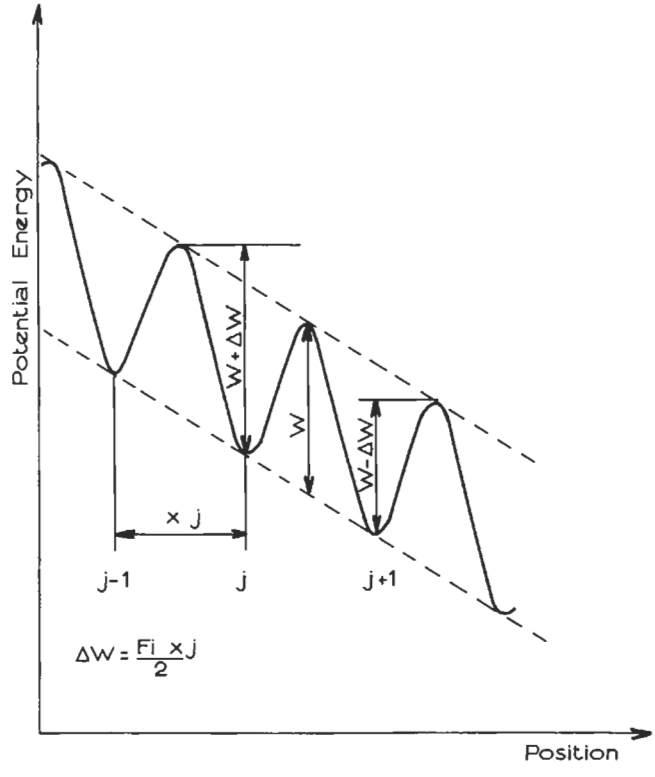

Fig. 6. Schematic representation of the potential energy diagram of the atoms when a constant force is present.

References: p. 651.

This expression is the *Nernst–Einstein relation.*

F_i has the following forms, according to the nature of the field acting on the atoms:

$$F_i = Z_i^* eE \text{ for an electric field,}$$

$$= -\frac{Q_{i\alpha}^*}{T}\frac{dT}{dx} \text{ for a thermal gradient,}$$

$$= -k\frac{\partial \log \gamma_i}{\partial x} \text{ for a concentration gradient,} \tag{37}$$

where Z_i^* is the effective valence, $Q_{i\alpha}^* = q_{i\alpha}^* - h_{fv\alpha}$, $q_{i\alpha}^*$ is the heat of transport for an α-type jump of the species i, $h_{fv\alpha}$ is the vacancy formation enthalpy on a site from which an α-type jump is possible, γ_i is the coefficient of activity of species i in the alloy at the position x; this last term can be evaluated from a thermodynamical study of the alloy; we will see in § 6 how it is possible to measure and calculate Z^* and Q^*. We observe that with the microscopic approach there are as many heats of transport as there are different types of jumps, whereas with the macroscopic approach the number of the heats of transport is equal to the number of species.

The expression for $\overline{X}$, eq. (36), is not complete because the diffusion mechanism can give rise to an additional term; in order to go further it is thus necessary to adopt a particular model for diffusion. We will consider the case of a binary alloy and a vacancy mechanism.

1.3.3. Binary alloys and vacancy mechanism

In the case of a vacancy mechanism there is a coupling between A and B fluxes through the vacancy flux. This coupling, known as the *vacancy flow effect*, contributes to $\langle v \rangle_i$ in addition to the force F_i. The calculation of this term is rather tedious and for more details we refer the reader to MANNING [1968]. Two cases have to be considered, depending on whether it is a dilute or a concentrated alloy. The diffusion models and results (expressions for L_{AA}, L_{AB} and L_{BB}) are given in § 4 for dilute alloys and § 5 for concentrated alloys.

1.3.4. Correlation effects

For most diffusion mechanisms the successive atomic jumps are not independent; as a result, the last term of eq. (30), $P = 2 \sum\sum \overline{x_i x_j}$, does not vanish. The *correlation factor* is defined as:

$$f = \frac{D_{\text{actual}}}{D_{\text{random}}} \tag{38}$$

and from eq. (30) we obtain:

$$f = 1 + \left(2 \sum_{i=1}^{n-1} \sum_{j=i+1}^{n} \overline{x_i x_j} \right) \Big/ \sum_{i=1}^{n} \overline{x_i^2} \tag{39}$$

Thus the expression for D, eq. (33), becomes:

$$D_{\text{actual}} = f\frac{\Gamma l^2}{6} \tag{40}$$

In order to calculate f we have to evaluate $P = 2\sum\sum \overline{x_i x_j}$, which will depend on the diffusion mechanism. BARDEEN and HERRING [1951] were the first to point out that point-defect diffusion mechanisms involve a non-random-walk motion for the atoms, and they calculated the correlation factor f for a vacancy mechanism.

The first useful estimation for f with the vacancy mechanism yields $f = 1 - 2/z$, where z stands for the coordination number of the lattice. Since, at each jump, the vacancy has the probability 1/z to perform a backward jump, a fraction 2/z of the number of jumps performed by a given tracer atom is lost, giving rise to an efficiency factor equal to $1 - 2/z$. This argument cannot be used as such for evaluating the correlation factor for solute diffusion, because the exchange frequency with a solute atom w_2 differs from that with the solvent w_0 and because the solvent jump frequencies themselves are altered in the immediate neighbourhood of the solute (see § 4.1). As a consequence, the walk of the defect around the solute must be considered in more detail. Since the pioneering work of BARDEEN and HERRING, numerous studies have been published on this topic; we refer the reader to the books or articles by ADDA and PHILIBERT [1966], MANING [1968] and LE CLAIRE [1970a].

The principal techniques used for the calculation of f are:

(i) *Computer simulations;* $\overline{X^2_{\text{actual}}}$ is obtained by Monte Carlo simulations and compared to X^2_{random}. For more details see § 1.5.2.

(ii) *The pair association method*; this technique is described in § 4; the fluxes are calculated from the diffusion model and by comparing with the macroscopic expressions we obtain D_{actual} and then f with eq. (38). This technique can only be used for dilute alloys.

(iii) *The random walk method*; this is the calculation of f from the expression (39). In this type of calculation it is necessary to evaluate the return probabilities of the defect on the neighbouring sites of the atom after the first exchange with this atom. To obtain these probabilities, several methods have been used:

– The BARDEEN and HERRING [1951] technique;
– the matrix method (LE CLAIRE and LIDIARD [1956], MULLEN [1961], HOWARD [1966]);
– the electrical analogue method (COMPAAN and HAVEN [1956, 1958]);
– the integral methods, which have now superseded the previous ones. The return probabilities are evaluated through 3–D integrals which are easily computed in a few seconds with a very high accuracy. Tackling with a slightly different problem, the ancestor paper introducing such integrals for random walk probabilities (MCCREA and WHIPPLE [1940]) has been followed much later by others more directly devoted to correlation calculations (MONTET [1973], BENOIST *et al.* [1977]; KOIWA [1978], ISHIOKA and KOIWA [1980]).

For self-diffusion, f is independent of temperature in isotropic materials (for vacancy mechanism $f = 0.72$ for bcc, 0.78 for fcc and hcp, 0.5 for diamond lattice; for divancancy

mechanism f = 0.475 for fcc and hcp lattice). For impurity diffusion see § 4.

In some cases the knowledge of the correlation factor can allow us to choose among several of the mechanisms of diffusion; it is then a very useful quantity, but as we will see later, experiment does not yield f alone. What is measured is the *isotope effect*, E, from which it is not obvious how to extract f (§ 1.4.3.3).

1.3.5. The limitation of Fick's Law

We present here a first restriction of Fick's Law, which is related to the discontinuous nature of the lattice (MARTIN and BENOIST [1977]). Let us consider the case of one-dimensional diffusion; the rate equations for an atomic plane n are:

$$\frac{dC_n}{dt} = \Gamma\left(C_{n+1} - 2C_n + C_{n-1}\right) \tag{41}$$

where Γ is the atomic jump frequency and C_i the concentration for the i^{th} plane.

We have to compare the solution of this rate equation, which takes into account the discontinuous nature of the lattice, with the macroscopic equation:

$$\frac{\partial C}{\partial t} = D\frac{\partial^2 C}{\partial x^2} \tag{42}$$

Let us suppose an infinite medium with an initial concentration variation according to a sine form:

$$C_{(0)} = C_1 + \left(C_2 - C_1\right)\sin\frac{2\pi x}{\lambda}$$

The solution will be:

$$C_{(t)} = C_1 + \left(C_2 - C_1\right)\left(\sin\frac{2\pi x}{\lambda}\right)e^{-\alpha t} \tag{43}$$

when $t \to \infty$, the concentration becomes homogeneous, $C \to C_1$.

By substituting eq. (43) in eqs. (41) and (42), we obtain:

$$\alpha_R = 2\Gamma\left[1 - \cos\frac{2\pi a}{\lambda}\right], \quad \alpha_F = \left(\frac{2\pi}{\lambda}\right)^2 D \tag{44}$$

where a is the interatomic distance, subscript R stands for the solution of eq. (41) and F for the solution of Fick's Law, eq. (42).

In expanding $\cos(2\pi a/\lambda)$ and taking into account the fact that $D = \Gamma a^2$ for this one-dimensional diffusion, we obtain:

$$\alpha_R = \left(\frac{2\pi}{\lambda}\right)^2 D\left[1 - \frac{2}{4!}\left(\frac{2\pi a}{\lambda}\right)^2 + \frac{2}{6!}\left(\frac{2\pi a}{\lambda}\right)^2 \ldots\right] \tag{45}$$

We clearly see by comparing eqs. (44) and (45) that the solutions of the rate equations and of Fick's equation are identical only when $2\pi a/\lambda << 1$, i.e., for large wavelengths.

Since a concentration profile can be expanded in a Fourier series, the short-wavelength components will evolve in a different manner than predicted by Fick's Law. This effect will be noticeable only for very short wavelengths (a_R and a_F differ by 3% for $\lambda = 10a$ and by 0.03% for $\lambda = 100$ a).

1.4. Jump frequency and diffusion coefficient calculation

We have shown above, eqs (33) and (40), that the diffusion coefficient is given as a function of the jump frequency Γ of the diffusing species. Its calculation comes therefore into the determination of this frequency, which itself can be done in the framework of the statistical mechanical theory of fluctuations (LANDAU and LIFSHITZ [1984], FLYNN [1972]). In fact the jump of an atom can be viewed as a particular fluctuation of the local energy density during which the system undergoing diffusion passes from a stable position to another over a barrier of higher energy, the so-called *saddle hypersurface* in the configurational space spanned by the 3 N position variables.The statistics of the fluctuations of the local energy density therefore control the jump frequency. The nature of this saddle hypersurface is defined by the nature of the crystalline lattice and by the mechanism at work (see § 1.1). Let us particularize for example to the case of a vacancy mechanism, the other cases being easily handled in the same framework.

1.4.1. Vacancy concentration

In this case the relevant fluctuation can be decomposed into two steps: the formation of the vacancy and the jump of a neighbouring atom into the vacancy. The probability to observe a defect on a neighbouring site of the atom under consideration is given by:

$$P_v = P_0 \exp\left(-G_v/kT\right)$$

with G_v the free enthalpy of the system containing the vacancy plus N atoms and P_0 a normalizing constant. The relative probability with respect to the non defective state, i.e. the vacancy concentration is therefore:

$$c_v = \exp\left(-\left(G_v - G_0\right)/kT\right) \tag{46}$$

with G_0 the free enthalpy of the perfect crystal. In the so-called quasi-harmonic approximation, which in most cases works fairly well up to near the melting point (LUTSKO *et al.* [1988]), these free enthalpies are given by:

$$G = W + kT \sum_{\alpha=1}^{3(N-1)} Ln\left(\frac{\hbar\varpi_\alpha}{k\,T}\right) + P_{ext}V$$

with W the potential energy of the system in the relevant state, the third term correspond to the work of the external pressure P_{ext} on the actual volume and the second, the so-called vibrational entropy, corresponds to a summation over the 3 (N−1) non-zero normal eigenfrequencies ϖ_α. The enthalpy difference in (46) takes now the form:

$$\Delta G_F = \Delta H_F - T\Delta S_F = W_v - W_0 + kT \sum_{\alpha}^{3(N-1)} Ln\left(\frac{\varpi_\alpha^v}{\varpi_\alpha^0}\right) + P_{ext}\left(V_v - V_0\right) \tag{47}$$

References: p. 651.

in which the eigenfrequencies ϖ_α^ν and ϖ_α^0 pertain to the system with and without a vacancy respectively; and V_ν and V_0 to the volume with and without the defect.

1.4.2. Vacancy jump

In order to handle the second step, the vacancy jump, two theories have been put forth and later refined, the theory of Rate Processes (WERT and ZENER [1949], VINEYARD [1957]), and the Dynamical Theory (RICE [1958], SLATER [1959], FLYNN [1968]). As will become clear, these two approaches emphasize different aspects of the jump, and are complementary rather than contradictory.

1.4.2.1. Rate theory of jumps. The probability of finding a vacancy as a first neighbour of an atom is a static property and as such the statistical thermodynamical treatment given above is rigorous. This is no longer the case for the jump which has a strong dynamic character: the jump proceeds as an hamiltonian trajectory in the phase space and the successive positions during the jump are strongly correlated. However, it is not possible to solve for them down to a calculation of the frequencies, so we need approximations. In the rate theory one neglects completely the dynamical aspects: the successive positions of the system during the jump are viewed as independent static positions with an occupancy given by their equilibrium statistical weight all along the jump path, including the saddle position. The dynamical correlations between successive positions are lost, and therefore the jumping particle has no "memory". Moreover the saddle hypersurface is supposed to be planar as a consequence of the hypothesis of harmonic interatomic interactions even at the saddle position.

The jump frequency of a vacancy, or the frequency in one direction for an atom (eq. 32), is defined as the *flux* J_S crossing the saddle hypersurface S, for a unit occupancy of the stable position, which in our example includes a vacancy on the proper site:

$$\Gamma_\nu = J_S/P_\nu \quad \text{with} \quad J_S = \int_0^\infty P_S s' \mathrm{d}s$$

where s is the unstable normal coordinate perpendicular to the saddle hypersurface S, s′ the corresponding "velocity" and P_S as above the statistical weight along S defined by:

$$\begin{aligned} P_S &= P_0 \exp\left\{-\left(G_S\right)/kT\right\} \\ G_S &= W_S + kT \sum_{\alpha=1}^{3(N-1)-1} \mathrm{Ln}\left(\frac{\hbar\varpi_\alpha^S}{k\,T}\right) + P_{\mathrm{ext}} V_S \end{aligned} \tag{48}$$

Now we have for the migration frequency:

$$\begin{aligned} \Gamma_\nu &= \frac{k\,T}{h} \exp\left\{-\left(G_S - G_V\right)/kT\right\} \\ G_S - G_V &= W_S - W_\nu + kT \sum_{\alpha=1}^{3(N-1)-1} \mathrm{Ln}\left(\frac{\hbar\varpi_\alpha^S}{k\,T}\right) - kT \sum_{\alpha=1}^{3(N-1)} \mathrm{Ln}\left(\frac{\hbar\varpi_\alpha^0}{k\,T}\right) + P_{\mathrm{ext}}\left(V_S - V_\nu\right) \end{aligned} \tag{49}$$

Notice that in this expression the eigenfrequencies ϖ_α^S corresponding to motions

restricted to the saddle hypersurface do not correspond one-to-one to the frequencies in the stable position, ϖ_α^0. Indeed the new modes of the system close to the saddle point have no counterpart in the perfect nor in the defective system in the stable position. Moreover the first product contains one fewer frequency than the second, for the reaction coordinate s is quenched at the saddle value. A more homogeneous formula is generally written as:

$$\Gamma_v = \nu_0 \exp\left\{-(G_S - G_V)/kT\right\} = \nu_0 \exp\left\{-(\Delta G_M)/kT\right\}$$
$$\Delta G_M = W_S - W_v + kT \operatorname{Ln}\left\{\nu_0 \prod_{\alpha^S}^{3(N-1)-1} \varpi_\alpha^S / \prod_{\alpha^0}^{3(N-1)} \varpi_\alpha^0\right\} + P_{\exp}(V_S - V_v) \tag{50}$$

which shows clearly that the so-called "attempt frequency", ν_0, has no physical meaning on its own, but only as a couple with the migration entropy. From (33) and (50) one recovers the well known expression of the diffusion coefficient in cubic structures:

$$D = \nu_0 a^2 \mathrm{f} \exp\left(\frac{\Delta S_F + \Delta S_M}{k}\right) \exp\left(-\frac{\Delta H_F + \Delta H_M}{kT}\right) \tag{51}$$

where, by comparison with eq. (50), one defines ΔS_M and ΔS_F, respectively the defect migration and formation entropies, ΔH_M and ΔH_F, the corresponding enthalpies, *'a'* the lattice parameter.

As said above, in this approach the dynamic aspect of the jump is neglected. However the system follows during the jump an hamiltonian trajectory in the phase space and its successive positions are therefore correlated. These short time correlations have two effects, multiple jumps one the one hand (DA FANO and JACUCCI [1977], DE LORENZI and ERCOLESSI [1992]) which can be viewed as a new diffusion mechanism, the existence of unsuccessful jumps on the other, in which the jumping particle turns back just after having passed the saddle point. Following BENNETT [1975] these unsuccessful events could amount to 10% of the jumps foreseen by the rate theory up to near the melting point in a Lennard–Jones crystal, but to a larger value for other kinds of interaction (GILLAN *et al.* [1987]). The main origin of this inefficiency lies in the anharmonicity of actual interatomic interactions allowing for a curved rather than planar saddle hypersurface; according to FLYNN [1987], a curved hypersurface can be crossed twice. An improvement to the Vineyard approach as been proposed by TOLLER and col. [1985] by considering the full manifold of the newtonian *trajectories* in the phase space, and not simply the *positions* of the system in the configuration space. Topological considerations allow to count now only the *successful trajectories* as a subset of all possible ones, instead of counting only the static state of the system in the saddle hypersurface, as in the rate theory approach. Using the first non-harmonic term, of third order, for describing the curvature of the saddle hypersurface, a part of the above mentioned 10% discrepancy is shown to be recovered, but the Molecular Dynamics method is needed to account for the remainder (FLYNN [1987]).

1.4.2.2. Dynamic theory of jumps. Contrarily to the rate theory, in the dynamic one the jump frequency is directly deduced from the atomic dynamics, the phonon contribution to the fluctuations of the atomic positions, and not from an occupancy hypothesis about the

states in configurational space. In this approach one defines a 1D reaction coordinate measuring the progress of the jump along the jump direction, according to the scalar product:

$$x = (\delta s_0 - \delta s_{col}) \cdot n$$

where δs_0 and δs_{col} are the 3D displacements with respect to the stable positions s_0 and s_{col}, respectively of the jumping atom and of the saddle point, and n the unit 3D vector along the jump path. The position s_{col} is generally defined as the center of gravity of the atoms defining the saddle gate. All these coordinates fluctuate as a result of the random superposition of phonons. The contribution of a phonon of frequency ϖ, wave vector k and branch λ to x is given by:

$$x(t) = \left(u^0_{\varpi\lambda} . n\right)\left(1 - \exp\left(i . k\ s_{col}\right)\right)\exp\left(i\left(k . s_0 - \varpi t\right)\right) \tag{52}$$

where $u^0_{\varpi\lambda}$ is the 3D amplitude vector of the phonon.

Last, it is assumed that the jump necessarily proceeds to completion, once a certain critical value δ of x has been reached. δ remains in the theory an adjustable parameter, which is supposed to depend only on the crystalline structure of the lattice.

It can be shown that upon superposition of harmonic vibrations of frequencies ν_i and amplitude x^0_i, the critical value δ is reached from below at a frequency w given by:

$$w = \left(\sum_i \left(\nu_i x_i^0\right)^2 / \sum_i \left(x_i^0\right)^2\right)^{1/2} \exp\left(-\delta^2 / \sum_i \left(x_i^0\right)^2\right)$$

The effect of the various phonons in (52) can be evaluated using $k_\lambda = \varpi_\lambda / v_\lambda$ in a Debye model, v_λ being the sound velocity along the phonon branch λ. At high temperature, $\hbar\varpi_\lambda / kT < 1$; denoting by $\varepsilon_{\varpi\lambda}$ the energy in the mode ϖ, λ, one has:

$$\left|u^0_{\varpi\lambda}\right|^2 = \frac{2\varepsilon_{\varpi\lambda}}{NM\varpi^2} \sim \frac{2kT}{NM\varpi^2}$$

and the summation over ϖ and λ gives:

$$w = \left(\tfrac{3}{5}\right)^{1/2} \nu_D \exp\left(-\frac{\delta^2}{kT}\ \frac{15M}{2\left(3v_l^{-2} + v_t^{-2} + v_{t'}^{-2}\right)}\right) \tag{53}$$

where v_l, v_t and $v_{t'}$ reflect the longitudinal and transverse sound velocities, ν_D is a mean Debye frequency and M the mass of the particles.

As in the rate theory approach, one recovers an Arrhenius-like form of the diffusion coefficient with the migration activation energy defined in the second bracket.

It is also possible to express this result as a function of the elastic constants, since $v^2 = c/\rho$ with ρ the specific mass. Using a properly weighted mean of the elastic moduli, c, and taking Ω as the atomic volume, FLYNN proposes:

$$w = \left(\tfrac{3}{5}\right)^{1/2} . \nu_D \exp\left(-\frac{c\,\Omega\,\delta^2}{kT}\right) \tag{53'}$$

Using a value of $\delta = .32$ for fcc metals and $\delta = .26$ for bcc ones, a quite good agreement

is found with experimental values of migration energies (FLYNN [1968]). Other values are sometimes used (SCHULTZ [1991]).

The most severe drawback of this approach lies in the implicit assumption that the normal modes remain untouched during the jump. Its main interest relies in its ability to handle the migration including the effects of the actual crystal dynamics. The summation in (52) can now be made without any approximation thanks to the availability of complete dispersion relations for various metals and to the development of the numerical simulations, allowing for example a deeper understanding of the bcc metals (see section 3.2).

1.4.3. Macroscopic parameters of diffusion

1.4.3.1. Variation with temperature. For self-diffusion in isotropic media, f is independent of T, so that from eq. (51), D has the well-known *Arrhenius form*:

$$D = D_0 \exp\left(-\frac{Q}{kT}\right) \quad \text{with} \quad D_0 = \nu_0 a^2 \, \mathrm{f} \exp\left(\frac{\Delta S_F + \Delta S_M}{k}\right) \quad \text{and} \quad Q = \Delta H_F + \Delta H_M$$

D_0 is the *frequency factor* and Q the *activation energy*.

For impurity diffusion, f depends on T and, strictly speaking, D has no longer the Arrhenius form, but if we want still to recast its variation into the form of an Arrhenius law, we can define Q as:

$$Q = -k \frac{\partial \log D}{\partial(1/T)} \quad \text{hence we obtain:} \quad Q = \Delta H_F + \Delta H_M - C$$

and $$D_0 = \nu_0 \, a^2 \, \mathrm{f} \exp\left(\frac{\Delta S_F + \Delta S_M}{k}\right) \exp\left(-\frac{C}{kT}\right) \quad \text{with} \quad C = k \frac{\partial \log \mathrm{f}}{\partial(1/T)}$$

If C depends on T, Q and D_0 will also depend on T but it is experimentally observed that C is small and more or less constant so that impurity and self-diffusion behaviours are qualitatively similar.

As a matter of fact, the Arrhenius plot (log D versus 1/T) is often curved; the departure from a straight line is more or less substantial (curvature only at high temperature, continuous curvature, two straight lines with different slopes). In general, the activation energy increases with T. Several explanations are possible:

(1) The enthalpy and entropy terms depend on T (GILDER and LAZARUS [1975], VAROTSOS and ALEXOPOULOS[1986]).

(2) Diffusion occurs by more than one mechanism. This is the case:
- for non homogeneous media; e.g. grain boundary + volume diffusion;
- when several types of jumps occur (DA FANO and JACUCCI [1977]);
- when several defects contribute to the diffusion. Monovacancies are responsible for most of the diffusion processes and, at the present time, the curvatures at high temperature are generally ascribed to the increasing contribution of the divacancies (SEEGER and MEHRER [1970]). If several defects contribute to the diffusion we have:

$$D = \sum_i D_i$$

D is the measured diffusion coefficient and D_i the contribution to the diffusion of the i th defect.

(3) There is an intrinsic domain at high temperature and an extrinsic domain at low temperature; this is mainly the case for semiconductors and ionic crystals. At high temperature (*intrinsic* region) the point-defect concentration is only a function of the temperature, whereas at low temperature (*extrinsic* region) the defect concentration is mainly controlled by the impurity content. More complex situations can occur for complex mechanisms (HOOD [1993])

Typically, for metals and alloys, D_0 is in the range of $10^{-6} - 10^{-4}$ m^2/s and Q in the range of 100–600 kJ/mole (~ 1–6 eV), depending on the melting point of the material.

1.4.3.2. Variation with pressure. According to eqs. (50) and (51) the pressure derivative of the activation enthalpy ΔG_M defines an activation volume ΔV along:

$$\left(\frac{\partial \log D}{\partial P}\right)_T \sim -\frac{(V_v - V_0) + (V_S - V_v)}{kT} = -\frac{\Delta V_F + \Delta V_M}{kT} \tag{54}$$

We have neglected the ∂ log f/∂P and all ∂ log ϖ_λ/∂P terms; the former is strictly zero for self-diffusion and the latter are generally small, of the order of 10^{-2} Ω (Ω is the atomic volume), with respect to the volume variation due to defect formation. $\Delta V = \Delta V_F + \Delta V_M$ is the *activation volume*, where ΔV_F and ΔV_M are the *defect formation* and *migration volumes*, respectively. In general, ΔV_M is small so that ΔV_F is not very different from ΔV. Typically ΔV varies from 0.5 to 1.3 Ω at least in the case of a monovacancy mechanism; in some cases ΔV is very small or even negative, which can be an indication of an interstitial-type mechanism.

1.4.3.3. Variation with atomic mass. From an experimental point of view, the *isotope effect* E is obtained by measuring simultaneously the diffusion coefficients D_α and D_β of isotopes α and β of the same element with masses m_α and m_β. It can be shown that E is given by:

$$E = \frac{D_\alpha/D_\beta - 1}{(m_\beta/m_\alpha)^{1/2} - 1} = f\Delta K \tag{55}$$

where f is the correlation factor. It is assumed that only the frequency ν of the isotope-vacancy exchange is altered by the mass difference according to:

$$\frac{d\ \mathrm{Ln}(\nu)}{-\frac{1}{2}\, d\ \mathrm{Ln}(m)} = \Delta K$$

where ΔK is the fraction of the kinetic energy in the unstable mode residing in the jumping atom. Its value is therefore smaller than 1, of the order of .8 to .9 for self-diffusion in simple fcc metals, and reflects the collective nature of the saddle position crossing during the jump (LE CLAIRE [1966]). Equation (55) holds if, and only if, f has the form:

$$f = \frac{u}{u + \nu}$$

where u is a term which depends on all the frequencies involved but ν. For fcc materials BAKKER [1971] has shown that eq. (55) is valid for vacancy, divacancy and impurity-vacancy pair mechanisms. For more complicated mechanisms such as the Miller mechanism, eq. (55) is no longer valid (see LE CLAIRE [1970a] and PETERSON [1975]). This is also the case for the the vacancy mechanism in ordered alloys with a **B2** structure.

Isotope effect measurements can contribute to identification of the diffusion mechanism through the correlation factor; but we have to know ΔK. Theoretical values of ΔK can be calculated in the framework of the above mentioned jump theories. Unfortunately they are not really sufficiently quantitative for that purpose. An expression has been established by LE CLAIRE [1966], which allows ΔK to be estimated if the defect formation volume ΔV_F is known:

$$\Delta K \sim \left(1 + \tfrac{\xi}{3}\left|(1 - \Delta V_F)\right|\right)^{-1} \tag{56}$$

In this expression, ξ is the number of neighbouring atoms when the jumping atom is in saddle-point position and ΔV_F is expressed as a fraction of the atomic volume. For more details about the isotope effect we refer the reader to LE CLAIRE [1970a], PETERSON [1975] and FLYNN [1987]).

1.5. Numerical simulation approaches

Thanks to the huge progresses of the power of the modern computers as well as of the presently available models of interatomic interactions, the numerical simulation route is now routinely used in diffusion studies (ADDA and CICCOTTI [1985]). The main goal of this approach is twofold. On the one hand numerical simulations are providing well-controlled experiments and allow a proper check of the validity of the various theoretical tools depicted above. Moreover, if realistic interatomic interactions are available, they provide a fairly reliable substitute to actual experiments. This is now almost the case for simple metals with s and p electrons (see for example GILLAN [1989]). On the other hand, like numerical methods, they easily allow for a full treatment of the actual problem: no approximation is needed, and the full anharmonicity can be introduced, which proves to be particularly important in diffusion studies due to the high temperatures involved and the strongly N-body character of the events.

The Molecular Dynamics (M.D.) and the Monte Carlo (M.C.) methods are the most used simulation tools. As explained in the previous paragraph the main observables of the diffusion theory, formation and migration energies for instance or the diffusion coefficient itself, appear as thermodynamic ensemble averages in the phase space of the system. Both of these methods aim therefore to furnish a full set of atomic configurations *using a properly choosen bias* for selecting the most important parts of the phase space, i.e. each configuration will be given a weight according to its Boltzmann factor in the proper ensemble.

References: p. 651.

In M.D., by solving the Newton equations of motion the full trajectory of the system in the phase space is built, and the proper weighting of the possible configurations follows as a consequence of the hamiltonian equations. The ensemble averages can be calculated as time averages thanks to the ergodic hypothesis. In M.C., a set of possibly uncorrelated configurations is built by *randomly moving* the particles according to a rule designed for achieving the proper importance sampling. The notion of trajectory, as well as of time scale, is therefore lost to a large extent.

1.5.1. Molecular Dynamics method

For a broad coverage of the field the interested reader can find almost everything in the following references: CICCOTTI and HOOVER [1986], ALLEN and TILDESLEY [1987], MEYER and PONTIKIS [1991].

In this method the hamiltonian equations of motion are solved by stepwise numerical integration for a system of N particles interacting by a properly chosen potential energy function U. This function can have any degree of complexity (and realism!) from the early empirical sum of interactions between pairs of atoms (GIBSON *et al.* [1960], RAHMAN [1964]), to the most recent quantum-mechanics-based N body potentials where the full contribution of the electrons to the cohesive energy of the system is taken into account (CAR and PARRINELLO [1985], LAASONEN [1994]). Periodic boundary conditions are generally used by repeating on all sides of the primitive system replicas of itself. In this way the spurious effects of free surfaces are avoided. Even in the largest simulations the maximum size is of the order of 10^6 atoms for a maximum duration lower than 10^{-9} seconds of actual time.

The first M.D. simulations were done at constant volume V and total energy E, in the microcanonical ensemble, noted NVE, but more recently new methods appeared which allow to produce trajectories in other ensembles: constant enthalpy (ANDERSEN [1980]), constant stresses (PARRINELLO and RAHMAN [1981]), constant temperature (NOSE [1984], HOOVER [1985]). One must be nevertheless careful when using these new ensembles since the dynamics of the fluctuations introduced is generally no longer the actual one. If needed, special techniques can be used, tailored for studying rare events or non equilibrium systems (BENNETT [1975], CICCOTTI [1991]).

Once a well-equilibrated system has been prepared, the thermodynamic average of the various physical observables can be calculated according to:

$$< f >= \lim_{\tau \to \infty} \frac{1}{\tau} \int_0^{\tau} f(t) dt$$

The observable f, determined as a function of time along the trajectory, can be an energy, enthalpy, temperature, pressure or stress, any correlation function, as well as the mean squared atomic displacement, of special interest here.

In diffusion studies, M.D. has been used either in a direct approach or in an indirect one. In the first the mean squared displacement of the atoms is directly computed from the record of the successive atomic positions. Albeit conceptually simple, this approach is limited by the available computing resources to calculation of diffusion coefficients

higher than 10^{-11} m²/s at most, which limits its application to the studies of liquids (RAHMAN [1964]), or of interstitial diffusion at a quite high temperature (GILLAN [1986], GENDRE *et al.* [1991]). In the indirect approach the M.D. is used for studying the elementary events of the diffusion: the atomic mechanism at work in a given material (BENNETT [1975], DOAN and ADDA [1987], DELAYE and LIMOGE [1993a]), and its various thermodynamic properties, e.g. formation and migration energies, entropies and volumes or associated local modes (WILLAIME [1990], DELAYE [1993]). At a high temperature, the jump frequencies of the defects can also be directly calculated, allowing for a direct check of the validity of the usual theoretical approaches in the diffusion theory.

1.5.2. Monte Carlo method

Now the notion of trajectory is lost: a set of successive configurations Π_i is generated by *randomly* moving one or several particles of a system. As in M.D., the system contains N particles interacting by a properly chosen potential energy function U (the limitations over N are of the same order as in M.D.), and periodic boundary conditions also are frequently used. The configurations resulting from these random moves will be taken as acceptable according to various rules which ensure that the set of configurations contains each state according to its thermodynamical weight in the proper ensemble (for a complete review of the field see VALLEAU and WHITTINGTON [1977] or BINDER ref. S, in the 'Further Reading' list). Such a set forms a Markov chain. It can be shown that it is sufficient that the acceptance rule, or transition probability p_{ij} between states Π_i and Π_j, satisfies the microscopic detailed balance:

$$\pi_j . p_{ji} = \pi_i . p_{ij}$$

for the various states Π_i will be represented in the stationary Markov chain proportionally to their proper Boltzmann weight π_i. Various acceptance rules have been devised, the most popular of which is the Metropolis scheme according to which:

$$\begin{aligned} &a)\quad p_{ij} = 1 && \text{if } W_j < W_i \\ &b)\quad p_{ij} = \exp\left(-\frac{W_j - W_i}{kT}\right) && \text{if } W_j > W_i \end{aligned} \tag{57}$$

if W_i and W_j are the potential energies of states Π_i and Π_j.
As a matter of fact the thermal averages are obtained simply as:

$$< f >= \frac{1}{m} \sum_{1}^{m} f(\Pi_i)$$

with m the length of the Markov chain. The precise form of the acceptance rule influences the rate of convergence towards the limit chain, but does not alter the stationary behaviour. In this approach one of the key point is the source of the random numbers used i) to generate the successive configurations ii) to decide of the acceptance or not in case 57b). The art of building "good" generators of pseudo-random numbers is a quite sophisticated one (see for example KNUTH [1968]). The best one for the present

purpose is probably the so-called "Feedback Shift Register" method (ZIERLER [1959], LEWIS and PAYNE [1973]).

The same comments apply here as in § 1.5.1 with respect to the extension of the method, originally developed for the canonical ensemble, to isoenthalpic, isostress or even Grand Canonical ones by using the proper weight. One of the subtleties of the M.C. method is that the time variable has disappeared, since successive configurations in the chain are not necessarily related by a physically possible path. However, this drawback can be removed (BOCQUET [1987], LIMOGE and BOCQUET [1988]).

Except for the dynamic aspects, the use of M.C. is identical to that of M.D.: defect structure and properties, thermodynamical averages calculation. Moreover, the M.C. approach is particularly well-suited for studying the properties of random walks. Indeed, in a random walk model, the full dynamics of the jump is condensed in a set of frequencies, allowing to calculate by the direct method the diffusion coefficient in a very efficient way. This method has proved to be particularly useful in complex systems, like concentrated alloys, disordered materials etc., where analytical solutions for random walk are not available (MURCH and ZHANG [1990]).

2. *Experimental methods*

We shall review the different techniques which allow the diffusion coefficients D to be measured; for the heats of transport and effective valence measurements the reader is referred to § 6. Two kinds of methods are used to measure D: macroscopic methods, which are based on Fick's Law, and microscopic methods. With the former, we compare the experimental concentration profiles (or a quantity which depends on it) with the appropriate solution of Fick's Law. The latter takes advantage of the fact that many physical phenomena depend on the atomic jumps (for instance, NMR or Mössbauer signals) and can be used to measure atomic jump frequencies. For the microscopic methods it is, in general, necessary to know the diffusion mechanism precisely in order to be able to deduce the jump frequency from the measured signal, whereas the macroscopic methods yield D without any assumption on the diffusion mechanism. Moreover it is not granted that the jumps detected are actually the ones involved in macroscopic diffusion (a drawback of spectroscopic techniques), nor that they are involved in the same manner as in actual diffusion (case of relaxation studies). But the macroscopic methods entail a macroscopic displacement of the atoms and thus a large number of jumps. At low temperatures, for small values of D, it is then necessary to perform long anneals. Conversely, because they only involve a small number of jumps, the microscopic methods require much shorter durations and they allow the variation of D with time to be studied for systems which are not in equilibrium (systems under irradiation, after quenching, during plastic deformation, etc.). For a given system the combination of both kinds of techniques can help to determine the diffusion mechanism (see for instance BRÜGGER *et al.* [1980]). We will successively discuss these two types of techniques.

2.1. Macroscopic methods

Most frequently the quantity which is measured is the concentration $C(x)$ at point x, and the resulting concentration profile is compared with the appropriate solution of Fick's Law; but any quantity which depends on the concentration or on the flux can allow the determination of the diffusion coefficient. In the first part we focus on methods which determine the profile $C(x)$; in the second part we briefly discuss other macroscopic techniques. For more details see ADDA and PHILIBERT [1966], or PHILIBERT [ref. C)].

2.1.1. D from the $C(x)$ curve

2.1.1.1. C(x) by sample sectioning. Generally the $C(x)$ profile is obtained by sectioning the diffusion zone and measuring the quantity of the diffusing species in each slice (thickness Δx).

For *sectioning*, several techniques can be used:
Mechanical sectioning with precision lathe (10 μm, 5×10^{-16} m^2/s), microtome (1 μm, 5×10^{-18} m^2/s) or grinding machine (1 μm, 5×10^{-18} m^2/s).
Chemical or electrochemical attack (50 Å, 10^{-22} m^2/s).
Sputtering by ionic bombardment (10 Å, 5×10^{-24} m^2/s).
The numbers in parentheses indicate, respectively, the minimum thickness of the slices and the minimum diffusion coefficient which can be obtained in practice.

The slice thickness, Δx, and the values of x can be measured by weighing; when Δx is too small, weighing becomes inaccurate and other techniques (optical methods, Talystep) have to be used. The techniques most frequently employed for the *determination of the concentration* $C(x)$ are activity counting (for the radioactive species) and mass spectrometry. Each of them can, in principle, be utilized with one of the sectioning methods described previously. They are very sensitive, especially activity counting which allows the detection of atomic fractions as small as 10^{-10}. Ionic sputtering is associated with mass spectrometry in commercial apparatus (ionic analyzers or SIMS, i.e. secondary ion mass spectrometry, see ch. 10, table 4) and with activity counting in several devices (see for instance GUPTA [1975]); both allow the determination of diffusion coefficients as small 5×10^{-24} m^2/s.

2.1.1.2. Non-destructive techniques. As a matter of fact all these techniques are methods of analysis which could be associated with the sectioning of the sample but they also allow the determination of the profiles without sectioning.

The Castaing microprobe (electron microprobe analyzer). A thin electron beam ($\phi \sim 1\mu m^2$; analyzed zone ~ 1 μm^3) stimulates the X-fluorescence radiation of the element to be studied (ch. 12, § 2.2); the profile $C(x)$ can be obtained by analyzing the sample along the diffusion direction. This technique is convenient for studying chemical diffusion. The sensitivity is of order of 10^{-3} and it is not possible to measure diffusion coefficients smaller than 10^{-15} m^2/s.

Nuclear reactions. The surface of the sample is bombarded with particles (α, protons, etc.) which induce a nuclear reaction with the element to be studied; the energy spectrum of the out-going particles created by this nuclear reaction allows the determination of the

concentration profile $C(x)$. These techniques are convenient for the analysis of light nuclei.

Back-scattering. As previously, the surface of the sample is bombarded and one studies the energy spectrum of the elastically back-scattered particles, from which it is possible to obtain the concentration profile. In contrast with nuclear reaction methods, the back-scattering method is convenient for the analysis of heavy nuclei.

For more details about these two last methods we refer the reader to the writings of ENGELMANN [1977], PHILIBERT [ref. C)] and CHU *et al.* [1978].

2.1.2. Other macroscopic methods

There are numerous macroscopic techniques which allow the determination of diffusion coefficients from measurements of properties depending on matter transport; one obtains generally as a result the *chemical diffusion coefficient.* The most important of these methods are the following:

– Measurement of the quantity of matter leaving or crossing a sample. This method is much employed for gases and volatile products.

– Measurement of the growth rate of a new phase. When the growth is controlled by diffusion it is possible to calculate D from the growth kinetics. This is fully explained by SCHMALZRIED [1974].

– Measurements of compaction and deformation kinetics. Sintering of powders and creep of crystals are in some cases controlled by bulk diffusion; it is then possible to deduce D from compaction or deformation kinetics (ch. 31, § 2.2).

– Measurements of the evolution of the concentration modulation by X-rays (or electrical resistance). This method was initially developed by COOK and HILLIARD [1969] and used for amorphous systems by ROSENBLUM *et al.* [1980], GREER and SPAEPEN [1985]. A film of periodic composition is deposited by evaporation or sputtering; this film tends to homogenize on heating, according to the solution given in § 1.3.5. The kinetics can be followed by X-rays and

$$D = -\frac{\lambda^2}{8\pi^2}\frac{\mathrm{d}}{\mathrm{d}t}\left(\ln\frac{I(t)}{I_0}\right)$$

where I is the intensity of the satellite peak in the neighbourhood of the central spot. It is also possible to follow this kinetics using the measurement of the electrical resistance of the sample; this provides a very convenient measurement tool in complex environments, like high pressures or irradiation (WONNELL *et al.* [1992]).

This technique allows the determination of very small coefficients of diffusion ($\sim 10^{-27}$ m^2/s).

The *Gorsky effect,* in spite of its being a macroscopic method, will be described in the next section, together with relaxation phenomena.

2.2. Microscopic (or local) methods

The methods described here pertain to two groups: on the one hand, studies of relaxation kinetics in out-of-equilibrium samples, on the other hand various spectroscopic methods involving transition matrices disturbed by atomic jumps.

2.2.1. Relaxation methods

The reader can find a very detailed theory of relaxation properties in solids as well as experimental results in NOWICK and BERRY [1972].

2.2.1.1. Thermodynamic aspects of relaxation. The internal energy of a system is defined by the state variables, stresses, temperature, fields, etc., and by a set of n internal variables, labelled v_i, the equilibrium values of which, v_i^e, are fixed by the values of the state variables. These internal parameters can be, for example, the order parameters in an alloy or the populations of the various energy levels that a system can occupy. If one of the state variables changes suddenly, the various internal variables which are coupled with it will relax to the new equilibrium values. In the cases of interest here, the diffusional mobility D controls the relaxation towards equilibrium. We can then measure a relaxation time τ, related to D by

$$D = k\frac{a^2}{\tau}$$

where a is a distance characteristic of the lattice, and k is a constant depending on the specific model involved.

The internal energy varies according to:

$$dU = TdS + dU_{ext} - \sum_i U_i dv_i \tag{58}$$

where dU_{ext} is the energy supplied by the external forces and the dv_i stand for the variations of the internal variables. U_i is the ordering energy associated with the i^{th} internal variable.

If the deviations from equilibrium, $v_i - v_i^e$, are not too large, the U_i can be expanded as

$$U_i = -\sum_j U_i^j \left(v_j - v_j^e\right) \tag{59}$$

When the time evolution of the v_i's is first-order, one speaks of relaxation phenomena. In this case:

$$\frac{dv_i}{dt} = -\sum_j w_i^j \left(v_j - v_j^e\right) \tag{60}$$

One sees easily that it is always possible to find a set of n normals modes V_i evolving in time as:

$$V_i(t) = V_i^e\left[V_i(t=o) - V_i^e\right]\exp\left(-t/\tau_i\right) \tag{61}$$

In eq. (61), τ_i is the relaxation time of the i th normal mode. In many cases the homogeneity of the sample is not perfect and, instead of a single-valued τ_i, we observe a distribution $\pi(\tau_i)$ of times, corresponding either to the distribution of atomic environments or to the various relaxation paths.

References: p. 651.

In diffusion studies of metals and alloys, the most frequently used external influences are mechanical stresses, magnetic field or temperature jumps.

2.2.1.2. Anelasticity. In the case of mechanical stresses one speaks of *anelasticity*. Two solicitation modes are used in these studies. The first one is the *mechanical after-effect*: a static stress (or strain) is applied and the strain (stress) relaxation is followed in time. The application for example of a constant stress leads to an instantaneous elastic response defining the *unrelaxed modulus* M_0. Afterwards the system displays a relaxation of the strain which corresponds at infinite time to the *relaxed modulus* M_∞. The after-effect anelasticity is then defined by three physical quantities:

– the relaxation intensity: $\Delta = (M_0 - M_\infty)/M_\infty$;

– the mean relaxation time $\bar{\tau}$;

– the width of the relaxation time spectrum β.

In many cases the experimental data are well fitted with a Gaussian spectrum (NOWICK and BERRY [1972]):

$$\pi(\tau) = \left(\beta\sqrt{\pi}\right)^{-1} \exp\, -\left(\ln\left(\tau/\bar{\tau}\right)/\beta\right)^2$$

The second mode is the *internal friction mode*. In this case, stress and strain are periodic with a frequency ω according to:

$$\sigma = \sigma_0 \exp i\omega t,\ \varepsilon = \varepsilon_0 \exp i(\omega t - \varphi)$$

The *phase factor* φ between stress and strain expresses the energy dissipation due to anelasticity. One can show that φ is related to $\bar{\tau}$ by:

$$\tan\varphi \sim \frac{\omega\bar{\tau}}{1 + (\omega\bar{\tau})^2} \tag{62}$$

The phase factor displays a Debye resonance versus ω, or versus temperature variation through the temperature dependence of $\bar{\tau}$; the maximum value, φ_{max}, is obtained for $\omega\bar{\tau} = 1$. In real experiments the measurements are made either in forced, or in free, damped oscillations. One can then measure the energy absorbed per cycle, $\delta w/w$, or the magnification factor at the resonance Q (inverse of Full Width at Half Maximum (FWHM) of the ε_0^2- *versus*-ω curve) as a function of temperature. In the free case one measures the logarithmic decrement $\delta = \ln\,[\varepsilon(t)/\varepsilon(t+T)]$, where T is the oscillation period.

All these physical quantities are related by:

$$2\pi \sin\varphi \sim \frac{2\pi}{Q} \sim 2\delta \sim \frac{\delta w}{w} \qquad \text{and} \qquad 2\mathrm{tg}\varphi_{max} \sim \frac{\Delta}{(1+\Delta)^{1/2}} \tag{63}$$

The study of the value of φ versus ω, at various temperatures, gives the relaxation time $\bar{\tau}$ versus temperature. We deduce D, the diffusion coefficient, as

$$D = \frac{k\,a^2}{\bar{\tau}}$$

A great variety of experimental set-ups have been used. The reader will find many references in NOWICK and BERRY [1972]. The most commonly used are the torsion pendulum, either in internal friction or in after-effect mode, and the resonant bar at higher frequency. The corresponding D's which can be measured are given in table 1.

2.2.1.3. Snoek relaxation. In body-centered cubic metals the interstitial defect has a tetragonal symmetry, in both octahedral and tetrahedral sites. Owing to this lower symmetry it can give rise to an anelasticity effect, the so-called *Snoek effect* (SNOEK [1939]). In most cases experimental results are, in bcc metals, in good agreement with the octahedral model (see fig. 7 and § 4.2.1). Under a uniaxial tensile stress σ along the Oz axis, there is a splitting of the energy levels of the three kinds of sites S_x, S_y, S_z, in favor of S_z sites. The ordering energy [eqs. (58) and (59) is: $U_i = \gamma\sigma$, where γ is the lattice parameter variation along Oz axis due to the redistribution from S_x and S_y to S_z sites. The associated internal variable is $v = (n_z - n/3)$, n and n_z being the total atomic fraction and the atomic fraction of solute on S_z sites, respectively. Taking Γ as the total solute frequency jump, one easily shows that $\Gamma = 2/(3\bar{\tau})$, and D is given by

$$D = \frac{a^2}{36\,\bar{\tau}} \tag{64}$$

where a is the lattice parameter. (See also ch. 22, § 4.3.)

2.2.1.4. Zener relaxation. In face-centered cubic metals, an interstitial solute has the same symmetry as the lattice. Therefore there is no anelasticity associated with interstitial solutes. On the other hand, a pair of substitutional solute atoms B of non-zero size effect in a solvent metal A represents a defect of orthorhombic symmetry. Their reorientation under stress then gives rise to an anelastic relaxation which can be seen in all lattices of higher symmetry. ZENER [1943, 1947] was the first to point out the existence of an internal friction peak in a 70:30 α-brass, which he further analyzed as the effect of the reorientation of solute pairs (now called the *Zener effect*). LE CLAIRE [1951] has analyzed the kinetics of their reorientation and shown how it allows the solute jump frequencies to be determined. Nevertheless this model in terms of solute pairs suffers from several weaknesses:

– Contrary to Snoek relaxation, the Zener effect can be observed only in concentrated alloys, because of its dependence on the square of the B concentration. The description in terms of isolated pairs therefore becomes less satisfactory.

– Several parameters of the relaxation (the anisotropy, the temperature dependence of D) are badly accounted for by the pair model.

– The solute mobility alone is involved in Le Claire's analysis of the kinetics. However, NOWICK [1952] has shown that the mobility of both species is needed to produce a relaxation.

Clearly we need a full description of the ordering under stress to give a good account of the Zener effect. LE CLAIRE and LOMER [1954] and WELCH and LE CLAIRE [1967] have given a solution to this problem in the framework of Cowley's order parameters (up to the second-nearest neighbours for the latter authors). The most elaborate analysis of the kinetics for the first model is due to RADELAAR [1970]. He simultaneously calculated

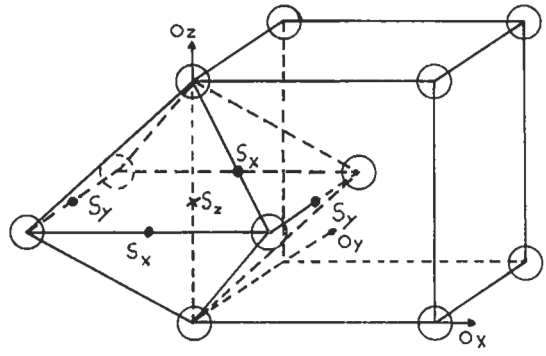

Fig. 7. Characteristics of octahedral interstitial sites in bcc lattices. There are three kinds of sites S_x, S_y and S_z. For an S_z site the first-neighbour distance in the z direction is $a/2$ and $a/\sqrt{2}$ in the xOy plane.

τ_R, the relaxation time for ordering, and $D^{AB}_{A^*}$ and $D^{AB}_{B^*}$, the tracer diffusion coefficients of respectively A* and B* in the alloy:

$$\tau_R \sim a^2 g(\alpha)\left(C_A/D^{AB}_{B^*} + C_B/D^{AB}_{A^*}\right) \tag{65}$$

where $g(\alpha)$ is a smooth function of α, the short range order parameter. No equivalent analysis exists for Welch and Le Claire's model.

One clearly sees that the (approximate) formula (65) does not allow one diffusion coefficients alone to be deduced from τ_R values. The relaxation time appears to be a "Zener-averaged" function of the various atomic jump frequencies and not that particular arrangement which gives the diffusion coefficients. In most cases for example, τ_R appears to be a thermally activated quantity, the activation energy of which is lower than that of either $D^{AB}_{B^*}$ or $D^{AB}_{A^*}$ (NOWICK and BERRY [1972]).

Nevertheless, while the use of Zener relaxation in measuring diffusion coefficients is a delicate task, this effect is of paramount interest in studies of the behaviour of point defects in alloys in, or out of, equilibrium (BERRY and OREHOTSKY [1968], BALANZAT and HILLAIRET [1980]).

2.2.1.5. Gorsky effect. Any defect B which produces a lattice dilatation is also able to give rise to an anelastic relaxation. This is the well known *Gorsky effect* (GORSKY [1935]) the complete theory of which was given by ALEFELD *et al.* [1970]. Indeed, the migration of positive (resp. negative) dilatation centres down (resp. up) a macroscopic strain gradient produces a relaxation of stresses, which is detectable if the diffusion coefficient is high enough (VÖLKL [1972]).

One easily shows that the diffusion coefficient D_{B^*} of the B defect is related to the relaxation time τ_R by (ALEFELD *et al.* [1970]):

$$D_{B^*} = \frac{1}{\varphi \tau_R}\left(\frac{d}{\pi}\right)^2 \tag{66}$$

where d is the length of the diffusion zone and φ the thermodynamic factor (§ 1.2.2). The main interest of the Gorsky relaxation is to give access to D_{B^*} without the need of any diffusion model. Note that here the length scale is d, the sample size, and not a, the atomic size [eqs. (64) or (65)]. We see in table 1 that this method is well suited for high diffusion coefficients.

2.2.1.6. Magnetic relaxation in ferromagnetic alloys. In ferromagnetic alloys the local interactions between a magnetic momentum and local order give rise to relaxation phenomena similar to those observed under stress. Their origin is to be found in the *induced anisotropy energy*, the theory of which was built up by NEEL [1951, 1952, 1954] and TANIGUCHI [1955]. We have an ordering energy U_i given by [see eqs. (58) and (59)]:

$$U_i = w \cos^2 \theta \tag{67}$$

where θ is the angle between the local moment and the symmetry axis of the defect under consideration. The origin of w lies in the perturbation by the defect of i) exchange integrals between magnetic atoms ii) spin–orbit coupling.

This anisotropy energy gives rise to three kinds of relaxations.

Table 1
Diffusion coefficient ranges accessible through different techniques.

Method	Relaxation time τ or Frequency ω	Range of D_{B^*} accessible (m^2/s)
Elastic after-effect (Zener or Snoek)	$10 < \tau < 10^5$ s	$10^{-25} < D_{B^*} < 10^{-21}$
Internal friction (Zener or Snoek)	1 Hz $< \omega < 10^5$ Hz	$10^{-20} < D_{B^*} < 10^{-15}$
After-effect and internal friction in Gorsky relaxation	Approximately same as above	$10^{-12} < D_{B^*} < 10^{-8}$
Torque measurement (magnetic anisotropy method)	$10 < \tau < 10^5$ s	$10^{-25} < D_{B^*} < 10^{-21}$
NMR field gradient	–	$10^{-13} < D_{B^*} < 10^{-8}$
Pulsed NMR	$10^{-7} < \tau < 0.1$ s	$10^{-19} < D_{B^*} < 10^{-13}$
Mössbauer	–	$10^{-15} < D_{B^*} < 10^{-11}$
Neutron scattering	–	$10^{-12} < D_{B^*} < 10^{-9}$

The first, analogous to the Snoek relaxation, is due to reorientation of interstitial impurities in bcc crystals during a change of field direction. The relationship between jump frequency, relaxation time and diffusion coefficient is the same as in the Snoek relaxation.

The second is the analogue of the Gorsky effect. In a domain wall the interaction between the magnetostrictive stresses and the strain field of interstitials can be minimized by diffusion through the wall. This diffusion gives rise to an after-effect. The relaxation

References: p. 651.

time is a factor $(\delta/a)^2$ larger than the preceding one (as in the mechanical case), δ being the domain wall thickness (KRONMÜLLER [1978]).

The third can be called a *magnetic Zener effect* and is due to the ordering of ferromagnetic alloys in a magnetic field. The theory was built up by NEEL [1954] in a quasi-chemical model and by VILLEMAIN [1970] with inclusion of second-nearest neighbour order. The link between relaxation time and diffusion is as difficult to establish as in the Zener effect. However, the sensitivity is extremely high and allows study of diffusion at exceedingly low defect concentrations ($10^{-8} - 10^{-10}$ vacancy fraction, CHAMBRON and CAPLAIN [1974]). (See also ch. 29, § 5.3.3.3).

2.2.1.7. Kinetics of short-range ordering. Any physical property sensitive to atomic order can be used to follow the kinetics of ordering and therefore to study atomic mobility: resistivity (RADELAAR [1966], BARTELS [1987], YU and LÜCKE [1992]), X ray-, electron- or neutron diffraction (PENISSON and BOURRET [1975]). Nevertheless we need to relate quantitatively the order parameter and the measured quantity. Further, the link between ordering kinetics and diffusion coefficients is as difficult to establish as in the Zener effect.

2.2.2. Spectroscopic methods

2.2.2.1. Nuclear magnetic resonance. In a static magnetic field $\mathbf{H}_0$ (say 10^3 Gauss) a nuclear spin of magnitude I takes a precession motion at the Larmor frequency ω_0. Simultaneously the degeneracy of the $2I+1$ energy levels is raised. A macroscopic sample is an assembly of nuclear spins and will then display a magnetic moment along $\mathbf{H}_0$, M_z, and a transverse part $M_\perp$, zero at equilibrium. If we apply a transverse radio-frequency magnetic field $H_\perp$ with a pulsation ω near ω_0, this field will induce transitions between the $2I+1$ Zeeman levels of each spin. Experiments show, and theory confirms in many cases (ABRAGAM [1961]), that the time evolution of the total moment of the sample $\mathbf{M}$ is given by the *Bloch equation*:

$$\frac{\partial \boldsymbol{M}}{\partial t} = \gamma \boldsymbol{M} \Lambda \boldsymbol{H} - \frac{M_\perp}{T_2} - \frac{M_z - M_z^{eq}}{T_1} + \nabla\left[D.\nabla\left(\boldsymbol{M} - \boldsymbol{M}^{eq}\right)\right] \tag{68}$$

where γ is the gyromagnetic ratio, $\mathbf{M}^{eq}$ the equilibrium value of the magnetic moment and D the diffusion coefficient of the nuclei. T_1 is the relaxation time of the longitudinal part M_z and corresponds to an energy transfer between lattice and spins system. T_2 is the relaxation time of the transverse part $M_\perp$. The values of T_1 and T_2 are fixed by various interactions between spins, either direct or indirect via electrons. On each nuclear site these interactions create a local field (approx. 1 Gauss) which fluctuates, due to atomic vibrations and jumps. It induces transitions between levels and then settles their lifetime. However, if the frequency of the atomic displacements becomes of the order of magnitude of the frequency of the precession motion due to this local field, the spins will be sensitive only to the time average of it. This average is zero and the lifetime is no longer limited by interactions: this is the so-called *motional narrowing* of absorption lines, which explains part of the variation of T_1 and T_2 with temperature.

Equation (68) shows that two techniques can be used to determine diffusion coefficients. Firstly, the last term of eq. (68) gives a time evolution of M when the sample is put into a field gradient G according to:

$$M_{\perp}(t) = M_0 \exp\left(-\frac{t}{T_2} - \frac{1}{3} D\gamma^2 G^2 \tau^2 t\right)$$

The measurements of $M_{\perp}$ versus time t then gives D without any further hypothesis (ABRAGAM [1961]).

We can also measure either the width of absorption lines in steady-state resonance (ω near ω_0), or the decay of M_z and $M_{\perp}$ parts with time after the perturbation by a "pulse" of $H_{\perp}$ field. In this last case, the decays fit the laws $M_z = M_0\,[1 - \exp(-t/T_1)]$ or $M_{\perp} = M_0 \exp(-2t/T_2)$. Now the BLOEMBERGEN *et al.* theory [1948] expresses T_1 and T_2 in terms of Fourier transforms of the time correlation function of dipolar interactions (the main interaction in many cases) due to nuclear motions. We then have to postulate a diffusion mechanism, to calculate correlation functions and to compare it with experimental T values in order to deduce a diffusion coefficient.

The original work of Bloembergen was done for diffusion in liquids and later extended to the case of random walk and defect mechanism in lattices (TORREY [1954]), including correlation effects (WOLF [1979]). Self-diffusion in aluminum was measured by NMR by SEYMOUR [1953] and by SPOKAS and SLICHTER [1959].

2.2.2.2. Mössbauer effect. Gamma rays can be emitted or absorbed by excited nuclei. According to the Heisenberg principle, and controlled by the half-life time τ of the nuclei, the width $\Gamma = \hbar/\tau$ of the corresponding lines can be very narrow, of the order of 10^{-9} eV for example. Owing to the recoil energy of the emitter, the emission line of free nuclei is shifted by a much larger amount. This shift then prevents the resonant absorption by other nuclei. On the other hand, if the emitter is embedded in a crystal a part of the emissions occurs without recoil. This is the Mössbauer effect. In this case resonant absorption can occur. However, if one of the emitting or absorbing nuclei is moving, either by thermal vibration or diffusion jumps, the line is broadened by self-interference effects. This broadening is the main effect which has been used to give access to atomic mobility. More precisely, SINGWI and SJÖLANDER [1960a] have shown that the emission, or absorption, cross-section is given by:

$$\sigma(\omega) = \frac{\sigma_0 \Gamma}{4\hbar} \int \exp\left[i(Kr - \omega t) - \frac{\Gamma}{2\hbar}|t|\right] G_s(r,t)\,\mathrm{d}r\,\mathrm{d}t \tag{69}$$

where $G_s(r,t)$ is the Van Hove autocorrelation function and K the wave vector of the γ photon of frequency $2\pi/\omega$. In a classical system G_s gives the probability of finding at (r,t) a particle located initially at (0,0). Therefore $G_s(r,t)$ contains all the information about diffusion processes. SINGWI and SJÖLANDER [1960a, b] have given the theory of diffusion broadening in the case of liquids and of random jumps on an empty lattice (i.e. interstitial case). In the last case the broadening is given by:

$$\Delta\Gamma = \frac{12\hbar}{b^2} D(1 - \alpha) \quad \text{and} \quad \alpha = \frac{1}{N} \sum_{n=1}^{N} \exp(iKR_n) \tag{70}$$

References: p. 651.

where b is the jump distance and R_n the N possible jump vectors. Equivalent formulas have been given for the vacancy mechanism (WOLF [1983]). This dependence can give very valuable informations about the anisotropy of diffusion (FLINN [1980]), as well as on the jump vectors (SEPIOL and VOGL [1993a]). Nevertheless the constraints of: (i) high recoilless fraction (large detectable signal), and (ii) measurable $\Delta\Gamma/\Gamma$, say between 10^{-1} and 10^{2}, limit the available tracers to ^{57}Fe, ^{119}Sn, ^{151}Eu and ^{161}Dy (JANOT [1976]).

The other aspects of the Mössbauer spectroscopy, the so-called hyperfine interactions, isomeric shift, magnetic dipolar and electric quadrupolar interactions, have also been used for studying the various jump frequencies of interstitial iron atoms in Al, Fe, Zr, Nb (YOSHIDA [1989]).

2.2.2.3. Quasi-elastic neutron scattering. A monoenergetic neutron beam can be scattered by nuclei embedded in a solid without any energy transfer, that is, without phonon emission or creation. This is the exact parallel, in the case of neutrons, of the Mössbauer effect for γ photons. More precisely, VAN HOVE [1954] has shown that eq. (69) gives the incoherent scattering differential cross-section for scattering vector K and energy transfer ω. In this case Γ has to be taken as zero, and σ appears to be the (r,t) Fourier transform of G_s. Therefore atomic motions, as given by $G_s(r,t)$, induce a broadening of the elastic peak, the measurement of which versus ω gives access to atomic mobility. The formula (70) works for describing the K and jump vectors dependences of the broadening.

Two experimental techniques can be used (SPRINGER [1972]). For the first, one uses small K values, corresponding to large r, where $G_s(r,t)$ is well represented by:

$$G_s(r,t) = (4\pi Dt)^{-3/2} \exp\left(-r^2/4Dt\right)$$

The quasi-elastic peak then has a Lorentzian shape with a FWHM of $2\,\hbar\,K^2\,D$. The use of this method, at low K, is therefore limited by the energy resolution of spectrometers.

In the second method, one starts from a diffusion model which allows G_s to be calculated. One then fits the parameters of the model to scattering measurements at various K vectors, using the K dependence of the broadening. If one works with fairly large K, then small r, the method is very sensitive to the details of the jump mechanism, (PETRY and VOGL [ref. M)], VOGL *et al.* [1989]).

Neutron scattering techniques, owing to an energy resolution of the spectrometers much more limited than in the case of Mössbauer spectroscopy ($\sim 10^{-7}$ with back-scattering geometry, against $\sim 10^{-9}$ eV), are best suited for fast diffusion, like that of hydrogen in metals (GISSLER [1972]), sodium self-diffusion (AIT SALEM *et al.* [1979]) or high temperature studies in β-Ti, a fast diffuser (PETRY *et al.* [1991]).

3. *Self-diffusion in pure metals*

The pure metals are undoubtedly the most studied with regards to their point defects and diffusion properties. The traditional distinction was between *normal* and *anomalous self-diffusion,* the latter taking place in about ten body-centered cubic metals. A detailed review on this point of view can be found in PETERSON [1978]. However, there has been

deep progress in the understanding of this aspect in the last years, and the paradigm has now changed to distinguish between diffusion in close-packed phases, i.e. fcc and hcp ones, as opposed to diffusion in bcc ones.

Diffusion parameters for various pure elements have been gathered in table 2.

According to LE CLAIRE [1976], normal self-diffusion complies with the three following empirical rules:

– the diffusion coefficient obeys the Arrhenius law: $D = D_0 \exp(-Q/kT)$;

– the D_0 values range from 5×10^{-6} to 5×10^{-4} m^2/s;

– the activation energy is related to the melting temperature by the expression: $Q = 34T_M$, (Q in calories per mole), or $0.14\ T_M$ (Q in kJ/mole), where T_M is the melting point of the metal (in Kelvin). This behaviour, forming the base of the Van Liempt relation, is well obeyed by compact metals (see fig. 8a for fcc ones). In bcc structures the dispersion is much greater (fig 8b).

All these properties can be qualitatively understood in the framework of the above mentioned theories of diffusion by the vacancy mechanism, keeping in mind that a proper formation energy for a vacancy has to be related to the cohesive energy of the material and therefore to its melting point.

The term of anomalous diffusion was formerly reserved for describing ten systems which present very low values of the frequency factor D_0 and of the activation energy Q: β-Ti, β-Zr, β-Hf, γ-U, ε-Pu, γ-La, δ-Ce, β-Pr, γ-Yb and β-Gd. All these metals also display a more or less important curvature of the Arrhenius plot (fig. 9b).

However, one often observes a slight positive curvature in the Arrhenius plot even in the so-called normal metals (Al, Ag, Au, Cu and Ni); it is frequently restricted to high temperatures but sometimes it is present over the whole temperature range. This curvature is always upward.

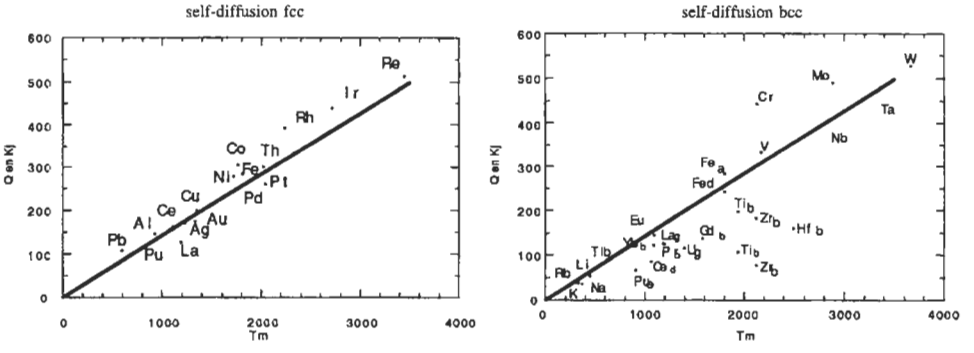

Fig. 8. Van Liempt relation for metals. Fig 8a) fcc metals, fig 8b) bcc metals. The straight line represents the Van Liempt relation: $Q = 0.14\ T_M$ in kJ/mole. bcc structures are widely dispersed around the line, contrarily to fcc ones.

References: p. 651.

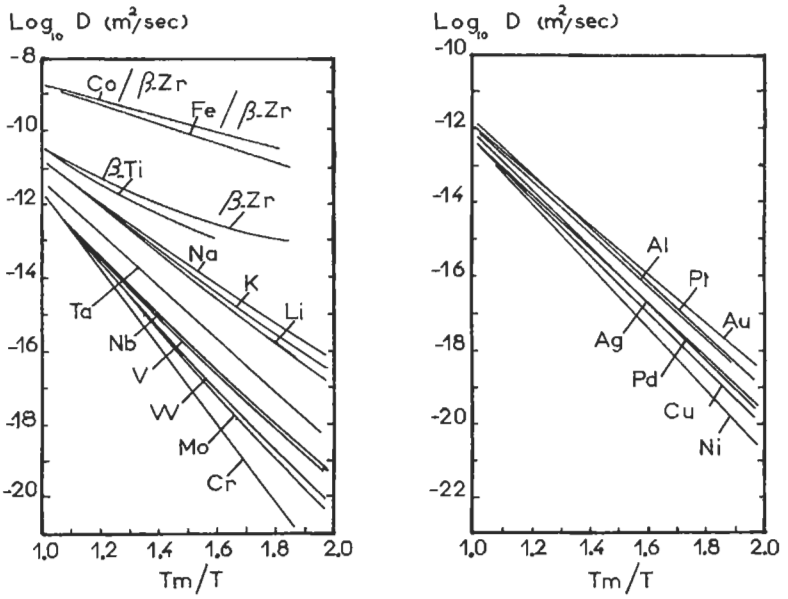

Fig. 9. Diffusion coefficients in an Arrhenius plot normalized to the melting point of the element considered. a) in fcc metals; the range of diffusion values is quite narrow and the curvatures, if any, are small. b) same curves in bcc metals; the diffusion coefficient varies widely from one element to the other according to a systematics controlled by the row number in the Mendeleev classification, the curvatures also are frequently strong.

3.1. Self-diffusion in fcc and hcp metals

The vacancy assumption for the diffusion in these metals is now well accepted by everyone (but see also § 4.2.2). Nevertheless there are still some controversies as regard to the origin of the possible curvature of the Arrhenius plots. In order to explain this curvature, three hypotheses can be retained among all the possibilities which have been discussed in § 1.4.3.1.:

– A vacancy mechanism occurs over the whole temperature range but because of a strong thermal expansion coefficient for the vacancy, (GILDER and LAZARUS [1975]), or due to the variation of the elastic constants with the temperature, (VAROTSOS and ALEXOPOULOS [1986]), D_0 and Q increase with temperature.

– Both vacancies and divacancies contribute to the diffusion, with an increasing participation of the latter at high temperatures (SEEGER and MEHRER [1970]).

Table 2
Self-diffusion parameters for pure elements.

Element (see comments at end)	C.S.	T_m (K)	D_0 (m^2s^{-1})$\times 10^4$	Q (kJ/mole)	Temp. range (K)	$Q = .1422T_m$ Van Liempt	$D(T_m)(m^2s^{-1})$	D (ph. tr.) (m^2s^{-1})	Reference
Ag	fcc	1234	$D_{01} = 0.046$ $D_{02} = 3.3$	$Q_1 = 169.8$ $Q_2 = 218.1$	594–994	175.5	4.9×10^{-13}		REIN and MEHRER (1982)
Al	fcc	933	2.25	144.4	673–883	132.7	1.85×10^{-12}		BEYELER and ADDA (1968)
Au	fcc	1336	0.084	174.1	1031–1333	190	1.3×10^{-12}		HERZIG *et al.* (1978)
Be	hex	1560	$\perp$ c 0.52 // c 0.62	157.4 165	836–1342 841–1321	221.8 id	2.79×10^{-10} 1.85×10^{-10}		DUPOUY *et al.* (1966)
Ca	bcc	1116	8.3	161.2	773–1073	158.7	2.36×10^{-11}		PAVLINOV *et al.* (1968)
Cd	hex	594	$\perp$ c 0.18 // c 0.12	82 77.9	420–587 id	84.5 id	1.11×10^{-12} 1.69×10^{-12}		MAO (1972)
Ce γ $T<999$	fcc	γ/δ 999	0.55	153.2	801–965	152.3*		5.37×10^{-13} (999 K)	DARIEL *et al.* (1971)
Ce δ $T>999$	bcc	1071	0.007	84.7	1018–1064	152.3	4.9×10^{-11}	2.36×10^{-11} (999 K)	LANGUILLE *et al.* (1973)
Co	fcc	1768	2.54	304	944–1743	251.4	2.65×10^{-13}		LEE *et al.* (1988)
Cr	bcc	2130	1280	441.9	1073–1446	302.9	1.86×10^{-12}		MUNDY *et al.* (1981)
Cu	fcc	1357	$D_{01} = 0.13$ $D_{02} = 4.6$	$Q_1 = 198.5$ $Q_2 = 238.6$	1010–1352	193	5.97×10^{-13}		BARTDORFF *et al.* (1978)
Er	hex	1795	$\perp$ c 4.51 // c 3.71	302.6 301.6	1475–1685 id	255.2	7.05×10^{-13} 6.2×10^{-13}		SPEDDING and SHIBA (1972)
Eu	bcc	1099	1	144	771–1074	156.2	1.43×10^{-11}		FROMONT and MARBACH (1977)
Fe α $T<1183$	bcc	α/γ 1183	121	281.6	1067–1168	257.2*		4.45×10^{-15} (1183 K)	GEISE and HERZIG (1987)
Fe γ $1183<T<1663$	fcc	γ/δ 1663	0.49	284.1	1444–1634	257.2*		1.4×10^{-17} (1183 K) 5.83×10^{-14} (1663 K)	HEUMAN and IMM (1968)
Fe δ $T>1663$	bcc	1809	2.01	240.7	1701–1765	257.2	2.25×10^{-11}	5.5×10^{-12} (1663 K)	JAMES and LEAK (1966)

Element	C.S.	T_m (K)	D_0 (m^2s^{-1}) $\times 10^4$	Q (kJ/mole)	Temp. range (K)	$Q = .1422T_m$ Van Liempt	$D(T_m)(m^2s^{-1})$	D (ph. tr.) (m^2s^{-1})	Reference
Gd β	bcc	1585	0.01	136.9	1549–1581	225.4	3.07×10^{-11}		FROMONT and MARBACH (1977)
Hf α $T<2013$	hex	α/β 2013	$\perp$ c 0.28 // c 0.86	348.3 370.1	1538–1883 1470–1883	355.5*		2.56×10^{-14} 2.14×10^{-14} (2013 K)	DAVIS and MCMULLEN (1972)
Hf β $T>2013$	bcc	2500	0.0011	159.2	2012–2351	355.5	5.19×10^{-11}	8.13×10^{-12} (2013 K)	HERZIG *et al.* (1982)
In	tetr	430	$\perp$ c 3.7 // c 2.7	78.5 78.5	312–417 id	61.1 id	1.08×10^{-13} 7.85×10^{-14}		DICKEY (1959)
Ir	fcc	2716	0.36	438.8	2092–2664	386.2	1.3×10^{-13}		ARKHIPOVA (1986)
K	bcc	336	$D_{01}=0.05$ $D_{02}=1$	$Q1=37.2$ $Q2=47$	221–335	47.8	1.32×10^{-11}		MUNDY *et al.* (1971)
La β $T<1134$	fcc	β/γ 1134	1.5	188.8	923–1123	169.6*		3×10^{-13} (1134 K)	DARIEL *et al.* (1969)
La γ $T>1134$	bcc	1193	0.11	125.2	1151–1183	169.6	3.62×10^{-11}	1.88×10^{-11} (1134 K)	LANGUILLE and CALAIS (1974)
Li	bcc	454	$D_{01}=0.19$ $D_{02}=95$	$Q1=53$ $Q2=76.2$	220–454	64.5	3.13×10^{-11}		HEITJANS *et al.* (1985)
Mg	hex	922	$\perp$ c 1.75 // c 1.78	138.2 139	775–906	131.1	2.59×10^{-12} 2.37×10^{-12}		COMBRONDE and BRÉBEC (1971)
Mo	bcc	2893	8	488.2	1360–2773	411.4	1.22×10^{-12}		MAIER *et al.* (1979)
Na	bcc	371	$D_{01}=57$ $D_{02}=0.72$	$Q1=35.7$ $Q2=48.1$	194–370	52.7	1.75×10^{-11}		MUNDY (1971)
Nb	bcc	2740	0.524	395.6	1354–2690	389.6	1.5×10^{-12}		EINZIGER *et al.* (1978)
Ni	fcc	1726	$D_{01}=0.92$ $D_{02}=370$	$Q1=278$ $Q2=357$	815–1193	245.4	9.35×10^{-13}		MAIER *et al.* (1976)
Pb	fcc	601	0.887	106.8	470–573	85.4	4.63×10^{-14}		MILLER (1969)
Pd	fcc	1825	0.205	266.3	1323–1773	259.5	4.9×10^{-13}		PETERSON (1964)

Element	C.S.	T_m (K)	D_0^- (m^2s^{-1})$\times 10^4$	Q (kJ/mole)	Temp. range (K)	$Q=.1422T_m$ Van Liempt	$D(T_m)$(m^2s^{-1})	D (ph. tr.) (m^2s^{-1})	Reference
Pr β $T>1068$	bcc	1205	0.087	123.1	1075–1150	171.3	4×10^{-11}		DARIEL *et al.* (1969)
Pt	fcc	2042	$D_{01}=0.06$ $D_{02}=0.6$	$Q1=259.7$ $Q2=365$	850–1265	290.3	1.4×10^{-12}		REIN *et al.* (1978)
Pu β $395<T<480$	m	β/γ 480	0.0169	108	409–454	129.8*		2.98×10^{-18} (480 K)	WADE *et al.* (1978)
Pu γ $480<T<588$	ort	γ/δ 588	0.038	118.4	484–546	129.8*		4.95×10^{-19} (480 K) 1.15×10^{-16} (588 K)	WADE *et al.* (1978)
Pu δ $588<T<730$	fcc	δ/δ' 730	0.0517	126.4	594–715	129.8*		3.05×10^{-17} (588 K) 4.66×10^{-15} (730 K)	WADE *et al.* (1978)
Pu ε $T>753$	bcc	913	0.003	65.7	788–849	129.8	5.22×10^{-11}	8.3×10^{-12} (753 K)	CORNET (1971)
Rb	bcc	312	0.23	39.3	280–312	44.4	6.05×10^{-12}		HOLCOMB and NORBERG (1955)
Re	hex	3453		511.4	1520–1560	491			NOIMANN *et al.* (1964)
Rh	fcc	2239		391	903–2043	318.4			SHALAYEV *et al.* (1970)
Sb	trig	904	$\perp$ c 0.1 // c 56	149.9 201	773–903	128.5	2.17×10^{-14} 1.36×10^{-14}		CORDES and KIM (1966)
Se	hex	494	$\perp$ c 100 // c 0.2	135.1 115.8	425–488	70.2	5.18×10^{-17} 1.1×10^{-17}		BRÄTTER and GOBRECHT (1970)
Sn	tetr	505	$\perp$ c 21 // c 12.8	108.4 108.9	455–500	71.8	1.29×10^{-14} 6.9×10^{-15}		HUANG and HUNTINGTON (1974)
Ta	bcc	3288	0.21	423.6	1261–2993	467.5	3.9×10^{-12}		WERNER *et al.* (1983)
Te	trig	723	$\perp$ c 20 // c 0.6	166 147.6	496–640	102.8	2.03×10^{-15} 1.3×10^{-15}		WERNER *et al.* (1983)
Th α $T<1636$	fcc	α/β 1636	395	299.8	998–1140	287.7*			SCHMITZ and FOCK (1967)
Ti α $T<1155$	hex	α/β 1155	6.6×10^{-5}	169.1	1013–1149	275.8*		1.48×10^{-16} (1155 K)	DYMENT (1980)

Element	C.S.	T_m (K)	D_0 (m^2s^{-1}) $\times 10^4$	Q (kJ/mole)	Temp. range (K)	$Q = .1422T_m$ Van Liempt	$D(T_m)$(m^2s^{-1})	D (ph. tr.) (m^2s^{-1})	Reference
Ti β $T>1155$	bcc	1940	$D(m^2s^{-1}) = 3.5\times 10^{-4}\times \exp(-328/RT)\times\exp\{4.1\ (T_m/T)^2\}$		1176–1893	275.8	3.11×10^{-11}	5.4×10^{-14} (1155 K)	KÖHLER and HERZIG (1987)
Tl α $T<507$	hex	α/β 507	$\perp$ c 0.4 // c 0.4	94.6 95.9	420–500	82*		7.16×10^{-15} 5.2×10^{-15} (507 K)	SHIRN (1955)
Tl β $T>507$	bcc	577	0.42	80.2	513–573	82	2.3×10^{-12}	2.29×10^{-13} (507 K)	CHIRON and FAIVRE (1985)
U α $T<941$	ort	α/β 941	0.002	167.5	853–923	199.8*		1×10^{-16} (941 K)	ADDA and KIRIANENKO (1962)
U β $941<T<1048$	tetr	β/γ 1048	0.0135	175.8	973–1028	199.8*		2.35×10^{-16} (941 K) 2.33×10^{-15} (1048 K)	ADDA *et al.* (1959)
U γ $T>108$	bcc	1405	0.0018	115.1	1073–1323	199.8	9.46×10^{-12}	3.29×10^{-13} (1048 K)	ADDA and KIRIANENKO (1959)
V	bcc	2175	1.79 26.81	331.9 372.4	1323–1823 1823–2147	309.3	3.05×10^{-12}		ABLITZER *et al.* (1983)
W	bcc	3673	$D_{01} = 0.04$ $D_{02} = 46$	$Q_1 = 525.8$ $Q_2 = 665.7$	1705–3409	522.3	1.7×10^{-12}		MUNDY *et al.* (1978)
Y α $T<1752$	hex	α/β 1752	$\perp$ c 5.2 // c 0.82	280.9 252.5	1173–1573	256.4		2.19×10^{-12} 2.43×10^{-12} (1752 K)	GORNY and ALTOVSKII (1970)
Yb α T<993	hex	α/β 993	0.034	146.8	813–990	156*		6.4×10^{-14} (993 K)	FROMONT *et al.* (1974)
Yb β T>993	bcc	1097	0.12	121	995–1086	156	2.08×10^{-12}	5.18×10^{-12} (993 K)	FROMONT *et al.* (1974)
Zn	hex	693	$\perp$ c 0.18 // c 0.13	96.3 91.7	513–691	98.5	9.92×10^{-13} 1.59×10^{-12}		PETERSON and ROTHMAN (1967)
Zr α T<1136	hex	α/β 1136	no value	Curved Arrh. plot	779–1128	302*		$\approx 5\ 10^{-18}$ (1136 K) 6.14×10^{-14} (1136 K)	HORVATH *et al.* (1984)
Zr β T>1136	bcc	2125	$D(m^2s^{-1}) = 3\times 10^{-5}\times \exp(-3.01/RT)\times \exp\{3.39(T_m/T)^2\}$		1189–2000	302	1.37×10^{-11}		HERZIG and ECKSELER (1979)

Comments on table

These self diffusion data have been extracted from the compilation by MEHRER *et al.* (Ref. B).

Column 1: Symbol of the metal.

Column 2: Crystal stucture. bcc = body centered cubic, fcc = face centered cubic, hex = hexagonal, m = monoclinic, ort = orthorhombic, tetr = tetragonal, trig = trigonal.

Column 3: Melting temperature. For the phases which do not melt (for instance Ce γ, Fe α etc.) we have given the temperature of the phase transition.

Column 4: Experimental D_0. The value in m^2s^{-1} is multiplied by 10^4 (so that it is in cm^2s^{-1}).
For some of the metals the Arrhenius plot is curved and D has the form: $D = D_{01}\exp(-Q_1/RT) + D_{02}\exp(-Q_2/RT)$, in these cases D_{01} and D_{02} are given (they are also multiplied by 10^4).
For Ti and Zr which have strongly curved Arrhenius plots special expressions are given for D (in m^2s^{-1}without any multiplying factor).

Column 5: Experimental Q in kJ $mole^{-1}$. Same remarks as for column 4.

Column 6: Temperature range of the experimental determination of D.

Column 7: Empirical value of Q according to the Van Liempt relation. For the phases which do not melt this value is followed by an *.

Column 8: Value of D at the melting point.

Column 9: For metals which display several phases the values of D are given at the temperature boundaries of the phase. For instance U_β is stable between 941 and 1048 K, D values at these temperatures are given in column 9.

Column 10: References.

– A vacancy mechanism occurs and the curvature is due to the dynamical correlation between successive jumps (vacancy double jumps) (DA FANO and JACUCCI [1977]).

Experimentally the following data are available: frequency factor D_0, activation energy Q, isotope effect E and activation volume ΔV. When the Arrhenius plot is curved, we notice that D_0 and Q increase with T whereas E decreases; for example, for silver self-diffusion, E decreases from 0.72 to 0.58 when T increases from 673 to 954°C. Any of the three assumptions can explain these experimental data: the decrease with temperature of the isotope effect is obvious for the mixed vacancy–divacancy mechanism since the correlation factor for the divacancy mechanism is smaller than for the vacancy mechanism. As a result, since the contribution of the divacancies to the diffusion increases with T, the apparent correlation factor and then the isotope effect will decrease. But this variation of E with T can also be explained with the two other assumptions. Likewise the variation of D_0 and Q with T is compatible with all three hypothesis. The variations of ΔV with P and T have not been frequently studied; in the case of silver ΔV increases with T, but remains constant for gold and aluminium. The increase with T has been interpreted as resulting from an increase of the divacancy contribution at high temperatures (REIN and MEHRER [1982]).

However, measurements of defect properties after quenching can only be understood if vacancies *and* divacancies are present (PETERSON [1978]); in addition, the analysis of tracer and NMR data on self-diffusion in sodium seems also to favour the mixed vacancy–divacancy mechanism (BRÜNGER *et al.* [1980]). Although these two statements are not very general *a consensus does exist in favour of the mixed vacancy–divacancy mechanism*. Thus, in general when the Arrhenius plots are curved the data are fitted by assuming a two-defect mechanism; in addition a possible dependence of enthalpies and entropies on temperature is sometimes taken into account (see for instance SEEGER and

MEHRER [1970] or PETERSON [1978]). Nevertheless the discussion is still open, since divacancies might also be formed *during* the quench, and the role of divacancies is among the "Unsolved Problems" for some experts (MUNDY [1992]).

In hcp metals the limited number of available data is compatible with a slight decrease of the ratio of the activation energies of the diffusion parallel to perpendicular to the c axis with increasing *c/a* ratio, the activation energies being the same in the ideal lattice (HOOD [1993]).

3.2. Diffusion in bcc metals

Self-diffusion in bcc metals presents three characteristics which do not comply with the previous picture. At first there is a much larger scatter of the diffusivity in bcc metals than in the compact phases, and some of them display an unusually large absolute value of D (fig. 9b); second, they frequently exhibit much larger curvatures than the fcc or hcp systems, much to large to be accounted for by a divacancy contribution; last they show a systematic variation of D with the position in the classification which has to be explained, e.g. metals of the same column, like Ti, Zr, Hf in the group 4, have for all of them a very small activation energy and a large curvature (fig 9b). Many explanations have been proposed in order to account for these anomalies: strong contribution of short-circuits, presence of extrinsic vacancies due to impurities, interstitial mechanisms, etc. All these assumptions have been ruled out by experiments. The very origin of this behaviour is now recognized to be linked to the electronic structure of the metal and to the structural properties of the bcc lattice.

At first the diffusion mechanism is now proved by quasi elastic neutron scattering experiments, to be the vacancy one with nearest-neighbour jumps, either in sodium (AIT SALEM *et al.* [1979]) or in β-Ti (PETRY *et al.* [1991]). A small fraction of N.N.N. jumps could also contribute, the fraction being independent of temperature. The same mechanism very likely is also at work in other bcc metals.

The key point now is the recognition that the bcc structure is intrinsically soft with respect to some specific shear deformations; moreover this intrinsic softness can be enhanced (as in β-Ti) or lowered (as in Cr) according to specific features of the electronic structure controlled by the number of d electrons (HO *et al.* [1983, 1984]). This softness is the very origin of the numerous martensitic phase transformations observed between bcc and hcp or ϖ phases, under ambient or high pressure in several of the metals displaying a range of stability in the bcc structure. It is also manifested by the presence in the phonon dispersion curves of a whole branch of soft phonons at large wave vector, from the longitudinal $q = 2/3[111]$ to the $q = 1/2[110]$ phonons. These phonons are precisely the ones which control most efficiently both the jump of the vacancy and the martensitic bcc to hcp phase transformation (1/2 [110]) or to ϖ phase (2/3 [111]). Being of low frequency, they contribute to large fluctuations of the reaction coordinate and therefore give rise to a small migration enthalpy as well as to high diffusion coefficients (see § 1.4.2.2 and eq. (52–53)) (HERZIG and KÖHLER [1987], PETRY *et al.* [1991]). Using experimental dispersion curves, in the framework of the dynamical theory, it is possible to calculate migration enthalpies in good agreement with the

experimental values (SCHOBER *et al.* [1992]). In this respect the 1/2[110] phonon is twice as efficient as the 2/3[111] one to promote the jump (WILLAIME [1991]).

Moreover, using inelastic neutron diffraction methods, the 1/2[110] phonon has been shown to be strongly anharmonic and to soften as temperature decreases in the "most curved" metals (Ti, Zr and Hf) (PETRY and col. [1991]). In this approach the curvature of the Arrhenius plots also can be qualitatively explained, as well as the decrease of the isotopic effect with decreasing temperature (from 0.285 at 916°C to 0.411 at 1727°C in Zr), in contrast with the data of isotope effects in self-diffusion in other structures.

In this picture the whole of the effect appears to be due to the migration term, being small and T-dependent. However we can also expect that these soft phonons will be linked with large relaxations around the vacancy, corresponding to specific features also for the formation contribution in bcc metals. Indeed it is recognized (SCHULTZ [1991], SCHOBER *et al.* [1992]) that in this respect Cr displays an anomalously large formation enthalpy and Ti an anomalously small one. In Cr the 1/2[110] phonon softens with increasing temperature. Since the diffusion activation enthalpy appears to be a constant in the whole temperature range, the formation enthalpy should then increase with T according to the preceding analysis (SCHOBER *et al.* [1992]). The analysis of the electronic structure of bcc metals indeed allows for a systematic variation of the vacancy properties with the number of d electrons: due to the presence of a quasi-band gap in the band structure for a number of electrons of 4, and a maximum around 2, the above mentioned variations of formation terms can be understood (WILLAIME and NASTAR [1994]).

Negative activation volumes have been found for δ-Ce and ε-Pu, pointing possibly to an interstitial diffusion mechanism resulting from specific electronic structure effects (CORNET [1971]).

In alkali metals the migration enthalpy is very low, of the order of one tenth of the formation part (SCHULTZ [1991]). The calculated vacancy formation enthalpy also forms a very important part of the experimental activation enthalpy, or is even greater than it. An interpretation in term of a Zener ring mechanism (see § 1.1.1), has been recently proposed (SEEGER [1993]).

3.3. Prediction of the self-diffusion coefficients

There are three possible ways to predict the diffusion coefficients:
- by theoretical calculations;
- by simulation (see § 1.5.)
- by empirical laws.

3.3.1. Theoretical calculations of D

Using one of the theories given in paragraph 1.4 and 1.5, the calculation of the enthalpies and entropies of formation and migration of the defect involved in the diffusion mechanism allows the determination of the diffusion coefficient. The techniques used in this type of calculation are beyond the scope of this review and we refer the

reader to the general references at the end of this chapter and to specialized treatises, for instance GERL and LANNOO [1978] (see also ch. 18 by WOLLENBERGER).

3.3.2. Empirical relations

Empirical relations are numerous, and we only present the most important;

– *The Zener formula* (ZENER [1951]). This has been established for interstitial solutions and therefore deals only with migration. The idea is that the migration free enthalpy is due to the elastic work required to strain the lattice so that the interstitial can jump. The relation has been empirically extended to self-diffusion. This expression relates the entropy of diffusion ΔS to the activation energy Q via Young's modulus (or shear modulus):

$$\Delta S = \frac{\lambda \beta Q}{T_M}$$

where λ is a constant which depends on the lattice ($\lambda = 0.55$ for fcc and 1 for bcc); $\beta = -\mathrm{d}\,(\mu/\mu_0)/\mathrm{d}\,(T/T_M)$, where μ is Young's modulus (or shear modulus) and μ_0 the value of μ at 0 K; T_M is the melting temperature. The review by LAZARUS [1960] shows that there is a pretty good agreement between experimental and calculated values of ΔS.

– *The Varotsos formula* (VAROTSOS [1978], VAROTSOS and ALEXOPOULOS [1986]). This is based on the idea that the free enthalpy of diffusion has the form $\Delta G = CB\Omega$, where C is a constant which depends on the lattice, B is the bulk modulus (the inverse of the compressibility χ) and Ω the atomic volume. Thus for cubic materials:

$$D = a^2 \nu \exp\left(-\frac{CB\Omega}{kT}\right) \qquad B = \frac{1}{\chi} = -V\frac{\partial P}{\partial V}$$

The agreement with experimental data seems fairly good.

– *Other empirical relations.* These include the *Van Liempt relation*: $Q = 32\ T_M$ (at present one prefers $Q = 34\ T_M$); the *Nachtrieb relation*: $Q = 16.5\ L_M$ (at present one prefers $Q = 15.2\ L_M$), L_M is the latent heat of melting; finally the *Keyes relation*: $\Delta V = 4\chi Q$, where ΔV is the activation volume.

4. *Self- and solute-diffusion in dilute alloys*

This section recalls the expressions of the tracer diffusion coefficients, correlation factors, and phenomenological coefficients L_{ij}'s as functions of the atomic jump frequencies in the frame of standard models which are today widely accepted as good descriptions of impurity effect in diffusion studies. The two methods which have been currently used in the past to establish the expression of the L_{ij}'s are also briefly reviewed. Finally, it is recalled how to determine the atomic jump frequencies starting from the experimental determination of various macroscopic quantities, together with the difficulties usually encountered.

The first part of this section deals with the substitutional alloys for which the vacancy mechanism is expected to be dominant. A short second part deals with the interstitial

dumbbell mechanism in substitutional alloys, since this case is encountered in irradiation experiments. The third part deals with those alloys which do not meet the requirements of a "normal" diffusion behaviour and in which the solute diffusivity is often much larger than the solvent diffusivity.

4.1. Vacancy diffusion in dilute A-B alloys

4.1.1. Standard models for bcc and fcc alloys

In the fcc lattice, the difference between the first and second neighbour distances is large enough to allow us to ignore the interaction between a solute atom and a vacancy beyond the nearest-neighbour distance. The same dissociative jump frequency w_3 is therefore attributed to the three possible dissociative jumps (fig. 10) which separate a vacancy from a neighbouring solute atom; w_4 is the frequency of the reverse jump. w_2 stands for the solute-vacancy exchange and w_1 for the vacancy jump around the solute atom which does not break the solute-vacancy complex. w_0 is a jump not affected by the solute atom. Detailed balancing implies that:

$$w_4/w_3 = \exp(-E_B/kT)$$

where E_B is the binding energy of the vacancy–solute pair (E_B is negative for an attractive binding). This is the so-called "five-frequency model".

All the physical quantities which will be compared to experimental diffusion data in dilute alloys are functions of only three independent ratios of these five jump frequencies, namely w_2/w_1, w_3/w_1 and w_4/w_0.

In the bcc lattice, conversely, the second-neighbour distance is close to the first-neighbour distance and the solute–vacancy interaction energy is not negligible at the second-neighbour distance. Four distinct dissociative frequencies are defined for a vacancy escaping from the first-neighbour shell (w_3, w_3' and w_3'') and from the second-neighbour shell (w_5). The frequencies of the reverse jumps are w_4, w_4', w_4'' and w_6, respectively (fig. 11). The solute–vacancy exchange frequency is w_2. If we denote the interaction energies at the first- and second-neighbour distances by E_{B1} and E_{B2}, respectively, detailed balancing requires that:

$$w_4'/w_3' = w_4''/w_3'' = \exp(-E_{B1}/kT)$$

$$w_6/w_5 = \exp(-E_{B2}/kT)$$

$$w_6 w_4/w_5 w_3 = w_4'/w_3'$$

The calculation of tracer diffusion coefficients has never been performed with the whole set of frequencies. Simplifying assumptions have always been made to reduce the large number of unknown parameters.

– *MODEL I* assumes that $w_4' = w_4'' = w_6 = w_0$. These equalities imply in turns $w_3' = w_3''$ and $w_3 w_5 = w_3' w_4$. All the physical quantities which will be compared to experimental data can be expressed as function of w_3/w_3' and w_2/w_3' only.

— *MODEL II* restricts the interaction to first neighbour distances and assumes that $w_3 = w_3' = w_3''$ and $w_5 = w_6 = w_0$. These equalities imply $w_4 = w_4' = w_4''$. The physical

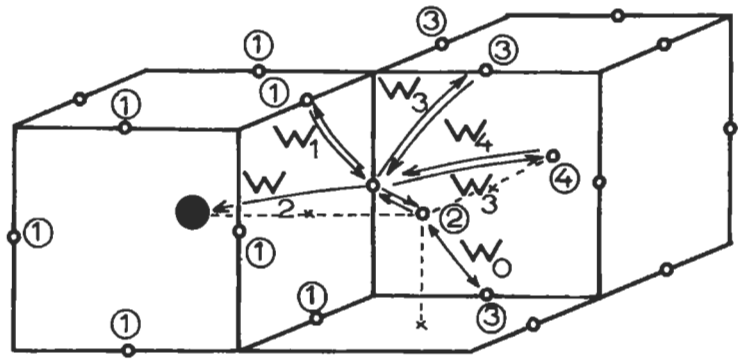

Fig. 10. Standard five-frequency model for solute diffusion in fcc lattices by a vacancy mechanism. The encircled figures denote more and more distant shells of neighbours around the solute atom (solid circle).

quantities which are to be compared with the experimental data are function of w_2/w_3 and w_4/w_0 only.

4.1.2. Kinetic expressions of the phenomenological coefficients L_{AA}, L_{AB}, L_{BA} and L_{BB}

The purpose of the calculation is to express these coefficients as functions of the jump frequencies, the solute and vacancy concentrations, and the various interaction energies between the species. Two methods have been used so far.

4.1.2.1. Kinetic theory. In this theory, also-called pair association method, the stationary fluxes J_A, J_B and J_V are calculated in the presence of a constant electric field E, which biases the jump frequencies of the vacancy. The bias can take two distinct values, ε_A and ε_B, according to the chemical nature of the atom which exchanges with the vacancy. Hence:

$$w_2^{\pm} = w_2(1 \pm \varepsilon_B), \qquad w_i^{\pm} = w_i(1 \pm \varepsilon_A) \text{ for } i \neq 2$$

where the superscript ± stands for a jump fequency in the direction of the electric field (+) or in the reverse direction (–). It can be shown that ε_A and ε_B are proportional to the thermodynamic forces $Z_A^* eE$ and $Z_B^* eE$, respectively, which act upon the species A and B. The final kinetic expressions of the fluxes are then compared with the phenomenological expressions in order to deduce the L_{ij}'s.

For an fcc lattice, the calculation has been carried out at first order in C_B and to an increasing degree of accuracy by including more and more distant shells from the solute (HOWARD and LIDIARD [1963], MANNING [1968], BOCQUET [1974]). For a bcc lattice the calculation has been published in the frame of the two approximations quoted above (SERRUYS and BREBEC [1982b]). For both structures, the common form of the results is the following:

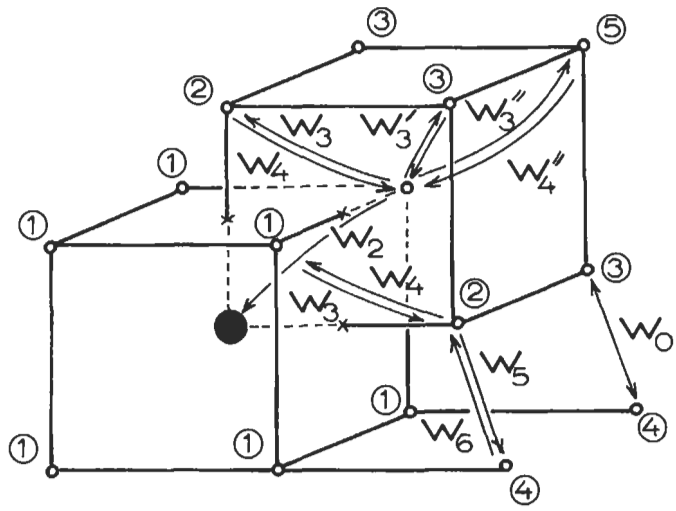

Fig. 11. Standard model for solute diffusion in bcc lattices by a vacancy mechanism.

$$L_{AA} = \frac{nD_{A^*}(0)}{f_0 kT}\left(1 + b_A C_B\right)$$

$$L_{AB} = L_{BA} = \frac{nC_B D_{B^*}(0)}{kT} G$$

$$L_{BB} = \frac{nC_B D_{B^*}(0)}{kT}$$

where n is the number of lattice sites per unit volume; D_{A^*} (0) and D_{B^*} (0) are the solvent and solute tracer diffusion coefficients in pure A ($C_B = 0$); G is the *vacancy wind* term L_{AB}/L_{BB} which accounts for the coupling between J_A and J_B through the vacancy flux J_V. Tables 3 and 4 summarize the expressions of D_{A^*} (0), D_{B^*} (0), b_A and G for both structures. A comprehensive series of papers by FRANKLIN and LIDIARD [1983, 1984], and LIDIARD [1985, 1986] gives a full account of a synthetic reformulation for this method.

The function **F**, always smaller than unity, is a correction to the escape frequency w_3 or w_3' which accounts for that fraction of the vacancies which finally returns in the neighbourhood of a tracer atom: the same function appears in the expression of the correlation factor and in the phenomenological coefficients for all the models where the solute vacancy interaction is restricted to a first neighbour distance (fcc model and bcc model II). More functions appear in the other case (bcc model I). The accuracy in the calculation of these functions increases with the size of the matrix used for the random walk calculation of the defect. The first evaluations (MANNING [1964]) have been recently revised by integral methods (KOIWA and ISHIOKA [1983]). In the same way, the

Table 3
Theoretical expressions of various quantities entering the phenomenological coefficients in an fcc lattice ($f_0 = 0.78145$)

$$D_{A^*} = 2s^2 C_v w_0 f_0, \qquad D_{B^*}(0) = 2s^2 C_v \frac{w_4}{w_3} w_2 f_B;$$

$$u = w_2/w_1, \qquad v = w_3/w_1, \qquad w = w_4/w_0;$$

$$D_{A^*}(C_B) = D_{A^*}(0)(1 + b_1 C_B);$$

$$f_B = (2 + 7\mathbf{F}v)/(2 + 2u + 7\mathbf{F}v);$$

$$b_1 = -34 + 16\frac{X_3}{f_0} + \frac{w}{f_0}\left(4\frac{X_1}{v} + 14X_2\right);$$

$$G = \frac{(3v - 2) + (7 - 7\mathbf{F})v(1/w - 1)}{1 + 3.5\mathbf{F}v};$$

$$b_A = -19 + w(4/v + 14) - \frac{14(1 - \mathbf{F})(1 - w)\left[3v - 2 + (1 + u + 3.5v)(1/w - 1)\right] + (w/v)(3v - 2)^2}{1 + u + 3.5\mathbf{F}v};$$

$$7\mathbf{F} = 7 - \frac{10w^4 + 180.3122w^3 + 924.3303w^2 + 1338.0577w}{2w^4 + 40.1478w^3 + 253.3w^2 + 595.9725w + 435.2839}$$

C_v is the vacancy concentration in pure A; s is the jump distance.

expression of the linear enhancement factor for self-diffusion b_1 contains coefficients X_1, X_2 and X_3 for the fcc lattice and X_1, X_2, X_3 and X_4 for the bcc one: these coefficients are functions of the partial correlation factors for the different solvent jump types in the vicinity of an impurity; they reduce identically to f_0 when all the jumps frequencies are equal, that is, for the case of self-diffusion. They have been numerically tabulated for the fcc lattice (HOWARD and MANNING [1967]) as well as for the bcc lattice (LE CLAIRE [1970b], JONES and LE CLAIRE [1972]). Defining a larger number of solvent jump types, revised and more accurate values have been obtained recently (ISHIOKA and KOIWA [1984]).

4.1.2.2. Linear response method. In the linear response method, a time-dependent (but spatially uniform) external field E(t) is applied to the alloy and instantaneous values of the fluxes J_A, J_B and J_V are calculated. It is shown that the calculation of the L_{ij}'s reduces to the solution, by a Green's function method, of closely related random-walk problems in the unperturbed (E = 0) state of the system. This general formalism has been adapted for the first time to mass transport in solids (ALLNATT [1965]): all the possible trajectories of the vacancy around the tracer atom are automatically taken into account and not only those contained in a few coordination shells, as was done in the pair association method.

The formalism has been illustrated by an application to various cubic structures (ALLNATT [1981], OKAMURA and ALLNATT [1983a]) and has confirmed (and generalised) the results previously obtained by the kinetic method, namely the general

Table 4
Theoretical expressions of various quantities entering the phenomenological coefficients in a bcc lattice ($f_0 = 0.72714$)

$$D_{A^*}(0) = \frac{4}{3} s^2 C_v w_0 f_0 \qquad D_{B^*}(0) = \frac{4}{3} s^2 C_v w_2 \frac{w_4'}{w_3'} f_B \qquad f_B = \frac{7\mathbf{F}w_3'}{2w_2 + 7\mathbf{F}w_3'}$$

$$D_{A^*}(C_B) = D_{A^*}(0)(1 + b_1 C_B)$$

Quantity	Expression	
	Model I	Model II
u	w_3/w_3'	w_4/w_0
v	w_2/w_3'	w_2/w_3
b_1	$-38 + \dfrac{6X_1 u + 8X_2}{f_0} + \dfrac{6X_3 + 18X_4}{f_0}$	$-38 + \dfrac{6X_1 + 8X_2}{f_0} u + \dfrac{6X_3 + 18X_4}{f_0}$
$\mathbf{F}_2$	$(u-2)^2 + 2\mathbf{F}_4(u-2)(u-1) + 3\mathbf{F}_3(3u + 3.096)$	
$\mathbf{F}_3$	$\dfrac{(u-1)^2}{u + 0.8082}$	
$\mathbf{F}_4$	$\dfrac{u + 0.1713}{u + 0.8082}$	
G	$-2\dfrac{(u-2) + \mathbf{F}_4(u-1)}{7\mathbf{F}\, A_1}$	$2\dfrac{u - 7(1-\mathbf{F})(u-1)}{7\mathbf{F}u}$
b_A	$7 + 6u - 2\dfrac{\mathbf{F}_2 + 2\mathbf{F}_3 v}{2v + 7\mathbf{F}}$	$-15 + 14u\left[1 - (1-F)\left(\dfrac{u-1}{u}\right)^2\right] - 2\dfrac{u^2 - 7(1-\mathbf{F})(u-1)^2}{(2v + 7\mathbf{F})u}$
$7\mathbf{F}$	$\dfrac{2u^2 + 5.175u + 2.466}{u + 0.8082}$	$\dfrac{3u^3 + 33.43u^2 + 97.38u + 66.06}{u^3 + 8.68u^2 + 18.35u + 9.433}$

forms for the phenomenological coefficients, and the number of distinct functions $\mathbf{F}$ to be used (ALLNATT and OKAMURA [1984]). Finally, the equivalence between the kinetic and linear response methods has been demonstrated by LIDIARD [1987], and ALLNATT and LIDIARD [1987a]: the former theory focusses on the jumps of a given chemical

References: p. 651.

species when paired to the defect which causes its migration and is well suited to dilute alloys where such pairs can be easily defined; the latter follows the path of a given species by separating it into a direct part when in contact with a defect, and a correlated part where the immobile species waits for the return of the defect. It is more general and can be applied to concentrated alloys (see below § 5).

4.1.3. Experimentally accessible quantities

We restrict ourselves to the experiments which are commonly used to deduce the vacancy jump frequencies at the root of the models for bcc and fcc lattices.

The measurements performed on pure solvent A consist in determining:
– the solvent and solute tracer diffusivities $D_{A^*}(0)$ and $D_{B^*}(0)$;
– the isotope effect for solute diffusion, $f_B \Delta K_B$. The ΔK_B factor must be evaluated in some way to extract f_B. Several theories have tried to determine ΔK_B as a function of the ratio m_B/m_0 where m_B and m_0 are the masses of the solute and of the solvent respectively (ACHAR [1970], FEIT [1972]): but they apparently do not fit with the experiments performed in lithium (MUNDY and MCFALL [1973]).

The measurements of alloying effects are performed on dilute A-B alloys and comparison is made with the same quantities determined in pure A, in order to extract the slope of the linear resulting variation. These measurements usually determine:
– The linear enhancement factor b_1 for solvent tracer diffusion $D_{A^*}(C_B)$, defined by

$$D_{A^*}(C_B) = D_{A^*}(0)(1 + b_1 C_B).$$

Tables 3 and 4 give the expressions for the enhancement factor b_1 which contain the coefficients X_1, X_2 and X_3 for the fcc lattice and X_1, X_2, X_3 and X_4 already defined above.

The solute diffusion coefficient D_{B^*} also varies linearly with the solute concentration, according to:

$$D_{B^*}(C_B) = D_{B^*}(0)(1 + B_1 C_B).$$

The expression of B_1 has been calculated only in the frame of simplified models which do not take into account the solvent partial correlation factors in the presence of solute pairs. But it introduces additional frequencies of the vacancy in the vicinity of two solute atoms (which were not necessary for b_1) as well as the binding energy between solute atoms. A thorough overview has been presented recently on this point (LE CLAIRE [1993]). It is experimentally observed that b_1 and B_1 often have the same sign and are roughly of equal magnitude whenever the diffusion mechanism is the same for A^* and B^* in the alloy (it is not true in Pb-based alloys, § 4.2.2). This means physically that the preponderant effect of the solute is to increase (or decrease if b_1, is negative) the total vacancy concentration, which affects solvent and solute diffusivity roughly to the same extent.
– The linear enhancement factors b_M and b_T for the shift of inert markers and solvent tracer markers in an electric field. If we denote the rates of these shifts by V_M and V_T, b_M and b_T are defined according to:

$$V_M(C_B) = V_M(0)(1 + b_M C_B), \quad V_{A^*}(C_B) = V_{A^*}(0)(1 + b_T C_B)$$

b_M and b_T have been calculated as functions of the vacancy jump frequencies (DOAN [1972]; BOCQUET [1973]; DOAN and BOCQUET [1975]; LIMOGE [1976a]) and are given by:

$$b_T = b_A + 1 + f_0 G \frac{Z_B^*}{Z_A^*} \frac{D_{B^*}(0)}{D_{A^*}(0)} \qquad b_M = b_A + f_0 \frac{D_{B^*}(0)}{D_{A^*}(0)} \left[\frac{Z_B^*}{Z_A^*}(1 + G) + G \right]$$

– The vacancy wind term $G = L_{AB}/L_{BB}$ can be measured from the solute enrichment or depletion in the neighbourhood of a sink (ANTHONY [1971, 1975]) or by combining tracer diffusion experiments with Kirkendall shift measurements in differential couples A + A – B (HEUMANN [1979]; HOSHINO *et al.* [1981a]; HAGENSCHULTE and HEUMANN [1989]).

4.1.4. Determination of vacancy jump frequencies

Jump frequencies depend on the interatomic potential which should, in principle, be deduced from ab-initio calculations. Unfortunately an accurate knowledge of these potentials is far from being currently acquired, except for particular systems, and one usually proceeds differently. Jump frequencies are instead fitted to the experimental results.

As already mentioned, diffusion data yield only three jump frequency ratios for an fcc lattice and only two for a bcc one; thus only three independent measurements are required in the former case and two in the latter. Any additional result is highly desirable and is used to check the consistency of the experiments. If this consistency cannot be maintained in view of a new result, this may mean that one (or more) experimental results are not worthy of confidence or that the model does not correctly represent the experimental system.

All the dilute alloys of fcc structure, for which we know the jump frequency ratios, are displayed in table 5. Whenever the number of experiments is equal to three, one reference only is quoted. When the experimental data are redundant, several references are given. The error bars on the final values of these ratios are large: at least 50% for the best cases, up to an order of magnitude for the worst. We have to keep in mind that any ratio which departs too much from unity (say less than 10^{-2} or larger than 10^2) may be an indication that the weak perturbation assumption at the root of the model is violated in the alloy under consideration. A similar table of jump frequency ratios has been published elsewhere (HERZIG *et al.* [1982]). For bcc alloys, similar tables can be found in fairly recent reviews (LE CLAIRE [1978], AGARWALA [1984]).

The search for the frequency ratios is not always straightforward, as can be seen from the following examples:

– Al-Cu: the value of the self-diffusion coefficient is still today highly controversial. At 585 K it is measured or evaluated to be 1.66 10^{-13} m^2/s (FRADIN and ROWLAND [1967]), 3.03 10^{-13} m^2/s (SEEGER *et al.* [1971]), 3.66 10^{-13} m^2/s (BEYELER and ADDA [1968]), 3.73 10^{-13} m^2/s (LUNDY and MURDOCK [1962]) and 4.51 10^{-13} m^2/s (PETERSON and ROTHMAN

Table 5
Jump frequency ratios for dilute fcc alloys.

Alloy	T(K)	D_{B^*}/D_{A^*}	f_B	b_1	b_T	G	Ref.	w_2/w_1	w_3/w_1	w_4/w_0
Ag–Cd	1060	3.8	0.41	4			c	2.6	0.3	0.85
	1133	3.28	0.71	9.2			b	0.49	0.07	0.52
	1153	3.18		6.5	−12		a	0.5	0.07	0.46
	1197	2.96	0.62	13.7			b	1.7	0.8	1.7
Ag–In	1064	5.7	0.35	17.5			c	4.7	0.7	1.9
Ag–Sn	1043	5.8	0.46	15.6			c	1.8	0.2	1.1
Ag–Zn	1010	4.1	0.52	12.6			d	1.53	0.27	1.15
	1153	3.9	0.57	12.7			d	1.54	0.39	1.30
	1153	3.9		12.7	6		a	1.20	0.26	1.12
Au–In	1075	8.6	0.26	71			e	212	45	5.5
	1175	7.5	0.26	49			e	40	7.3	4.2
Au–Sn	1059	16.4	0.16	130			e	NO SOLUTION		
		16.4	0.16	73			f	1.5	1.2	6.3
	1129	12.93		73		−0.5	n	31.2	4.2	7.1
Au–Zn	1058	6.2	0.15	24			e	942	85	2.9
	1117	5.7	0.15	23			e	973	85	2.6
Cu–Au	1133	1.15	0.9	8.1			g	0.2	0.1	0.6
Cu–Cd	1076	10.2		35		−0.7	h	0.1	1	3
	1076	10.2	0.22	35			h	7.6	0.6	2.8
Cu–Co	1133	0.81	0.85	0			g	2	4.2	1.2
	1133	0.81	0.88	0			g	0.3	0.4	0.76
Cu–Fe	1293	1.1	0.8	−5			i	0.4	0.09	0.3
Cu–In	1005	13.3		42		−0.71	j	18	0.5	3
	1089	11.4		43		−0.57	j	11	1	4
	1089	12	0.07	43			e	33	0.8	3.2
Cu–Mn	1199	4.2	0.36	5			c	3.4	0.35	0.95
Cu–Ni	1273	0.36		−5		0.07	k	0.2	1	1
	1273	0.36		−5.3		0.12	l	0.27	0.42	0.53
Cu–Sb	1005	24.1		79		−1.2	j	15	0.40	5
Cu–Sn	1014	15.5		40		−1.06	j	13	0.2	2
	1014	17	0.15	40			e	7.5	0.14	1.7
	1089	13.6		48		−0.84	j	7	0.33	3
	1089	14.1	0.15	48			e	11	0.5	3.3
Cu–Zn	1168	3.56	0.47	7.3			m	2.5	0.5	1.2
	1168	3.3		8		−0.22	k	3	0.5	1
	1220	3.4	0.47	8.8			m	3.6	0.9	1.5

[a] DOAN and BOCQUET [1975]; [b] BHARATI and SINHA [1977]; [c] HERZIG *et al.* [1982]; [d] ROTHMAN and PETERSON [1967]; [e] HILGEDIECK [1981]; [f] REINHOLD *et al.* [1980]; [g] ECKSELER and HERZIG [1978]; [h] HOSHINO *et al.* [1981b]; [i] BOCQUET [1972]; [j] HOSHINO *et al.* [1982]; [k] HIRANO [1981]; [l] DAMKÖHLER and HEUMANN [1982]; [m] PETERSON and ROTHMAN [1971]; [n] HAGENSCHULTE and HEUMANN [1989].

[1970]). Using ANTHONY's result, which establishes that no detectable solute redistribution occurs in the neighbourhood of a vacancy sink, very different values of $G = L_{AB}/L_{BB}$ are deduced according to the value which is retained for the self-diffusion coefficient. It is easy to check that one obtains $G = -0.4; -0.01; +0.203; +0.226$, and $+0.43$, respectively. The jump frequency ratios which stem from such scattered values of G are highly different of course; in addition they do not fit with the measurement of inert marker shifts in dilute alloys (LIMOGE [1976a]).

Finally, according to SEEGER *et al.* [1971], 40% of the total diffusivity at 858 K is due to divacancies. This fact cannot be ignored any longer, and a revised version of the atomic model should be presented to take properly into account the contribution of the divacancies to diffusion and electromigration.

– Au-Sn: the extracted value for b_1 is sometimes very sensitive to the way chosen for the fitting whenever $D_{A^*}(C_B)$ exhibits a pronounced curvature. A rough fitting extracts a value which is not compatible with the other data and does not allow to deduce the jump frequency ratios (HERZIG and HEUMANN [1972]); a more careful fitting gives reasonable values (REINHOLD *et al.* [1980]). It must be noted however that the direct measurement of the vacancy flow factor G at a slightly different temperature on dilute couples yields noticeably different values (HAGENSCHULTE and HEUMANN [1989]): the departure from the previous ones cannot be accounted for by the small temperature difference, or would imply unusually high activation energies for these frequency ratios.

Although the partial correlation factors are not analytically known, it is possible to check the internal consistency of the experimentally determined quantities in the frame of a given diffusion mechanism. For instance, once the ratio D_{B^*}/D_{A^*} is known, a constraint on the possible values for u,v and w is imposed, which in turn, restrains the possible range for other quantities like b_1 or G. For instance, b_1 is kept to a minimum if the vacancy spends most of its time in exchanging with the solute ($u = w_2/w_1 \to \infty$) and keeping the exchanges with the solvent to the lowest possible value which is compatible with the solute diffusion ($v = w = 0$). Assuming that $X_3 = f_0$ and using the tabulated value $X_1(u \to \infty, v = w = 0) = 0.4682$ yields (MILLER [1969]):

$$b_1^{\min} = -18 + 1.945 \frac{D_{B^*}}{D_{A^*}}$$

If the experimental value for this term is noticeably smaller, it means that the vacancy mechanism alone cannot account for the diffusional behaviour of the system and that, probably, other diffusion mechanisms must be looked for. A similar limitation has been established for the bcc structure, although no simple analytical formula is available (LE CLAIRE [1983]). In the same spirit, it has been shown that the vacancy flow term G in bcc alloys ranges from –2 to a maximum value which depends on the same ratio D_{B^*}/D_{A^*} and on the model (I or II) to be chosen (IIJIMA *et al.* [1985]).

– Pb-Cd: self-diffusion in lead meets the usual requierements of normal diffusion. On the other hand, the solute diffusivity is roughly 20 times larger than the solvent diffusivity: this fact alone is not an indisputable proof that another mechanism is operating. MILLER

[1969] pointed out that the linear enhancement factor b_1 exhibited a value which was noticeably smaller than b_1^{min}. This is the reason why he proposed a new mechanism with interstitial-vacancy pairs (§ 4.2.2).

Like the fcc alloys, there are several bcc systems in which the b_1 factor is too small to be compatible with the high value of the solute-to-solvent diffusivity ratio, namely Zr-based alloys (Co, Cr, Fe), Ti–Co, Nb–Fe and U–Co. The isotope effect measurements, when available in these systems (ABLITZER [1977]; ABLITZER and VIGNES [1978]), are not compatible with the frequency ratios in the frame of a pure vacancy mechanism: another mechanism resting on a dissociative model similar to MILLER's one for Cd in Pb is commonly thought to come into play.

4.1.5. Determination of the solute–vacancy binding energy

The only relevant quantity for determining the binding energy E_B of the solute–vacancy complex is the ratio w_4/w_3, which cannot be deduced from the knowledge of w_2/w_1, w_3/w_1 and w_4/w_0.

DIRKES and HEUMANN [1982] worked out a simple procedure for simulating the vacancy trajectory around the solute and proposed to extract from this trajectory the desired quantity. It is true that the only knowledge of the ratios w_2/w_1, w_3/w_1 and w_4/w_0 is sufficient to determine, at each step of a Monte Carlo simulation, the direction of the most probable next jump. But these authors used an incorrect definition of the vacancy concentration on a first neighbour site of the solute. This concentration is not related to the number of times that the vacancy was located on a first-neighbour site of the solute, but rather to the time the vacancy actually spent on this site.

This definition needs the knowledge of the mean residence time of the vacancy on each site (that is, the inverse of the total escape frequency from this site). It is easily checked that the fraction of the total time which has been spent on a first-neighbour site involves one more independent frequency ratio w_1/w_0 (BOCQUET [1983a]). Moreover, the assumption $w_2 + 4w_1 + 7w_3 = 12w_0$ which is invoked here and there in the diffusion literature for the fcc alloys has no physical justification and is totally arbitrary.

Diffusion experiments by themselves are not sufficient to determine this binding energy. Experiments of another kind must be added: for instance a direct determination of the total vacancy concentration in a dilute alloy, by comparing the macroscopic thermal expansion and the increase in lattice parameter as already done for Al–Ag and Al–Mg (BEAMAN *et al.* [1964]; BEAMAN and BALLUFFI [1965]).

4.2. Dumb-bell interstitial diffusion in dilute A-B alloys

The self-interstitial atom in a compact structure is too large to content itself with an octahedral or tetrahedral position as smaller solute atoms do; it minimizes the distortion of the surrounding lattice by sharing a lattice site with a neighbouring atom and making up a dumb-bell-shaped defect denoted by I_{AA} aligned along <100> (<110>) direction in a fcc (bcc) structure. The migration mechanism involves a translation to a first neighbour site combined to a rotation of its dissociation axis (see chap. 18). The diffusion coeffi-

cient of a substitutional solute atom has been calculated with this mechanism at work for bcc and fcc lattices, under the assumption that it can be incorporated into the defect under the form of a mixed dumb-bell I_{AB} which does not possess necessarily the same symmetry (BOCQUET [1983b, 1991]); the phenomenological coefficients have been calculated for the fcc lattice by the kinetic method (ALLNATT *et al.* [1983]) as well as by the linear response one (OKAMURA and ALLNATT [1986], CHATURVEDI and ALLNATT [1992], SINGH and CHATURVEDI [1993]). But these models cannot be checked experimentally as thoroughly as in the vacancy case, since the frequencies cannot be determined by a clever combination of diffusion experiments; the interstitial defects are necessarily produced by irradiating the solid, and their contribution to diffusion is intricately linked with that of thermal and irradiation-produced vacancies.

4.3. A-B alloys with a high solute diffusivity

4.3.1. Purely interstitial solutes

Light elements like H, C, N, O are known to dissolve interstitially in many bcc and fcc metals. No theoretical criterion has yet been found to predict with confidence the localization of the interstitial atom in the host lattice. In many bcc metals C, O and N are believed to be located on octahedral sites; but dual-occupancy models (octahedral + tetrahedral position) have been invoked to account for the upward curvature of their Arrhenius plot at high temperatures (FARRARO and MCLELLAN [1979]). For the case of hydrogen, a simple empirical rule has been proposed (SOMENKOV and SHIL'STEIN [1979]): H dissolves in the tetrahedral position in all the host metals which have an atomic radius larger than 0.137 nm (Sc, Ti, Y, Zr, Nb, La, Hf, Ta, W) and in the octahedral position for the others (Cr, Mn, Ni, Pd). Vanadium is the link between the two groups and is believed to have a dual occupancy. In Fe, H is expected to be located in octahedral sites although no clear experimental proof has ever been given. The insertion into the host lattice is accompanied by a (generally) large distortion of the surroundings, which can give rise to Snoek-type or Gorsky-type relaxations (§ 2.2).

Although in an interstitial location, the solute atom is believed to interact with vacancies of the host; the diffusivity and the phenomenological coefficients have been calculated with the linear response method (OKAMURA and ALLNATT [1983b]).

The diffusivity of such interstitials in metals has been measured over orders of magnitude by complementary techniques (relaxation methods, tracers, out-gassing, etc...). The Arrhenius plot is straight or exhibits a small curvature at high temperatures. This curvature has been tentatively explained by different models (FARRARO and MCLELLAN [1979]), either a single mechanism with a temperature-dependent activation energy or several mechanisms (or defects) acting in parallel.

For very light interstitials like hydrogen and its isotopes, or the positive muon μ^+, quantum effects play a significant role at low temperatures. Several regimes are expected to be observed in the following order with increasing temperature (STONEHAM [1979]; KEHR [1978]):

(i) *coherent tunneling*, the interstitial propagates through the lattice like a free electron;

(ii) *incoherent (or phonon-assisted) tunneling*, the ground state levels of an occupied and an unoccupied interstitial site have different energies; the tunneling process requires the assistance of phonons which help to equalize the levels of neighbouring sites;
(iii) *classical regime*, the jumping atom receives from the lattice the amount of energy which is required to overcome the potential barrier of the saddlepoint configuration;
(iv) *high-temperature regime*, the residence time on a site is comparable to the time of flight between two neighbouring sites.

The second and third regimes have been observed in many systems. Whether coherent tunneling can actually be observed in real systems or not is still controversial (STONEHAM [1979]; GRAF *et al.* [1980]).

Let us mention the reversed isotope effect which is observed in fcc metals at low temperatures: tritium is found to diffuse faster than deuterium, which diffuses faster than hydrogen. Several models have been proposed to account for this anomaly (TEICHLER [1979]; KAUR and PRAKASH [1982]). See also ch. 18, § 3.3.2.7 for the interaction of self-interstitials with solute atoms.

4.3.2. Complex diffusion mechanisms

The most widely studied case is that of dilute Pb-based alloys.

In lead, several solute atoms (Cu, Ag, Au, Pd, Ni, Zr) diffuse from 10^3 to 10^6 times faster than the solvent tracer. Other elements (Na, Bi, Sn, Tl) diffuse roughly at the same rate. A third group (Cd, Hg) diffuses at rates between the two extremes. It is well established that these properties are in no way related to any short-circuit diffusion path and that they reflect a bulk property. We already mentioned in § 4.1.4 why a pure vacancy mechanism should be rejected for cadmium diffusion in lead.

The high value of the diffusivities led many investigators in the past to think in terms of an interstitial-like diffusion mechanism; it can be shown however, by particular examples, that a purely interstitial mechanism would not yield a value of the linear enhancement factor b_1 consistent with experiment. This is why many authors proposed more complex mechanisms involving interstitial-vacancy complexes, interstitial clusters, and today the consensus is roughly as follows:
– very fast diffusers dissolve partly as substitutionals and partly as interstitials in lead. The total diffusivity is therefore the sum of both contributions; pairs made up of an interstitial solute and a host vacancy are expected to play a dominant role; the phenomenological coefficients L_{ij} have been calculated for this mechanism (HUNTLEY [1974], OKAMURA and ALLNATT [1984]);
– multidefects (interstitial solute atoms sharing one substitutional lattice site) are necessary to account for the diversity of experimental results, especially for the signs and the orders of magnitude of the linear enhancement coefficients b_1 and B_1 (WARBURTON [1975], KUSUNOKI *et al.* [1981]), as well as for the low value of the isotope effect measurements;
– solute atoms which diffuse roughly as fast as the solvent dissolve presumably as substitutionals (except Sn: DECKER *et al.* [1977]);

A general and detailed atomic model including all these defects is still lacking, apart from an attempt by VANFLEET [1980]. The reader is referred to an extensive review by

WARBURTON and TURNBULL [1975].

Lead is not a unique case however, since similar problems arise in other polyvalent metals like Sn, In or Tl (WARBURTON and TURNBULL [1975]; LE CLAIRE [1978]), in the α-phase of Zr, Ti and Hf (HOOD [1993], NAKAJIMA and KOIWA [1993], KÖPPERS *et al.* [1993]), in bcc metals like Nb (ABLITZER [1977]; SERRUYS and BREBEC [1982a]), and for rare-gas diffusion (He) in fcc metals like Au, Ni, Al (WILSON and BISSON [1973]; MELIUS and WILSON [1980]; SCHILLING [1981]). The interaction energy between the smaller solutes and the intrinsic point defects of the host, namely the vacancy one, is believed to be high (above 1 eV); this feature, when combined with a very low solubility in the host, can lead to behaviours, which have puzzled the experimentalists for long. The general interpretation (KÖPPERS *et al.* [1993]) distinguishes three different temperature ranges: in the first (high-temperature) one, the native intrinsic vacancies are more numerous than those trapped by the impurity atoms, and the self-diffusion is normal; at intermediate temperatures (second range), the extrinsic vacancies trapped by the impurity atoms become dominant, and the apparent activation energy for self-diffusion is markedly decreased; at the lower temperatures (third range) where the impurity atoms precipitate into clusters, the number of trapping sites is reduced to such an extent that the intrinsic defects play again the dominant role. It ensues an unusual downward curvature of the Arrhenius plot over the low and intermediate temperature ranges. Depending on the ratio of the melting temperature to the α–β transformation temperature, the interaction energies between impurity and vacancies and between impurities themselves, not all the three regimes are automatically observed. In α-Zr, which has been for long the archetype, the (practically unavoidable) Fe impurity has been found to give rise to the regimes 2 and 3 with the downward curvature observed for self- as well as solute-diffusion; the determining experiments have been carried out only recently since ultra-high purity Zr was not available before (HOOD [1993]). For α-Hf, only regimes 1 and 2 are observed, but the impurity which is responsible of the upward curvature is not yet identified (KÖPPERS *et al.* [1993]). At last for α-Ti, the impurity is believed to be oxygen which is easily incorporated into this highly reactive metal (NAKAJIMA and KOIWA [1993]).

5. *Diffusion in concentrated alloys*

We shall restrict ourselves to binary alloys. The first two sections are devoted to the diffusion of A* and B* tracer atoms in homogeneous disordered and ordered alloys. The third section will deal with chemical diffusion, that is, diffusion in the presence of chemical gradients.

5.1. Diffusion of A* and B* tracers in homogeneous disordered alloys

5.1.1. Experimental results

Diffusion measurements in concentrated binary alloys are legion, but only few alloys have been investigated throughout the whole composition range: Ag–Au (MALLARD *et al.* [1963]), Au–Ni (KURTZ *et al.* [1955]; REYNOLDS *et al.* [1957]), Co–Ni (MILLION and KUCERA [1969, 1971], HIRANO *et al.* [1962]); Cu–Ni (MONMA *et al.* [1964]), Fe–Ni

(CAPLAIN and CHAMBRON [1977], MILLION *et al.* [1981]), Fe–Pd (FILLON and CALAIS [1977]), Ge–Si (MCVAY and DUCHARME [1974]), Nb–Ti (GIBBS *et al.* [1963]; PONTAU and LAZARUS [1979]), Pb–Tl (RESING and NACHTRIEB [1961]). For Fe–Ni, the diffusion has been studied both through a magnetic relaxation method which yields apparent values for the formation and migration energies of the vacancy and by tracers.

Two general trends can be outlined:

– The same kind of empirical correlation as for self-diffusion in pure metals are observed between the preexponential factors D_0 and the activation energy Q, or between Q and the melting temperature T_m of the alloy.

– The diffusion coefficients $D_{A^*}^{AB}$ and $D_{B^*}^{AB}$ for a given temperature and composition do not differ by more than one order of magnitude. When they do, it might be an indication that the diffusion mechanism for the two tracers is not the same (Ge–Si or Pb–Tl). Some cases still offer matter for controversy, like Ge–Si alloys (PIKE *et al.* [1974]). For brevity, $D_{A^*}^{AB}$ and $D_{B^*}^{AB}$ will be denoted by D_{A^*} and D_{B^*} in what follows.

5.1.2. Manning's random alloy model

In this model, the simplest which can be thought of, the alloy is assumed to be random and the vacancy exchanges at rate w_A with A atoms, and w_B with B atoms, whatever the detailed atomic configuration of the local surroundings (fig. 12). The most important finding lies in the fact that the vacancy no longer follows a random walk; its successive jumps are correlated and a vacancy correlation factor f_V smaller than unity shows up in the final expressions (MANNING [1968], [1971]):

$$D_{A^*(B^*)} = \lambda s^2 C_V f_{A(B)} w_{A(B)} \qquad D_V = \lambda s^2 f_V \bar{w}$$

where $f_v = (C_A w_A f_A + C_B w_B f_B)/f_0$ and $f_0 = M_0/(M_0 + 2)$ is the correlation factor for self-diffusion, $\bar{w} = C_A w_A + C_B w_B$, and finally, $f_{A(B)} = M_0 f_v\, \bar{w}/(M_0 f_v\, \bar{w} + 2w_{A(B)})$ for A(B).

Consistent expressions of the phenomenological coefficients L_{ij} have been established in this frame:

$$L_{AA} = n \frac{C_A D_{A^*}}{kT}\left(1 + \frac{2C_A D_{A^*}}{M_0 D^*}\right)$$

$$L_{AB} = L_{BA} = 2n \frac{C_A C_B D_{A^*} D_{B^*}}{kTM_0 D^*}$$

$$L_{BB} = \frac{nC_B D_{B^*}}{kT}\left(1 + \frac{2C_B D_{B^*}}{M_0 D^*}\right)$$

where n is the average number of sites per unit volume, and D^* is the average $C_A D_{A^*} + C_B D_{B^*}$. At last it can be easily shown that the vacancy wind corrections showing up in the expressions of the intrinsic diffusivities [see eqs. (17)] are given by:

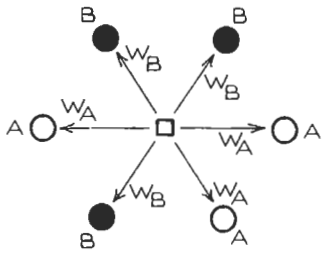

Fig. 12. Manning's random alloy model.

$$r_A = 1 + 2\frac{C_A(D_{A^*} - D_{B^*})}{M_0 D^*}$$

$$r_B = 1 + 2\frac{C_B(D_{B^*} - D_{A^*})}{M_0 D^*}$$

The L_{ij}'s are not independent since they are functions of D_{A^*} and D_{B^*} only; they obey the relationship:

$$L_{AB} = \frac{f_0(L_{AA} + L_{BB})}{2(1 + f_0)}\left[\left(1 + 4\frac{(1 - f_0^2)L_{AA}L_{BB}}{f_0^2(L_{AA} + L_{BB})^2}\right)^{1/2} - 1\right]$$

The same expressions have been later recovered following two different routes:

i) in a formal derivation resting on two macroscopic assumptions related to the invariance of the functional relationship between mobility and flux between the pure substance and the average alloy (LIDIARD [1986]);

ii) in a mean-field treatment of the diffusion problem, resting on the adoption of a preliminary consistency equation over the diffusivities, namely:

$$C_A D_{A^*} + C_B D_{B^*} = f_0 C_v D_v$$

the right-hand side of the above equality being nothing but the tracer self-diffusivity in the average alloy (BOCQUET [1987]).

Manning's approximation appeared fascinating and very appealing since the only independent quantities are the easily accessible tracer diffusivities. It has been the object of very numerous Monte Carlo simulations, which can take into account the detailed occupancy of the sites surrounding the vacancy and can check the accuracy of the approximation. These simulations essentially show that the approximation is indeed quantitatively excellent over the whole concentration range, as long as the disparity between the jump frequencies is not too large, say $10^{-3} < W_A/W_B < 10^3$ (BOCQUET [1973], DE BRUIN *et al.* [1975], [1977], ALLNATT and ALLNATT [1984]). An analytical more sophisticated method for the self-consistent decoupling of the kinetic equations has been worked out and yields the same conclusion (HOLDSWORTH and ELLIOTT [1986], ALLNATT [1991]). Even in dilute alloys, the approximation turns out to be satisfactory

for all quantities but the linear enhancement factor b_1 (ALLNATT and LIDIARD [1987b]).

In the same spirit, the same kind of approximation has been worked out for the dumbbell interstitial mechanism in random two-frequency alloys on fcc and bcc lattices. Although no simple analytical expressions can be established for the tracer diffusivities (BOCQUET [1986]), a similar functional dependence of the L_{ij}'s versus the D_{i*}'s as above can be proposed after replacing f_0 by the product $f_0\mu_0$ (BOCQUET [1987]), where μ_0 is the ratio of the tracer average squared jump length to that of the defect. $\mu_0 = 1/2$ for fcc structures and 7/15 for bcc ones (BOCQUET [1983b, 1991]). The numerical simulations show a good agreement only in special cases for the fcc lattice, and a disagreement for all the cases investigated in the bcc lattice (BOCQUET [1990b]): the reason for these discrepancies has not been elucidated so far, in spite of a recent treatment involving the more sophisticated linear response method (CHATURVEDI and ALLNATT [1994]).

5.1.3. Atomic models for diffusion in non-random disordered alloy

The attempts to improve the alloy model beyond the random approximation and to include the effect of short-range ordering on diffusion have historically followed two different routes.

The first one consisted in extending the dilute alloy models by including more and more solute clusters of increasing size together with the corresponding modifications of the solute and solvent jump frequencies in their neighbourhood. This route turned out to be not well fitted to this purpose, due to the rapidly increasing number of unknown parameters which yielded intractable results, together with the intrinsic impossibility to deal with cluster overlap (BOCQUET [1973]); only rough approximations can be proposed by selecting a few solute clusters which are believed to have a dominant influence (FAUPEL and HEHENKAMP [1987]). But this choice is totally arbitrary and physically unjustified; as a consequence, this route has now been abandoned.

The second route, at the expense of some loss of accuracy, approximates the effect of the local surroundings on the height of the potential barrier by using a small number of pair interaction energies for the stable (E_{ij}) and the saddle-point (E'_{ij}) configurations. The merit of such a description lies in the fact that it connects simply and consistently the thermodynamics (reflected in the E_{ij}'s) and the kinetic behaviour of the alloy (reflected in the E'_{ij}'s). The model was used first to account for the kinetics of short-range ordering in Ag–Au alloys (RADELAAR [1968, 1970]) and Fe–Ni alloys (CAPLAIN and CHAMBRON [1977]). Later it was improved to take into account correlation effects in short-range ordered alloys (STOLWIJK [1981], ALLNATT and ALLNATT [1992]): the analytical formula obtained for the tracer diffusivities and the associated correlation factors are in fair agreement with Monte-Carlo simulations over a reasonably large range of the thermodynamic parameter mastering the order, namely $[2\,E_{AB} - (E_{AA} + E_{BB})]/kT$. The agreement deteriorates to some extent for the lower temperatures where systematic departures show up.

Independently from the search for better expressions of the D_{i*}'s, a systematic investigation of the phenomenological coefficients L_{ij}'s has been carried out numerically by simulating non-random alloys using such pair energies; and the most intriguing result of the last ten years is that the functional dependence of the L_{ij}'s upon the D_{j*}'s

established by Manning for random alloys is still preserved in non-random ones with a fairly good quantitative agreement (MURCH [1982a, 1982b, 1982c], ZHANG *et al.* [1989a], ALLNATT and ALLNATT [1991]), except at the lower temperatures or dilute concentrations; the latter restrictions are not a surprise, since they correspond to those actual situations where the departure from randomness is expected to be the largest. The basic reason for such an agreement is still not understood. Following previous tentative papers (HEUMANN [1979]; DAYANANDA [1981]), an active research effort has recently been undertaken to establish more general relationships between the L_{ij}'s and the various diffusivities (tracer, chemical) (ALLNATT and LIDIARD [1987c], LIDIARD *et al.* [1990], QIN and MURCH [1993a]).

Before closing this section, the main limitations of such models in the present state of the art must be recalled:

– they do not calculate D_{A^*} and D_{B^*} but only the activation energies for diffusion Q_{A^*} and Q_{B^*}, with the correlation effects included in the best case. The preexponential factors D_{0A} and D_{0B} are not known and are arbitrary assumed to remain constant, since no model is available which would account for their variations throughout the whole composition range.

– they use pair energies and assume implicitly that the energy of the alloy can be summed in this way, which is not always true (namely, transition metals). Even if effective pair energies can be defined, the electronic theory of alloys must be used to predict the variations of these pair energies as function of the composition on physically grounded arguments for each specific alloy (DUCASTELLE [1978]).

– finally, they cannot have any predictive power: while pair energies in the stable position can be deduced from thermodynamic measurements, saddle-point pair energies conversely can only be deduced from experiments involving diffusion jumps, that is, from the diffusion experiments themselves.

5.2. Diffusion of A^* and B^* tracers in ordered binary alloys

In the last ten years, intermetallics have been the object of intensive study for their attractive practical properties: some of them are indeed characterized by a high melting temperature, high elastic limit (see ch. 24), high resistance against corrosion and (or) creep (LIU *et al.* [1992]). Before reviewing in more detail the different ordered structures, some preliminary and general ideas should be recalled here.

The progress in the understanding of phase stability from *ab initio* calculations based on the local density functional approximation (LDF) has allowed research people to address very basic points, namely, the physical reasons leading a given alloy to adopt a well-defined structure or symmetry. Such calculations are able to explain the reason why Ti Al_3 is tetragonal (DO_{22}), while Ti_3 Al is hexagonal (DO_{19}) and Ti Al is cubic ($L1_0$); or why Ni_3 Al ($L1_2$) exists whereas there is no corresponding close-packed phase for Ni Al_3 (PETTIFOR [1992]). However, the problem of the point defects has not yet been addressed.

The existence of the so-called constitutional (or structural) defects is probably connected to the preceding point but has not yet received an unambiguous experimental

confirmation as well as a firmly grounded theoretical explanation. Starting with the simple case of the B2 structure as an illustration, the stoichiometric A-B alloy is perfectly ordered at 0 K and the N_A (N_B) atoms occupy the α (β)-sites. When the temperature is raised, several kinds of defect are believed to appear:
– *antistructure* or *substitutional defects*: A atoms can occupy β-sites and are denoted A_β, their number is $N_{A\beta}$, B atoms can occupy α-sites (B_α, $N_{B\alpha}$);
– *vacancies* denoted by V_α on α-sites and V_β on β-sites. Depending on the atomic interactions, the alloy will choose preferentially one type of defect or the other (or some combination of the two). Up to this point, these defects have been introduced as a pure manifestation of thermal excitation in a stoichiometric alloy.

However, for a non-stoichiometric alloy, one must think of the way to accommodate the departure from stoichiometry. The same defects (antistructure atoms or vacancies) have been also invoked; but in this case they are expected to be much more numerous than in the thermal case, since their concentrations will be of the order of the stoichiometry offset (up to several percent) and to survive even at O K unlike thermal ones. The difficult point in looking at actual systems at finite temperatures is to decide which part of the observed vacancies or antisite defects has a thermal origin and which part has a structural one. The undisputable fingerprint of structural defects (their non-null concentration at 0 K) is unfortunately very difficult to use practically: in many systems indeed, high concentrations of vacancies (at room temperature and above) have undoubtedly been evidenced by a careful comparison between density and lattice parameter measurements: but their apparent migration energy has often be found to be large, and one cannot safely state that equilibrium properties rather than quenched-in defects ones are measured. Phenomenological models like bond-breaking pictures (NEUMANN [1980], KIM [1991]) or the Miedema "macroscopic atom" model (DE BOER *et al.* [1988]) using rough expressions for configurational entropies cannot claim to be anything but guiding approximations to decide which type of defect is most likely to appear. A rapidly growing number of model defect calculations using semi-empirical potentials is presently observed (CLERI and ROSATO [1993], REY-LOSADA *et al.* [1993]) but the approximations involved are probably still too crude to solve this question. The problem requires undoubtedly accurate *ab initio* calculations of ground-state energies, together with a minimisation procedure which would allow charge transfers (KOCH and KOENIG [1986]), local relaxations as well as the settlement of an arbitrary vacancy concentration: such calculations would tell us whether the ternary (A,B,V) is most stable in the investigated lattice structure at low temperatures or whether a phase separation between ordered phases of other symmetries (and, or) concentrations occurs. If the existence of these *structural vacancies* can be theoretically proven, one must remember however that their properties are in no way different from those of the so-called *thermal* ones although they have received a different name. Indeed, the total vacancy concentration at finite temperatures minimizes the free-energy of the alloy: but in the present case, the existence of two sublattices and of suitable atomic interactions implies that the result of the calculation is more sensitive to a small variation of the composition, than to a temperature change, unlike the case of the disordered alloy at the same concentration.

Tracer diffusion measurements are still performed and are still highly desirable, as a

first insight into the transport mechanisms. Correlation factors have been calculated in various structures and for various jump mechanisms (BAKKER [1979], ARITA *et al.* [1989], WEILER *et al.* [1984], SZABO *et al.* [1991]). While isotope effects were measured with the hope of determining the jump mechanism, it was shown later that, for B2 structures, such a measurement does not yield the correlation factor (ZHANG *et al.* [1989b]); this is rather unfortunate since these (very difficult) experiments have been performed only on alloys with this symmetry (PETERSON and ROTHMAN [1971], HILGEDIECK and HERZIG [1983]).

Spectroscopic methods like nuclear magnetic resonance (NMR), quasi-elastic Mössbauer line broadening (QEMLB) and quasi-elastic neutron scattering (QENS) appear today as the best candidates to clarify the atomic diffusion mechanisms in ordered alloys; NMR techniques measure the frequency (ies) of the diffusing species (TARCZON *et al.* [1988]), while QEMLB and QENS give besides access to the individual jump vectors (see § 2.2.2 and VOGL *et al.* [1992]). Although some intermediate modelling is still necessary for the final interpretation, they yield the most confident information gained so far. The most important result obtained up to now is that diffusion in ordered structures seems to proceed simply via nearest-neighbour jumps of a vacancy defect. Finally, the ability of the positron annihilation (PA) technique to measure vacancy concentration with confidence is also being currently improved (BALOGH *et al.* [1992]).

The preceding point helps to solve old ill-formulated problems about the migration mechanisms in ordered alloys. The 6–jump cycle was initially designed for transporting atoms without altering the long-range order (MCCOMBIE and ELCOCK [1958], ELCOCK [1959], HUNTINGTON *et al.* [1961]): this condition is unnecessarily stringent since local and thermally activated fluctuations of the long-range order (LRO) must necessarily occur in a real system, the only requirement being the conservation of the average LRO through detailed balancing: this remark has been the starting point of a new formalism (Path Probability Method or PPM) for the evolution of cooperative systems (KIKUCHI [1966]; SATO [1984]). The 6–jump cycle is thus not necessary. Moreover, it is also very improbable: many computer simulations show that such cycles never go to completion and are destroyed while underway by strongly correlated backward jumps (ARNHOLD [1981]). In the same way, the triple defect has been introduced only for thermostatistical reasons (large difference between vacancy formation energies on both lattices): but it was implicitly thought that it should migrate as a whole, that is, without dissociating. This unnecessary constraint has led previous investigators to imagine a mechanism of highly concerted vacancy jumps (STOLWIJK *et al.* [1980], VAN OMNEN and DE MIRANDA [1981]), which has never been clearly evidenced neither experimentally nor theoretically.

At last, a growing body of practical knowledge has been gained through the use of macroscopic measurements like chemical diffusivity (DAYANANDA [1992]), kinetics of long range order recovery after irradiation or plastic deformation (CAHN [1992]), internal friction (GHILARDUCCI and AHLERS [1983]), degradation of superconducting temperature in A_{15} compounds (BAKKER [1993]): these experiments yield effective quantities which are of importance for mastering the practical properties of these materials. But a detailed atomistic model is still lacking which would link these effective energies to the usual parameters deduced from tracer diffusion experiments.

References: p. 651.

For sake of space, the reader will be referred to a recent compilation of experimental results (WEVER [1992]).

5.2.1. Ordered alloys with B2 structure

The B2 structure has been more extensively studied than the others: it is made of two interpenetrating simple cubic lattices, α and β. Each α-site is surrounded by eight first-neighbour β-sites and conversely. The existing alloys belong to two distinct groups:

(i) In the first group (AgCd, AgMg, AgZn, AuCd, AuZn, BeCu, BeNi, CuZn, NiZn) the defects are mainly antistructure defects on *both* sublattices (A_β and B_α) the departure from stoichiometry is compensated by A_β defects for A-rich alloys and B_α defects for B-rich alloys. The apparent formation energy E_F^V of thermal vacancies can be different on the two sublattices.

(ii) In the second group (CoAl, FeAl, NiAl, PdAl, CoGa, NiGa, PdIn), for which α will denote the sublattice of the transition metal A, maintenance of equal α and β site numbers allows formation of paired defects only ($A_\beta + B_\alpha$ or $V_\alpha + V_\beta$). If V_β costs more energy than $A_\beta + V_\alpha$, then $V_\alpha + V_\beta$ converts into the triple defect $A_\beta + 2V_\alpha$. Symmetrically, if B_α costs more than $2V_\alpha$ (mainly due to size effects), then $B_\alpha + A_\beta$ converts also into the same triple defect. The departure from stoichiometry is therefore compensated in two different ways: for an A-rich alloy the major defect is A_β; for a B-rich alloy, the major defect is V_α. In the latter case, very high structural vacancy concentrations on one sublattice are expected and (indeed) experimentally observed (up to 10% in CoGa on the gallium-rich side). All the theoretical calculations performed so far (e.g., EDELIN [1979]) are based on a zeroth-order treatment (BRAGG and WILLIAMS [1934]); not withstanding their crudeness, they account qualitatively well for all the presently known experimental situations, provided reasonable values of the adjustable pair energies E_{ij} are chosen.

A first and simple explanation has been proposed to account for the fact that a particular alloy belongs to the first or to the second group (NEUMANN [1980]). Using a crude bond-breaking picture, this author shows that the number of substitutional defects is dominant whenever the mixing enthalpy ΔH_f is (algebraïcally) higher than –0.3 eV/atom; the number of triple defects is dominant otherwise. It is very gratifying to ascertain that this correlation is very well obeyed. The existence of structural defects (namely in CoGa) has been however questioned recently on the basis of a similar model (KIM [1991]): but the controversy rests entirely on the relative values of the bond energies, which are nothing but phenomenological parameters and which cannot be extracted from experimental quantities by undisputable procedures.

In a growing number of experimental systems, a combination of lattice parameter and sample length measurements (SIMMONS and BALLUFFI's technique; ch. 18, § 2.2.2.2) yields the *total* vacancy concentration *increase* between a reference state at room temperature and the high temperature state: (CoGa: VAN OMNEN and DE MIRANDA [1981]; AlFe: HO and DODD [1978], PARIS and LESBATS [1978]; GaNi: HO *et al.* [1977], CoSc and InPd: WAEGEMAEKERS [1990]). The concentration of vacancies for the reference state is determined by a density measurement at room temperature. PA techniques have also been used, which confirm the previous determinations. But the concentration of anti-site defects is usually not directly reachable through spectroscopic

methods; only an indirect determination of their number is possible if such defects can be associated with some macroscopically measurable quantity. As an example, from the measurement of the quenched-in magnetisation of a Co–Ga alloy, the number of antisite atoms Co_{Ga}, which are the only Co atoms to be surrounded by like neighbours and, as such, are assumed to be the only ones to bear a magnetic moment, is indeed found equal to half of the number of vacancies. This beautiful result points strongly in favor of the very existence of the triple defect in this alloy (LO CASCIO [1992]).

Other experimental techniques are necessary in order to gain a sharper insight into the defect populations on each sublattice. First results have been obtained through positron annihilation in CuZn (CHABIK and ROZENFELD [1981]) or direct observation in a field ion microscope in AlFe (PARIS and LESBATS [1975]); but extracting meaningful values from the raw data requires a delicate analysis of positron trapping at vacancies for the first technique, and a careful analysis of image contrast for the second.

5.2.1.1. Experimental results. Most of the experiments measured the tracer diffusion coefficients D_{A^*} and D_{B^*} as a function of temperature and composition. The reader is referred to a recent compilation for the detailed results and references (WEVER [1992]]. Without entering into details, the following trends can be outlined:

– At constant composition, the activation energy for diffusion is higher in the ordered than in the disordered phase (when it exists). There is a break of the Arrhenius plot at the critical temperature T_c of ordering, and a large fraction of the increase in activation energy is due to correlation effects. In the ordered phase, the Arrhenius plot is often more or less curved (KUPER *et al.* [1956]). Simple models show that the migration and formation energies (E_M, E_F) of the vacancy and, therefore, the total activation energy Q, exhibit a quadratic dependence upon the long-range order parameter S (GIRIFALCO [1964]):

$$E_M = E_M^0\left(1 + \alpha_M S^2\right) \quad E_F = E_F^0\left(1 + \alpha_F S^2\right) \quad \text{and} \quad Q = Q_0\left(1 + \alpha_D S^2\right).$$

The experiments are not entirely conclusive however:

– In CuZn, the diffusion *coefficients* of Cu^* and Zn^* tracers (KUPER *et al.* [1956]) have been plotted logarithmically as function of $(1+\alpha_D S^2)/T$ (GIRIFALCO [1964]). The Arrhenius plot is a straight line only if the *theoretical* values S_{BW} of the long-range order parameter (BW stands for Bragg and Williams) are arbitrarily replaced by the *experimental* values S_{exp} which have been determined by X-ray measurements. It has been checked however that S_{exp} is not well accounted for by a Bragg–Williams approximation and that a more sophisticated treatment including short-range order (SRO) must be used instead (COWLEY [1950]). An interesting observation is that S^2_{Cowley} is equal to S_{BW} at the same temperature: therefore the quadratic dependence of Q upon S^2_{exp} can be interpreted as a linear dependence of Q on S_{BW} as well. The last difficulty lies in the fact that, as already mentioned above, most of the change in the activation energy comes from the temperature dependence of the correlation factor, which is not included in Girifalco's analysis.

– In AlFe alloys, the migration energy of the vacancies which have been retained by quenching varies roughly as S^2 (RIVIERE and GRILHE [1974]). But it is clear from the data that the results, within the error bars, can as well be accounted for by a linear law.

– In CoFe alloys, the observation of a Portevin–Le Chatelier effect is related to vacancy

migration and the effective migration energy varies quadratically over a large range of S extending from 0.1 to 0.9 (DINHUT *et al.* [1976]).

– At constant temperature, the diffusion coefficients vary with composition and exhibit a minimum at stoichiometry (or in the close neighbourhood of stoichiometry). This minimum is more or less pronounced (V-shaped curve for AgMg or AlNi) and corresponds to a maximum of the activation energy. The existence of this maximum is understandable, since the formation and migration energies of the vacancy are both increasing functions of the long-range order parameter which goes through a maximum at stoichiometry. D_{A^*} and D_{B^*} differ by no more than a factor of two or three for the alloys in which the defects are predominantly of substitutional type (AgMg, AuCd, AuZn).

– For alloys belonging to group ii), a marked asymmetry between hypo-and-hyper stoichiometric compositions is exhibited: very high vacancy contents show up which correspond to an excess of B component (Ga in NiGa and CoGa; Al in FeAl or CoAl). The difference between D_{A^*} and D_{B^*} is more pronounced than above for the alloys (between one and two orders of magnitude).The apparent vacancy formation energy is usually low (typically 0.4 eV per vacancy), and a minimum shows up at stoichiometry. An effective migration energy can also be determined by following the kinetics of thermal equilibration through the macroscopic length of the sample: the previous analysis of NiGa and CoGa in terms of two diffusion mechanisms (nearest-neighbour plus next-nearest-neighbour jumps: VAN OMNEN and DE MIRANDA [1981]) has been recently revisited: with the only assumption that the departure from the equilibrium value of the vacancy concentration follows a first order kinetics, it turns out that a simple vacancy mechanism with NN jumps only can account fairly well for the observed kinetics (WAEGEMAEKERS [1990]). A puzzling result however is that the sum of the effective formation and migration enthalpies is approximately equal to the activation energies for tracer diffusion in NiGa, but significantly lower in the case of CoGa.

5.2.1.2. Atomic mechanisms for diffusion in ordered B_2 alloys. Several atomic mechanisms have been proposed: nearest-neighbour (NN) or next-nearest-neighbour (NNN) jumps. The triple-defect (TD) has been unnecessarily assumed to migrate as a whole and the migration of the divacancy $2V_\alpha$ was supposed to occur through a correlated sequence of NN vacancy jumps with species A and NNN vacancy jumps with B. The direct determination of jump vectors has been performed only very recently on FeAl alloys. The most probable path for Fe diffusion consists of sequences of two consecutive NN jumps, implying a transitory residence on a β-site and resulting in the net displacements along <110>, <100> and <111> depicted on figure 13a (SEPIOL and VOGL [1993b]).

5.2.2. Ordered alloys with $L1_2$ structure

The $L1_2$ structure of the A_3B compound is such that the B component occupies one of the four sc lattices which make up the host fcc lattice: each B atom has twelve nearest-neighbour A atoms, whereas each A atom has four unlike neighbours and eight like ones. Due to this last property, it is commonly believed that A should diffuse

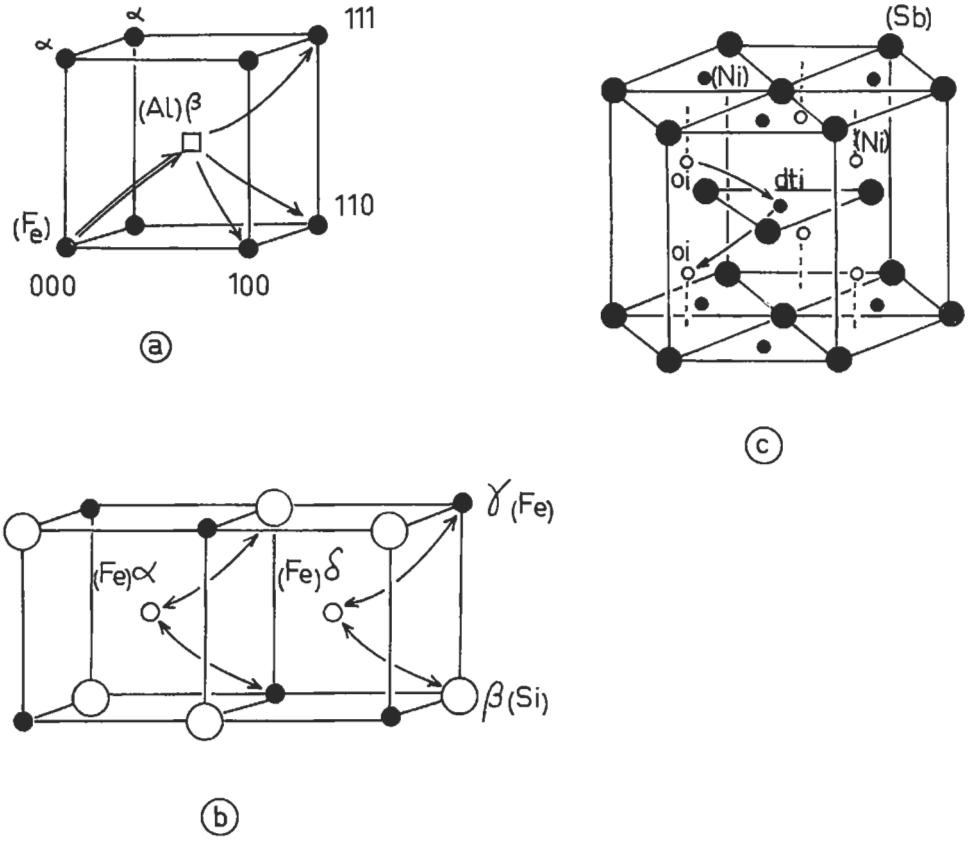

Fig. 13. Observed jump mechanisms for ordered alloys by QEMLB: (a) B2 structure with a → b → a jump sequences; (b) DO_3 structure with $\alpha \leftrightarrow \beta$, $\alpha \leftrightarrow \gamma$, $\beta \leftrightarrow \beta$ and $\gamma \leftrightarrow \delta$ jumps; (c) B8 structure with (oi) ↔ (dti) jumps.

markedly faster than B species: it has been experimentally checked only recently on Ni_3Ge where Ni (as well as Fe or Co tracer) diffusivity is indeed found to be one order of magnitude larger than Ge diffusivity (YASUDA *et al.* [1993]). Direct measurements of vacancy concentrations in Ni_3Al suggest that mainly antistructure atoms accommodate the departure from stoichiometry (AOKI and IZUMI [1975]): model calculations with the embedded atom method (EAM) agree with this picture and predict low vacancy concentrations on both sublattices, with a marked preference for the sublattice of the major component (FOILES and DAW [1987]; XIE and FARKAS [1994]); the same results are suggested by EAM calculations for Cu_3Au (JOHNSON and BROWN [1992]). It is worth noticing that Ni_3Al is the only alloy in which the vibrational entropy has been *measured* in the ordered and disordered phase (ANTHONY *et al.* [1993]): the reduction in entropy when passing to the ordered phase is equal to 0.3 k_B per atom. In Co_3Ti alloys, on the

Ti-poor side, the diffusivity of Co tracer increases with approaching stoichiometry and the isotope effect, which can be shown to equal $f\Delta K$ in $L1_2$ structures (ITO *et al.* [1990]), is small (ITOH *et al.* [1989]).

5.2.3. Ordered alloys with $L1_0$ structure

The $L1_0$ compound AB is such that the (001) planes of the host fcc lattice are alternately filled with A and B atoms. In TiAl alloys, the diffusion of Ti tracer complies the empirical rules of normal diffusion in compact structures (KROLL *et al.* [1993]) and no structural vacancies are expected from PA measurements on either side of the stoichiometric composition (SHIRAI *et al.* [1992]).

5.2.4. Ordered alloys with DO_3 structure

The DO_3 structure for this A_3B compound can be viewed as the occupancy by B atoms (Al, Si, Sn, Sb) of a fcc lattice (named β), the parameter of which is twice that of the host bcc lattice; the others sites belong to three other fcc lattices with the same lattice parameter (α, γ, δ) which are occupied by A atoms (Fe, Ni, Cu, Ag). A_α and A_δ have 4 $A_\gamma + 4B_\beta$ as first neighbours, while A_γ and B_β have $4A_\alpha + 4A_\delta$ (fig. 13b). As a consequence, B atoms have only unlike nearest neighbours. The major component has generally the larger diffusivity which increases with increasing the concentration of the minor component: Cu_3Sn (PRINZ and WEVER [1980], ARITA *et al.* [1991]); Cu_3Sb (HEUMANN *et al.* [1970]), Ni_3Sb (HEUMANN and STÜER [1966]). QEMLB in stoichiometric Fe_3Si (SEPIOL and VOGL [1993a]) and QENS in $Ni_{3-\varepsilon}Sb_{1+\varepsilon}$ (SEPIOL *et al.* [1994]) indicate that the transition metal (Fe, Ni) atoms diffuse by NN jumps between α, γ and δ sublattices; the departure from stoichiometry for $Fe_{3+\varepsilon}Si_{1-\varepsilon}$ is accommodated by antisite Fe_β which are shown to participate also strongly to diffusion. PA measurements in $Fe_{3+\varepsilon}Al_{1-\varepsilon}$ cannot separate V_{Fe} from V_{Al} and gives an apparent vacancy formation energy of 1.2 eV (SCHAEFER *et al.* [1990]): structural vacancies are not expected from the data.

5.2.5. Ordered alloys with B8 structure

The B8 structure for this AB compound is made of a compressed hcp lattice for the B component (In, Sn, Sb, As, Ge) with a *c/a* ratio of the order of 1.3; the A component (Ni) occupies either the octahedral interstices (oi) or the doubly tetrahedral ones (dti). Antistructure atoms Ni_{In} are however believed in NiIn. The large number of (oi) + (dti) sites allows the compounds to accommodate a significant positive departure of Ni atoms from stoichiometry, while still maintaining high concentrations of vacancies on the (oi) sites as large as several percent, even for Ni-rich alloys. The Ni* diffusivity is roughly 10^2 times that of Sb* (HÄHNEL *et al.* [1986]) or Sn* (SCHMIDT *et al.* [1992a, 1992b]). The determination of Ni jump vectors in NiSb compounds shows that Ni atoms jumps essentially from (oi) to (dti) sites, the vacancies on (oi) sites being crucial for allowing easy (dti) to (oi) backward jumps (fig 13c). Direct (oi–oi) or (dti–dti) jumps are excluded (VOGL *et al.* [1993]).

5.2.6. Ordered alloys with $B3_2$ structure

The $B3_2$ structure for this AB compound is made of two interpenetrating diamond lattices. Only two ordered alloys have been investigated so far, namely β-Li-Al and β-Li-In. Structural vacancies V_{Li} and antisite Li_{Al} (or Li_{In}) are believed to be the dominant defects, both defects coexisting at stoichiometry with noticeable concentrations. Li diffusion studied by NMR relaxation exhibits an activation energy of the order of one tenth of an eV and a diffusion coefficient in the range 10^{-6}–10^{-7} cm^2s^{-1} at room temperature. A significant interaction is found between the immobile Li_{Al} or Li_{In} antisite atom and the vacancy on the Li sublattice (attraction for the first, repulsion for the second). (TARCZON *et al.* [1988], TOKUHIRO *et al.* [1989]).

5.2.7. Ordered alloys with A15 structure

The A15 structure for this A_3B compound is made of a bcc lattice for B atoms (Ga, Sn, Au, Si), together with a split interstitial A-A (A = Nb, V, Cr) dissociated along <100>, <010> and <001> directions in the faces (001), (100) and (010) of the elementary cubic cell, respectively. When bringing together the cubic cells, the split interstitials make up linear chains along the corresponding directions. The only alloy in which both diffusivities have been measured is V_3Ga: the activation energy of the transition element is high (4.3 eV), and Ga, which is found to diffuse in grain-boundaries with an unexpectedly high activation energy, is probably the slowest component in bulk diffusion (BAKKER [1984]). Superconductivity occurs along the chains of the transition metal; the thermal disorder, which is believed to be mainly antistructural by analogy with Nb_3Sn (WELCH *et al.* [1984]), can be retained by quenching from higher temperatures: it degrades the superconducting transition temperature T_c in a reversible way, since a subsequent annealing restores the original value. A simple model relates the drop of T_c to the amount of antistructural defects (the vacancies, which are necessary for atomic transport, are neglected) (FÄHNLE [1982]]. An apparent formation energy of 0.65 eV for antisite defects is deduced from the variation of T_c with the quenching temperature (VAN WINKEL *et al.* [1984]). The healing kinetics of T_c, attributed to vacancy bulk migration, is dominated by the slowest bulk diffusivity of Ga atoms: it has been measured at different temperatures with an apparent migration energy of 2.2 eV; however one is left with the contradiction that Ga is the slowest component with the lower activation energy (VAN WINKEL and BAKKER [1985]). Further studies on these compounds are currently in progress (LO CASCIO *et al.* [1992]).

5.3. Chemical diffusion

When diffusion takes place in a region of the sample where the chemical gradients cannot be ignored, the diffusion coefficients of the various components are no longer constant, as in homogeneous alloys, but depend on space and time through the composition.

In what follows, we examine the case of chemical diffusion and the Kirkendall effect in binary alloys. The reader is referred to more extensive reviews for the case of multiphase and multi-component systems (ADDA and PHILIBERT [1966], KIRKALDY and

YOUNG [1987]). The interdiffusion of two elements having different partial molar volumes implies a volume change of the sample which must be taken into account for an accurate measurement of chemical diffusivities (BALLUFFI [1960]). The change of the average atomic volume in neighbouring parts of the sample induces however the birth and the development of stresses, which are usually partially released by some amount of plastic deformation. The inclusion of such effects in the analysis of Kirkendall effects started only recently and is currently under progress (STEPHENSON [1988]; SZABO *et al.* [1993]); they will be ignored in what follows.

5.3.1. Chemical diffusion in binary systems and Kirkendall effect

5.3.1.1. Description and interpretation of a typical experiment. The simplest diffusion experiment to carry out consists in clamping together two pieces of pure metals A and B, to anneal this couple long enough and to determine, at the end of the run, the concentration profile all along the sample. What is observed is a spreading of the initially step-like profile together with a shift of the initial welding interface (defined by inert markers such as oxide particles or tungsten wires) with respect to the ends of the couple which have not been affected by the diffusion (fig. 14). This shift results from the *Kirkendall effect* and finds its origin in the fact that the diffusivities D_A and D_B are not equal. Indeed, if D_A is larger than D_B, species A penetrates into B at a faster rate than B into A: as a consequence, the B-rich part of the sample must increase its volume to accommodate the net positive inward flux of matter. This increase will be achieved at the expense of the A-rich part by shifting the interface towards A. This observation was reported for the first time by SMIGELKAS and KIRKENDALL [1947] on copper–zinc alloys: the zinc is the faster diffuser and the welding interface (called *Kirkendall plane*) shifts towards the zinc-rich side of the couple. This experiment was a milestone in the history of solid-state diffusion: it definitely ruled out the assumption of a direct exchange $A \leftrightarrow B$ mechanism which was formerly proposed and which would have implied equal diffusivities for both species.

It must be noted that a Kirkendall effect has also been observed in fluids: it is expected indeed to be very general, since the first convincing interpretation of the phenomenon is not based on any detailed mechanism for matter transport (DARKEN [1948]).

The simultaneous measurements of the displacement rate v of the Kirkendall plane and of the chemical diffusivity $\tilde{D}$ in that plane yield the intrinsic diffusion coefficients D_A and D_B for the composition of the Kirkendall plane. In order to know D_A and D_B at several concentrations, one should prepare the corresponding number of differential couples, which are made of two alloys with different compositions. In fact it can be shown that a single experiment is needed, provided that a complete set of inert markers has been inserted on both sides of the welding interface (CORNET and CALAIS [1972]).

In what follows we suppose that the observed effect is unidirectional, and that only one space coordinate x is needed, in conjunction with the time variable t, to describe the evolution of the system. The transformation $x/\sqrt{t} \rightarrow \lambda$ in Fick's second Law shows that the solution C(x,t) can be expressed as a one-variable function $C(\lambda)$. We know from

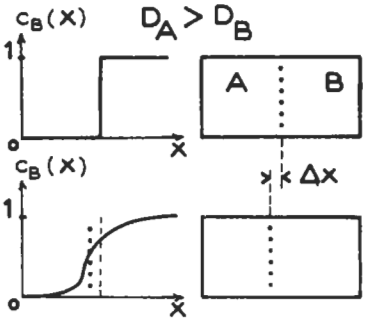

Fig. 14. Kirkendall effect experiment with a diffusion couple made of two pure metals A and B.

experiment that the Kirkendall plane has a constant concentration during the diffusion anneal, and accordingly that it is characterized by a constant value of λ. As a consequence, the Kirkendall shift Δx varies as $\sqrt{t}$; no exception to this simple law has ever been reported.

A similar behaviour has also been observed for any inert marker which is not located in the Kirkendall plane at $t=0$; after a time lag, the duration of which depends on the distance from the Kirkendall plane, the inert marker starts moving with the same time law (LEVASSEUR and PHILIBERT [1967]; MONTY [1972]).

Up to now no atomic mechanism for matter transport has been mentioned; but if we know it, something more can be said about the Kirkendall plane.

We suppose in the following that the vacancy mechanism is operating. In all the experiments performed so far, the inert markers are invariably made of materials which have a high melting temperature. The formation and migration energies of the vacancy in such materials are significantly larger than in the surrounding matrix. As a consequence, the markers are impermeable to the vacancy flux. Under this condition, it can be shown that such a marker shifts along with the lattice planes (KRIVOGLAZ [1969]), whatever the type of its interface with the matrix (coherent or incoherent). Thus the measurement of the Kirkendall shift is nothing but the measurement of the lattice plane shift.

The above formalism can be easily enlarged to account for the case in which the average atomic volume varies with the concentration of the alloy (BALLUFFI [1960]).

5.3.1.2. Vacancy wind effect — Manning's approximation. In the original formulation of the Kirkendall effect, the flux J_A of species A stems only from the chemical potential gradient $\nabla\mu_A$ of species A (DARKEN [1948]).

At infinite dilution, the solid solution becomes ideal ($\varphi = 1$) and the intrinsic diffusion coefficient D_A must tend towards the tracer diffusion coefficient D_{A^*} . Hence:

$$D_A = D_{A^*} \cdot \varphi, \qquad D_B = D_{B^*} \cdot \varphi.$$

These relationships are known as *Darken's equations*; we know however, from the thermodynamics of irreversible processes, that the off-diagonal term cannot be neglected. More general expressions can be established [see eqs. (6)]:

$$D_A = \frac{kT}{n}\left(\frac{L_{AA}}{C_A} - \frac{L_{AB}}{C_B}\right)\varphi \quad D_B = \frac{kT}{n}\left(\frac{L_{BB}}{C_B} - \frac{L_{BA}}{C_A}\right)\varphi$$

There is no simple way to relate theoretically the L_{ij}'s to experimentally accessible quantities such as tracer (or intrinsic) diffusion coefficients. This has been done only in the particular case of a simplified random-alloy model (MANNING [1968]) for which $\varphi = 1$. These expressions are arbitrary assumed to hold even for a non-random alloy where the thermodynamic factor φ is no longer unity. Hence the final expressions for the intrinsic diffusivities are still given by eqs. (17) with the random values of the *vacancy wind* corrections r_A and r_B recalled in § 5.1.2. Hence:

$$\tilde{D} = \left(C_A D_{B^*} + C_B D_{A^*}\right)\varphi\left[1 + 2\frac{C_A C_B\left(D_{A^*} - D_{B^*}\right)^2}{M_0 D^*\left(C_A D_{B^*} + C_B D_{A^*}\right)}\right]$$

The last term in the brackets is called a *vacancy wind* term since it reflects the coupling between the transport of species A and B through the vacancy flux. We note that Manning's equations predict a chemical diffusion coefficient $\tilde{D}$ always larger than that given by Darken's equations. The match of both sets of equations with experimental results will be reviewed in the following section.

Before closing this section, a last remark should be made concerning the structure of Darken's or Manning's expressions: in both sets of equations the thermodynamic factor φ enters in a multiplicative way. In some cases the variations of φ with the respect to concentration or temperature may outweigh the variations of other factors. This situation can be met accidentally as in Au-80 at % Ni (REYNOLDS *et al.* [1975]) but is also expected to happen in well-defined situations: for any alloy which tends to unmix at low temperatures, φ goes through zero at the top of the coexistence curve at some critical temperature T_c. It is easy to show that the maximum of the coexistence curve is such that the second derivative of the molar free energy, d^2f/dC_B^2, vanishes. A short derivation yields:

$$\frac{d^2 f}{dC_B^2} = \frac{kT}{C_A C_B}\left(1 + \frac{d\log\gamma_A}{d\log C_B}\right) = \frac{kT}{C_A C_B}\varphi$$

where γ_A is the activity coefficient of species A.

A convincing illustration of a vanishing $\tilde{D}$ has been reported for Nb-34 at % H (VÖLKL and ALEFELD [1978]). At critical temperature T_c, the Arrhenius plot of $\tilde{D}$ bends downwards and $\tilde{D}$ falls several orders of magnitude, whereas the Arrhenius plot of the hydrogen tracer diffusion exhibits a normal behaviour. This phenomenon is called *critical slowing down*; the top of the coexistence curve is the very point where the alloy hesitates between two conflicting forms of behaviour:

– high-temperature behaviour where all the concentration fluctuations flatten out ($\tilde{D} > 0$);
– low-temperature behaviour where the concentration fluctuations of large wave-lengths are amplified ($\tilde{D} < 0$) in order to allow the system to decompose into two phases of different compositions (spinodal decomposition).

5.3.1.3. Experimental check of vacancy wind effect. Let us recall first that accurate measurements are difficult: in many cases the Kirkendall shift is of the same order of magnitude as the diameter of the inert markers; cavities are often observed on the side of the faster diffusing species, indicating a local vacancy supersaturation; the thermodynamic factor is not known better than within 5–10 percent (ELDRIDGE and KOMAREK [1964]). The departure of the actual experimental conditions from the theoretical assumptions (vacancies everywhere at thermal equilibrium, purely unidirectional fluxes, etc.) probably induce further errors of unknown magnitude.

Only a few systems have been explicitly studied to compare Manning's and Darken's formulations, namely: AgAu (MEYER [1969], DALLWITZ [1972], MONTY [1972], AgCd (BUTRYMOWICZ and MANNING [1978], IORIO *et al.* [1973], AlNi (SHANAR and SEIGLE [1978], AuCu (HEUMANN and ROTTWINKEL [1978], CuZn (SCHMATZ *et al.* [1966], TiVa (CARLSON [1976]). Without entering into great detail, two general trends can be extracted from these studies:

– In most cases, Manning's vacancy wind correction to Darken's expressions for D_A and D_B improves the agreement of the experimentally measured values of the Kirkendall shift Δx and of the ratio D_A/D_B with the corresponding calculated quantities. "Calculated" means that D_A and D_B are evaluated by plugging the experimental values of D_{A^*}, D_{B^*} and φ into Manning's or Darken's equations.

– However, whereas the ratio D_A/D_B is fairly well accounted for, the individual values of D_A and D_B are often larger than the calculated ones (by a factor of two in the case of AuCu!) and the experimental Kirkendall shift has also a tendency to be larger than the theoretical one. (Except for AlNi, where $\tilde{D}_{meas}$ is smaller than $\tilde{D}_{theor}$ for both models.)

The reason for the discrepancy is not yet clearly understood. As pointed out by CARLSON [1978], Manning's correction to Darken's expressions holds only for a random alloy, a condition which is never fulfilled in real systems. But, as outlined above, Manning's approximation is quantitatively reasonable even in the non-random case; the problem of the experimental accuracy should be clarified first.

5.3.2. Ternary alloys

The expressions of the three matter fluxes J_1, J_2, J_3 in the lattice reference frame introduce nine independent phenomenological coefficients (or intrinsic diffusion coefficients if the chemical potentials gradients are expressed as concentration gradients). Neglecting the vacancy concentration C_v against the matter concentrations C_1, C_2 and C_3 and eliminating one of the concentrations (say C_3) yields flux expressions with only six independent new coefficients. Expressing at last, the three fluxes in the laboratory reference frame, together with the condition $J_1^0 + J_2^0 + J_3^0 = 0$ we are finally left with only four independent chemical diffusion coefficients $\tilde{D}_{11}^3$, $\tilde{D}_{12}^3$, $\tilde{D}_{21}^3$, $\tilde{D}_{22}^3$, the superscript '3' recalling that C_3 is the dependent concentration and is evaluated through $C_3 = 1 - C_1 - C_2$ and the tilde (~) recalling that interdiffusion coefficients are determined (BOCQUET [1990a]). A beautiful analytical approach has been worked out on simplified systems, where the above diffusion coefficients are assumed to be concentration independent, a condition which holds in practice whenever the terminal concentrations of the diffusion couples are close to one another (differential couples). This analysis enlightens all the

characteristic features to be encountered in the practical studies of ternaries, namely, the existence of maxima in the concentration–penetration curves, the possible occurrence of zero-flux planes, together with the general properties of diffusion paths (THOMPSON and MORRAL [1986]). The extension to concentration dependent diffusivities can be made straightforwardly with the help of numerical methods.

6. *Electro- and thermomigration*

At temperatures where diffusion is noticeable, atoms of a pure metal, or of an alloy, are caused to drift by a gradient of electric potential or temperature. We saw (§ 4.1.2) that this phenomenon, also called the *Soret effect* in the case of thermal gradients, has been used to study phenomenological coefficients. It has also been used practically to purify some refractory metals. Last, but not least, it is a way to study the electronic structure of point defects (vacancies, impurity atoms) at high temperatures and its variation during a jump. Careful reviews of all aspects of electromigration can be found in VERBRUGGEN [1988] and HO and KWOK [1989].

6.1. Thermodynamic aspects

Starting with the equations (1)–(5) in § 1.2.2., if J_e and J_q are the electron and the heat flux, respectively, we define (DOAN [1971]) the valency and the heat of transport by:

$$z_A^* = \left(\frac{J_e}{J_A}\right)_{J_B=E=0} \quad \text{and} \quad q_A^* = \left(\frac{J_q}{J_A}\right)_{J_B=\nabla T=0} \tag{71}$$

The effective valence Z_A^* and the reduced heat of transport Q_A^* introduced in § 1.2.2. are then given by:

$$Z_A^* = z_A - z_A^* \quad \text{and} \quad Q_A^* = q_A^* - \Delta H_{FV} \tag{72}$$

and the equivalent relations for the B component.

The form of Q_A^* is due to the effect of the temperature gradient on the vacancies. It is derived under the hypothesis of a local equilibrium concentration of vacancies. It has therefore no counterpart in the electric field case. Any deviation from this equilibrium (see § 8) invalidates the comparison between microscopic evaluations of q* and experimental Q*.

In self-diffusion, B stands for an isotope of A, so eqs. (1)–(5) give, in the case of electromigration:

$$J_{A^*} = -D_{A^*}\nabla n_{A^*} + Z_A^* \frac{eE}{kT} n_{A^*} \frac{D_{A^*}}{f_0}$$

where f_0 is the self-diffusion correlation factor. The thermomigration case is given by an analogous equation, Q_A^* and $-\nabla T/T$ replacing Z_A^* and E.

Such self-diffusion experiments then give access to the true values Z_A^* and Q_A^*. For solute diffusion, one calculates easily (dropping the ∇n_{B^*} term):

$$J_B = n_B D_{B^*} \frac{eE}{kT}\left[Z_B^* + Z_A^* \frac{L_{AB}}{L_{BB}}\right] = Z_B^{**} n_B D_{B^*} \frac{eE}{kT}$$

Measurements can then give access only to the *apparent* effective valence Z_B^{**} (or heat of transport Q_B^{**}). This value differs from the true one, Z_B^*, by the vacancy wind term $Z_A^* L_{AB}/L_{BB}$ (MANNING [1968]). The ratio L_{AB}/L_{BB} varies approximately from +2 to –2 and can then give a very large correction to Z_B^*, especially in polyvalent solvents. Equations (1)–(5) are written in the lattice frame, and so are defined the Z_B^{**} and Q_B^{**} values. But if the fluxes are, for some reason, measured in another reference frame, they give access to other values of coupling coefficients. For example in the laboratory frame, one obtains:

$$J_B^0 = n_B D_{B^*} \frac{eE}{kT}\left(Z_B^{**} - \frac{D_{A^*}}{D_{B^*}} Z_A^{**}\right)$$

where the bracketed term defines the apparent effective valence in the fixed frame.

6.2. Microscopic analysis

Atoms in a metal under a gradient of potential or temperature are submitted to a force which has a double origin. On one hand, one finds a static part called *direct* in the electric case, or *intrinsic* in the thermal one. The direct force is due to the unscreened action of the electric field on the true ionic charge [eq. (72), term z_A] and the intrinsic contribution corresponds to the enthalpy transfer due to an atomic jump (WIRTZ [1943], BRINKMAN [1954], LE CLAIRE [1954]). In this approximation the heat of transport q_A^* [eq. (72)] is nothing else than a part of the migration enthalpy (HUNTINGTON [1968]). On the other hand electrons and phonons in metals are highly mobile carriers, either thermal or electrical. Therefore their scattering at atoms which are neighbours of a vacancy gives rise to a second contribution: the electron or phonon *breeze*.

In the case of electromigration FIKS [1959] and HUNTINGTON and GRÖNE [1961] have given a model of this scattering part, treating electrons as semiclassical particles. BOSVIEUX and FRIEDEL [1962] have used the free-electron model in the Born approximation to give a quantum-mechanical expression of the z* term. More rigorous treatments of this term have been developed later, either in the framework of the linear response theory, or of the muffin-tin approach (KUMAR and SORBELLO [1975], TURBAN *et al.* [1976], SCHAICH [1976], RIMBEY and SORBELLO [1980], GUPTA [1982], VAN EK and LODDER [1991]). Controversies are still running on the existence either of a screening effect in z*, which could partially or exactly cancel the direct force (TURBAN *et al.* [1976], LODDER [1991]), or other contributions behind the carrier scattering (GUPTA [1986]). However all these treatments give essentially the same basic results, their main interest being to define more precisely the range of validity for the preceding models. The results are the following:

(i) For a free electron gas the scattering part of the effective valence is given by:

$$Z_i^* = -\frac{z_A}{2}\left[100\frac{\Delta\rho_i^{\text{saddle}} + \Delta\rho_i^{\text{stable}}}{\rho_0} - f_0\right] \tag{73}$$

where $\Delta\rho_i^{\text{saddle}}$ and $\Delta\rho_i^{\text{stable}}$ are the residual resistivities (expressed in $\mu\Omega$cm per at%) of atoms of species i (i = B or A) in saddle or stable position (their sum, $\Delta\rho_i^{\text{saddle}} + \Delta\rho_i^{\text{stable}}$, is denoted by $\Delta\rho_{E_M}$ in table 8, below); ρ_0 is the matrix resistivity and f_0 is a correction term due to the neighbouring vacancy (zeroed for an interstitial solute). We find that in normal metals, owing to the order of magnitude of Δr and ρ_0, the (possible) direct term is completely negligible.

(ii) In polyvalent metals, or transition metals, with a hole conductivity, one has to take into account the details of the Fermi surface and of the scattering atom, electron velocities, wave function character, anisotropic scattering. Schematically two opposite contributions like eq. (73) are found, one for electrons and one for holes, which yields a partial compensation between them. The link with the residual resistivities is lost. In that case, the effective valence is much lower, and the calculations are quite involved (FIKS [1973], HUNTINGTON and HO [1963], LIMOGE [1976b], GUPTA [1982], VAN EK and LODDER [1991]).

The situation is more troublesome in thermomigration. FIKS [1961], GERL [1967] and SORBELLO [1972] have calculated the phonon scattering contribution. The result, as given by Gerl, is a positive term, of the order of 100 kJ/mole (or lower after CROLET [1971]) and linear in temperature, contrary to SCHOTTKY's calculation [1965]. The electron term is more firmly established and according to GERL [1967]:

$$q_{el}^* \propto Z^*$$

and so gives a negative contribution in normal metals. The final Q^* is then the result of the compensation between four terms, and theoretical calculations are very questionable (DOAN *et al.* [1976]). Some years ago, it was proposed to use directly the thermodynamic definition of q* eq. (71) to calculate it (GILLAN [1977]); but this way has not been much followed till now to give quantitative results.

6.3. Experimental methods

In electro- or thermotransport, three techniques have been used. In the first, one measures the total atomic flux $J_a + J_b = -J_v$. This is done by measuring the displacement of inert markers with respect to the ends of the sample. This method can be used only for self-diffusion but is able to yield a good accuracy if vacancy elimination conditions are well controlled (GERL [1968]; LIMOGE [1976a]).

In the second method one establishes a steady state between the external force, either E or ∇T, and the induced concentration gradient. Measurement of the contration profile gives access to effective valence, or heat of transport, *in the laboratory frame* (fig. 15a). The accuracy is generally not very high and the method is restricted to solute diffusion. Moreover the assumptions concerning the equilibrium vacancy concentration must be

carefully checked.

In the third method one uses a thin deposit of tracer between two bulk samples of solvent. This deposit will spread (§ 1.2.5.), as a Gaussian in electromigration, and simultaneously displace (fig. 15b) due to the external force. This displacement with respect to the welding interface gives the coefficient Z**, or Q**. The accuracy is very high and the method is as suitable for self-diffusion as for solute diffusion (GILDER and LAZARUS [1966], DOAN [1971]), although its use in thermomigration needs some care (CROLET [1971]).

6.4. Experimental results and discussion

The reader can find an exhaustive review of experimental results on electromigration in PRATT and SELLORS' monograph [1973]. For thermomigration he is referred to ORIANI's article [1969], see also WEVER [1983].

Let us first discuss thermomigration results.

6.4.1. Thermomigration

In table 6, the heat of transport q_B^* for interstitial solutes are displayed: this case does not raise of course the delicate problem of the vacancy local equilibrium! It can be noticed first that q_B^* has generally the same sign for all solutes in a given solvent. There is also some correlation between Z_B^* and q_B^*, but opposite to the one predicted by Gerl's model. According to NAKAJIMA *et al.* [1987] there is a good correlation between the q_B^* and the migration enthalpies of the three isotopes of Hydrogen in V, Nb and Ta. In table 7, we display the heat of transport in self-diffusion in common metals. The strong scattering of the experimental values can be seen at once, either for a given

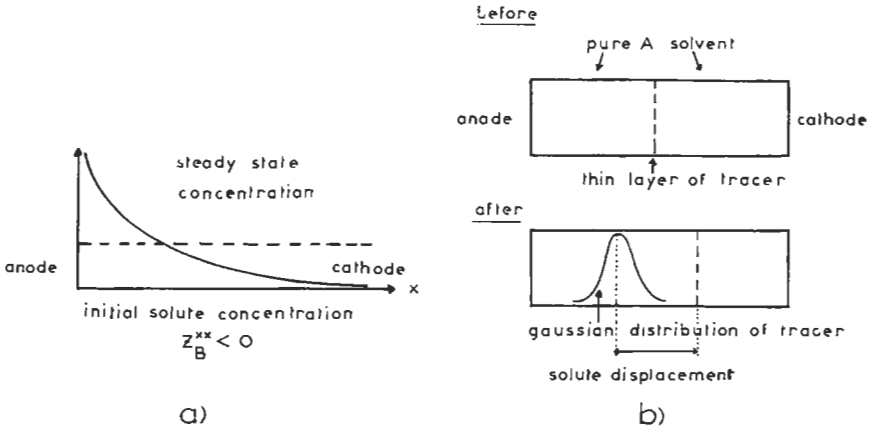

Fig. 15. Experimental methods in electro- and thermomigration. (a) Steady state method: initially the sample has a homogeneous solute concentration; during the current flows a steady-state gradient of concentration is established, the force due to the current flow being equilibrated by the force due to the gradient. (b) The tracer, initially deposited as a thin layer, is spread as a Gaussian in electromigration and also displaced as a whole with respect to the welding interface.

References: p. 651.

Table 6
Effective valences and heats of transport of interstitial impurities.

Solvent	Solute	Z_B^*	q_B^* (kJ/mole)
Ti	H	−1 [e]	+21.7 [b]
	C	>0 [a]	–
	O	<0 [a]	–
V	H	1.5 [d]	1.4 [j]
	O	1 to 1.5 [e]	17 to 29 [e]
	N	–	17 to 29 [e]
	C	–	−42 [i]
Fe_α	H	0.25 [a]	−33 to −23 [b]
	D	0.4 [a]	−33 to −23 [b]
	C	4.3 [a]	−71 to −100 [b]
	N	5.7 [a]	−75 [b]
Ni	H	0.5 [a]	−6.3 to −0.8 [b]
	D	0.7 [a]	−6.3 to −0.8 [b]
	C	–	–
Y	H	−0.3 to −0.9 [a]	–
	N	−0.9 to −2.8 [a]	–
	O	−1.2 to −2.6 [a]	–
Zr_β	C	>0 [a]	–
	N	–	>0 [b]
	O	<0 [a]	–
Nb	H	2.5 [d]	12 [j]
	C	0.6 [a]	54 [h]
	O	6.5 to −2 [a]	−67 [f]
Pd	H	>0 [a]	–
Ta	H	0.5 [d]	28.5 [j]
	O	0 to 2 [g]	−20 to −80 [g]
	N	–	−10 to −40 [g]

[a] PRATT and SELLORS [1973]; [b] ORIANI [1969]; [c] MARECHE *et al.* [1979]; [d] ERCKMANN and WIPF [1976]; [e] MATHUNI *et al.* [1976]; [f] PETERSON and SMITH. [1982]; [g] MATHUNI *et al.* [1979]; [h] CARLSON and SCHMIDT [1981]; [i] UZ and CARLSON [1986]; [j] NAKAJIMA *et al.* [1987].

element or for similar elements. This underlines the experimental difficulties and also a possible departure from equilibrium of the vacancy distribution (§§ 1.2.2, 6.1 and 8.1). Transition metals display large Q_A^* values. This has been explained by HUNTINGTON [1966] as the result of additive contributions of electrons and holes, contributions which are of opposite sign in electromigration, leading to small Z*.

6.4.2. Electromigration

In table 6 are also given the Z_B^* values for interstitial solutes. As in thermomigration, most interstitial solutes migrate in the same direction in a given solvent. The hole

Table 7
Thermomigration — effective heats of transport in self-diffusion, after ORIANI [1969].

Metal	Q_A^* (kJ/mole) [a]
Na	−6.3
Al	−6.3 to −8.4; +46
Cu	−22.6; 0; +16.7
Ag	0
Au	−27; 0
Pb	+8.8
Zn	−0.8; 0; +9.6 to 14.6
Fe_α / Fe_γ	<0; 0; +38 to 314
Co	+221 to +1380
Ni	<0
Pt	+38 to +56
Ti	<0; +773
Zr	−29 to −502

[a] For some elements there are several experimental values from different authors, separated by commas.

contribution is clearly seen in transition metals with hole conductivity. In table 8 are displayed Z_B^* of various solutes in copper, silver and aluminium. We have also shown the residual resistivities $\Delta\rho_M$ given by resistivity measurements in dilute alloys and $\Delta\rho_{EM}$ deduced from electromigration studies using relation (73) (LIMOGE [1976b]). Unlike thermomigration, we see that our predictive understanding of the electron breeze term is fairly good in these quasi free-electron metals, provided experimental resistivities are used. The solute valence effect, varying as $z_B(z_B - z_A)$, is for example well reproduced in copper and silver. The case of aluminium is less satisfactory, probably owing to (i) a badly accounted-for vacancy wind effect and (ii) fairly strong band-structure effects in this polyvalent metal. For the same reason the solvent and the various solutes have low Z^* in lead, smaller than in Al (ROCKOSCH and HERZIG [1983]). Transition metal solutes give rise to large valences due to the formation of a virtual bound level.

6.5. Electromigration in short-circuits

Migration under external forces, mainly an electric field, takes place also in diffusion short-circuits, such as surfaces and grain boundaries (GB) (ADAM [1971]). A first manifestation of this phenomenon is the *induced migration of GB* under an electric field.

This result is now well established both at high temperatures, $T/T_m > 0.7$ (LORMAND [1970]) and at lower temperatures, $T/T_m \sim 0.3$ (HAESSNER *et al.* [1974]). The interpretation however is not clear; namely, it is not obvious how to deduce the migration of an atomic configuration, such as a GB, from the sum of the forces exerted on the constituent atoms. A second manifestation, of great technological impact, is the large matter transport along short circuits in the samples which have a high ratio (surface + GB

Table 8
Valence effect in solute electromigration in normal solvents
(after LIMOGE [1976b]).

Solvent	Solute	Z_B^* (a)	$\Delta\rho_{EM}$ [b] ($\mu\Omega$cm/at%)	$\Delta\rho_M$ [c] ($\mu\Omega$cm/at%)
Copper	Cu	− 8	0.98	0.33
(1300 K)	Ag	− 6	0.62	0.35
	Cd	− 9	1.14	1.31
	In	− 16	2.36	3.95
	Sn	− 30	5.13	8.3
	Sb	− 40	6.64	10.9
Silver	Ag	− 7.5	0.43	0.38
(1150 K)	Zn	− 18.7	2.1	2.9
	Cd	− 30	3.8	2.2
	In	− 43.5	5.7	6.1
	Sn	− 69	9.9	11.6
	Sb	− 103	15	15
Aluminium	Al	− 13.7	0.73	<0.9
(900 K)	Cu	− 6.2	0.26	1.5
	Ag	− 17.3	1.01	2.1
	Cd	− 16.9	1.02	1.5
	Au	− 19.4	1.21	>2.2
	Fe	− 148	9.9	11.6

[a] Z_B^* is the true effective valence.
[b] The resistivity sum $\Delta\rho_{EM}$ is deduced from Z_B^* by eq. (73).
[c] $\Delta\rho_M$ is the resistivity sum as directly measured.

area)/(bulk). This is the case for the very thin stripes of evaporated aluminium used as electrical connections in solid-state electronic devices, run through by current density as high as 10^6 Amp/cm^2. The local divergences of atomic fluxes (triple junctions, hot points) tend to develop vacancy supersaturations and stresses, leading to the formation of voids and hillocks. Rapid breaking or short-circuits intervene, even at low temperatures (D'HEURLE [1971]). Experiments done under well-controlled conditions, for solute diffusion in silver bicrystals (MARTIN [1972]) or in thin aluminium films (D'HEURLE and GANGULEE [1972]), do not show any striking difference between volume and grain boundary valences. Nevertheless, a theory of the GB electromigration force remains to be built. The addition of some solutes (copper, chromium, magnesium) that segregate and/or precipitate at grain boundaries, can enhance the life time by orders of magnitude (D'HEURLE and GANGULEE [1972]). The precise role of these solute is not well understood (LLOYD [1990], SMALL and SMITH[1992]).

6.6. Electromigration as a purification process

Reviews of this topic have been done by PETERSON [1977] and FORT [1987]. The basis of the method is very simple: if a solute impurity displays a non-zero effective apparent valence Z_B^{**}, it will segregate to one end of a sample, of length l, during an

electromigration experiment (see fig. 15a). There remains then a depleted, purified, zone elsewhere. But as the time needed is proportional to $4l^2/(Z_B^* D_b)$, one easily sees that this method is especially efficient for interstitial solutes, or in the liquid state. In fact it has been used mainly for interstitial gaseous impurities in refractory metals, but also for transition metal solutes in Zr (ZEE [1989]) or rare earth (FORT [1987]).

7. *Diffusion along short-circuits*

Short-circuits consist of all the regions of the lattice which have lost their perfectly ordered structure: dislocations, grain boundaries and interfaces, free surfaces. They have in common the following properties:
– The diffusivity is much higher than in the bulk and is detectable in a temperature range where bulk diffusion is negligible.
– The disordered regions interact chemically with the point defects, the diffusing species and with the components of the alloy: the concentrations in the short-circuits are different from those in the bulk.
– They can be modified by the diffusion process itself, which can lead to changes in the ledge and kink densities on a surface, diffusion-induced migration of a grain boundary, etc.
– Their detailed atomic structure is often unknown; when an approximate knowledge is available (as in the case of low-index surfaces), the structure always appears very complex. Extensive simulation work in the last ten years have tried to correlate the macroscopic properties of the boundary (energy per unit area, cleavage fracture energy) to basic microscopic properties (compacity and orientation of the crystalline planes brought into contact) through the use of various semi-empirical potentials: the densest planes seem generally to give rise to low energy grain-boundaries with high cleavage fracture energy (see WOLF [1990a, 1990b, 1991] and references therein). However, no relationship with the behaviour at higher temperatures is available, where point defect generation and possible reconstruction are expected.
– The properties of point defects at surfaces and grain boundaries (formation and migration energies, interaction with the substrate or with other defects) are not yet firmly established.

We recall first the phenomenological approach which has been fruitfully used to interpret grain-boundary diffusion experiments, as well as some recent progress in this area. We next treat the atomistic approach to grain-boundary diffusion and will mention the use of molecular dynamics calculations. The case of surface diffusion will be treated separately.

7.1. Phenomenological approach

The basic idea of the continuous models consists of modeling the (one-) two-dimensional short-circuit as a (pipe) slab, along which the diffusion coefficient D' is much larger than that in the bulk D.

The diffusion equations are then written in both media with suitable matching

conditions at the interfaces. For the grain boundary depicted in fig. 16, the two following equations are written:

$$\frac{\partial c}{\partial t} = D\Delta c \quad |x| > a$$

for the balance equation in the bulk; 2a is the thickness of the boundary, and

$$\frac{\partial c'}{\partial t} = D' \frac{\partial^2 c'}{\partial y^2} + \frac{D}{a} \frac{\partial c}{\partial x}\Big|_{a+\varepsilon} \quad |x| < a, \varepsilon \to 0^+$$

for the balance equation in the grain boundary; the first term is the usual flux divergence term along the y direction; the second term accounts for the lateral exchanges between the slab and the bulk; the concentration inside the boundary is assumed independent of x.

The matching conditions at the interface $x = \pm a$ depend on the problem under consideration:

– for self-diffusion, $c' = c$,

– for solute diffusion $c' = kc$, where k is the grain-boundary segregation factor and under the assumption that c' remains much smaller than the solute concentration inside the boundary at saturation. For the case of a grain boundary in a concentrated alloy or the case of an interface in a two-phase system, the reader is referred to BERNARDINI and MARTIN [1976]. (See also ch. 13 concerning equilibrium grain-boundary segregation, especially § 4).

The solution has been calculated only under simplifying assumptions pertaining to the geometry of the short-circuit or the type of the source. Only one isolated short-circuit is considered; it is assumed to be perpendicular to the surface where the source is deposited.

– Whenever the source is of finite thickness, its concentration is uniform along the plane $y = 0$; the surface diffusion coefficient of the deposited species is taken to be infinitely

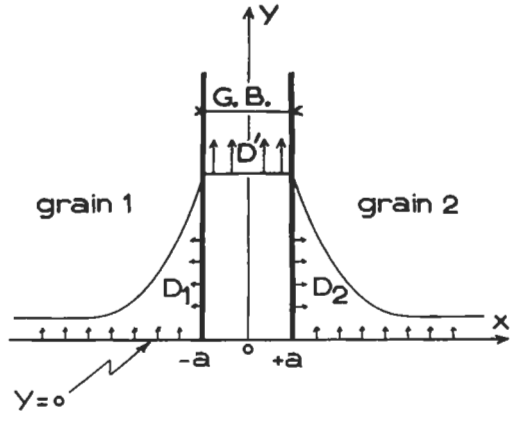

Fig. 16. Equiconcentration profile in the continuous model of grain-boundary diffusion. The slab thickness is 2a; $y = 0$ is the plane of the tracer deposit.

fast to prevent any depletion of the tracer in the area where the short-circuit emerges from the bulk.

7.1.1. Semi-infinite bicrystal

The problem of an infinite source (constant surface concentration) has been solved in an approximate way by FISHER [1951] and in exact form by WHIPPLE [1954]. The problem of the finite source has been solved by SUZUOKA [1961a, b, 1964].

The theoretical quantity which is used to analyze the experiments is not the concentration C(x,t) but its integral $\overline{C}$ along a plane at depth y from the surface:

$$\overline{C}(y,t) = \int_{\infty}^{-a} C(x,y,t)\mathrm{d}x + \int_{+a}^{-a} C'(y,t)\mathrm{d}x + \int_{a}^{\infty} C(x,y,t)\mathrm{d}x$$

It is ascertained that:

– The grain-boundary diffusion coefficient D′ cannot be directly determined, because it shows up in all the expressions in the form 2akD′. A separate measurement of k and an evaluation of 2a is needed to go further.

– The overall shape of the solution is practically independent of the initial condition (infinite source or thin layer) provided that the quantity $b=(D'/D)[ka/(Dt)^{1/2}]$ is large enough (in practice, larger than 5). In that case, log $\overline{C}$ varies as $y^{6/5}$ (LE CLAIRE [1963]). A more detailed discussion of the validity of the above solution can be found elsewhere (MARTIN and PERRAILLON [1979]).

7.1.2. Semi-infinite crystal with an isolated dislocation

A revised version of the calculation has been proposed (LE CLAIRE and RABINOVITCH [1981]). It is shown that log $\overline{C}$ varies linearly with y for distances which are large compared to the penetration depth into the bulk $[y > 4(Dt)^{1/2}]$:

$$\frac{\partial \log \overline{C}}{\partial y} = -A\Big/\left(k\ a^2\ \frac{D'}{D} - a^2\right)^{1/2}$$

where A is a slowly varying function of the time and a the radius of the pipe. The slope of the straight line is thus nearly independent of time in the case of diffusion along an isolated dislocation pipe: this is in contrast with the case where the dislocations are closely arranged into walls or boundaries and in which the slope varies as $t^{-1/4}$ (LE CLAIRE [1963]). The calculation of correlation effects in dislocation pipe diffusion requires an atomistic modelling of the dislocation core: the two attempts made so far on simple structural models show that the usual form of the correlation factor can be used even in the case where bulk and pipe diffusivities are widely different (ROBINSON and PETERSON [1972], QIN and MURCH [1993b, 1993c]). Molecular Dynamics (MD) simulations of vacancy and interstitial diffusion along a dissociated edge dislocation in copper show that the mobility of the interstitial defect is much larger than that of the vacancy; but that their respective contribution to mass transport are comparable; at last, the existence of the stacking-fault ribbon extends the dimensionality of their migration path to 2–D, slowing down their mobility accordingly (HUANG *et al.* [1991]).

References: p. 651.

7.1.3. Short-circuit networks

In actual crystals, short-circuits are present in high concentration and their orientations with respect to the diffusion direction are more or less random. They make up some kind of connected network along which diffusion is much faster than in the bulk. Three diffusion regimes can be distinguished, according to the bulk penetration depth $(Dt)^{1/2}$ being smaller than, equal to or larger than a characteristic length l of the network: l is the average diameter of the grains in the case of a grain-boundary network and the average distance between two pinning points in the case of a dislocation network (HARRISON [1961]):

(i) When bulk diffusion is totally negligible and when the penetration depth along the network is larger than l, the concentration profile is expected to be similar to a bulk diffusion profile with D′ instead of D. This is called *Harrison's C regime.*

(ii) When bulk diffusion is not negligible but $(Dt)^{1/2}$ remains much smaller than l, the short-circuits do not interact with each other: no significant amount of the diffusing species which has diffused through and out of a first short-circuit ever reaches another short-circuit. It can be shown that an approximate value of $2akD'$ (or ka^2D') can be deduced from plotting log $\bar{C}$ as a function of y (LEVINE and MACCALLUM [1960]): this is called *Harrison's B regime.*

(iii) Whenever the bulk diffusion depth is larger than l, the diffusion fields of neighbouring short-circuits overlap and none of the solutions quoted above can be used. This is *Harrison's A regime.* A simple expression of the effective diffusivity D_{eff} can be proposed, taking into account the fraction f of the lattice sites which belong to the short-circuits (HART [1957]):

$$D_{eff} = fD' + (1 - f)D$$

A detailed mathematical analysis of the penetration profiles versus dislocation density shows that the effective diffusion coefficient D_{eff} is reasonably given by Hart's formula, as soon as the bulk penetration distance $(Dt)^{1/2}$ is larger than 10 l; this limit, which is grounded on a firmer basis, is one order of magnitude lower than that determined by Harrison (LE CLAIRE and RABINOVITCH [1983]). The same analysis shows further that the influence of existing dislocation densities upon the determination of bulk diffusivities in pure metals performed so far should be negligible (LE CLAIRE and RABINOVITCH [1982]).

Harrison's classification has been later extended to the case where the grain boundaries are moving at rate V (CAHN and BALLUFFI [1979]); Harrisson's A regime is encountered whenever $(Dt)^{1/2}$ or Vt is larger than l; Harrison's B regime is split into distinct regimes according to the velocity of the grain boundary; Harrison's C regime remains untouched.

Let us mention that a continuous approach has been proposed for Harrison's A regime (AIFANTIS [1979]; HILL [1979]). A diffusion field is associated with each family of high-diffusivity paths. The total solution results from the superposition of these diffusional fields, which are connected with each other and with the bulk through quasi-chemical reactions. Interesting new features have been predicted, in particular a non-Fickean character of the diffusion in simple cases.

7.1.4. Experimental results

The reader is referred to the compilation of experiments by MARTIN and PERRAILLON [1979]. It is observed that:

– For self-diffusion, the apparent activation energy in a grain boundary is roughly 0.4–0.6 times the activation energy for bulk diffusion.

– For solute diffusion, the apparent activation energy includes the interaction energy of the solute with the boundary.

– For diffusion along the interface separating two phases of different chemical compositions, the results are still too scarce and somewhat controversial. The first experiments in Ag–Fe (BONDY *et al.* [1971]; JOB *et al.* [1974]) or Ag–Cu (PERINET [1975]) showed unusually large activation energies; recent experiments in α/γ interfaces of stainless steels (JUVE–DUC *et al.* [1980]), however, exhibit activation energies which agree fairly well with the activation energy for diffusion along grain boundaries of the γ-phase.

7.2. New advances in grain-boundary diffusion

7.2.1. Impurity effects

This topic is treated in chapter 13, § 5.2.

7.2.2. Diffusion-induced grain-boundary migration (DIGM)

The diffusion of two chemically different species along a grain boundary may under certain conditions induce a lateral displacement of this boundary (DIGM). In the same way, a thin liquid film (during sintering for instance) often migrates towards one grain at the cost of the other (LFM). Contrarily to the initial observations, the condition of a vanishingly small lattice diffusion is not a prerequisite; and the displacement is observed in a fairly large temperature range and for an increasing number of alloy systems. This lateral movement (perpendicular to the grain-boundary plane) is not necessarily uniform along the boundary and as a consequence the latter is very often distorted. The swept area which is left in its wake has a different chemical composition from that of the bulk (fig. 17) and may correspond to a better mixing of the alloy or to phase separation. The *driving force* of this evolution is still highly controversed. A first series of models attributes its origin to the free energy decrease which accompanies the change in chemical composition of the swept area (FOURNELLE [1991]). In a second series of models, the driving force stems from the release of elastic energy: the solute diffusing in the grain-boundary leaks out of the latter and changes the composition of the nearby zone, building up a coherency strain with respect to the undiffused bulk (a situation which prevails only if the bulk diffusivity of the solute is not too large, that is, if the solute does not migrate as fast as an interstitial); the elastic constants are generally anisotropic and the amount of elastic energy will necessarily be different in the two adjacent grains. The grain with the higher elastic energy will shrink and dissolve at the benefit of the other by the sweeping movement of the boundary or of the liquid film (BAIK and YOON [1990]). In both cases, the free energy loss over-compensates the energy increase due to the increase of the grain boundary surface. The only *mechanism* proposed so far invokes the climb of grain-boundary dislocations (BALLUFFI and CAHN

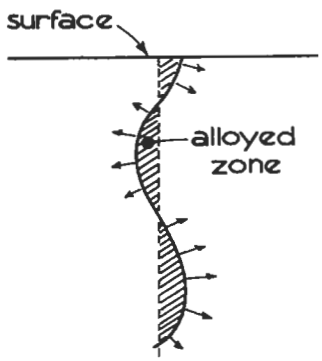

Fig. 17. Lateral displacement of a grain boundary due to a Kirkendall effect along the boundary. The hatched regions have a composition different from that of the surrounding matrix. The dashed line is the initial position of the boundary.

[1981]); it embodies no driving force in itself but offers only a means to move laterally the boundary. It holds however only for DIGM and not for LFM. Beautiful experiments on carefully oriented Cu bicrystals (symmetrical and asymmetrical tilt boundaries) immersed in Zn vapor suggest that the coherency strain model, together with the climb of dislocations in the core of the grain boundary, accounts only roughly for the experimental results concerning the low misorientations (KING and DIXIT [1990]); but the results depend heavily on the detailed structure of the boundary which varies while changing its orientation during the experiments. On the other hand, the calculated elastic effects are often found to be much too low to be consistent with the heavy curvatures of the boundaries sustained in many experiments (LIU *et al.* [1989], KUO and FOURNELLE [1991]); this observation points back to the relevance of the chemical effects.

7.3. Atomistic approach to diffusion in short-circuits

7.3.1. Atomic model for grain-boundary diffusion

The continuous approach has proved its efficiency for interpreting the experimental results which have been collected up to now. However, it raises several questions:
– What is the grain boundary thickness? How can it be defined in a precise way?
– What is a diffusion coefficient inside a grain-boundary?
– Is the assumption of local equilibrium between the bulk and the grain boundary justified?
– What does the solution looks like for very short times, i.e. , times smaller than a jump period in the bulk?

BENOIST and MARTIN [1975a, b]) were able to answer these questions with the following simple model. The grain boundary is modelled as a (100) plane of a simple cubic array, in which the atom jump frequency is Γ' and is supposed to be larger than the jump frequency Γ of the atom in the rest of the lattice. Γ_i and Γ_0 stand for the atom

jump frequencies from the bulk into the grain-boundary and conversely. The starting transport equation is written as follows:

$$\frac{\partial C(r,t)}{\partial t} = \sum_{r'} \left[C(r',t)\Gamma_{r'\to r} - C(r,t)\Gamma_{r\to r'} \right],$$

where C(r,t) stands for the tracer concentration on site r at time t; $\Gamma_{r'\to r}$ for the jump frequency from site r′ to site r; $\Sigma_{r'}$ is extended to sites r′ which are first neighbours of site r. The solution is calculated with a boundary condition corresponding to the instantaneous source of the continuous approach. The main results can be summarized as follows:

– In the limit of large bulk penetration (more precisely, a large number of jumps in the bulk, i.e. $t >> 1$), the solution is equivalent to Suzuoka's solution (see § 7.1.1).

The expression for the parameter β is:

$$\beta = \frac{D'}{D}\frac{ka}{(Dt)^{1/2}} = \frac{\Gamma'}{\Gamma}\frac{\Gamma_i}{\Gamma_0}\frac{1}{2(\Gamma t)^{1/2}}.$$

Since the bulk diffusion coefficient is Γb^2 (b is the lattice parameter), the comparison of the two solutions yields $D' = \Gamma' b^2$; the segregation factor k is equal to Γ_i/Γ_0 and the grain-boundary thickness is b.

In the case where the grain boundary is modelled as p parallel planes, it is found that its thickness is pb. It must be noticed that this thickness is not altered even if the bonds between the sites in the bulk and the sites in the boundary are stretched perpendicularly to the boundary plane. The "thickness" of the grain-boundary is not related to the actual atomic relaxations at the grain-boundary but only to the *number* of high-diffusivity paths which are available for the tracer.

– In the limit of a small penetration depth into the bulk, the identification with the continuous solution is impossible. At very short times ($\Gamma t < 0.1$) the exact solution tends towards a Gaussian with $\Gamma' b^2$ as diffusion coefficient.

This model has been modified to account for more realistic grain-boundary structures, but still disregard the correlation effects. We refer the reader to the original papers (COSTE *et al.* [1976]).

For long, the sophistication of the modelling has been several steps forward with respect to the available experimental information. Only recently, an impressive series of grain-boundary Ag diffusivity measurements, using a clever accumulation method of improved accuracy, has been undertaken in Au bicrystals of well-controlled tilt angle (MA and BALLUFFI [1993a]); the diffusion coefficients (and the activation energies as well) do not exhibit any cusp at those particular orientations which correspond to coincidence site lattice boundaries (CSLB) of short-period and low-Σ. This was taken as an indication that the core of the boundary is made up of several structural units derived from relatively short-period delimiting boundaries which are nearby in the series; in this picture, the change in tilt angle is reflected in a continuous change in the mixture of these structural units. An atomistic modelling resting on the embedded atom method (EAM) suggests that vacancy, direct interstitial and intersticialcy mechanisms are

References: p. 651.

probable candidates for matter transport along the boundary. The change in activation energy experimentally observed is accounted for by additional jumps of higher energies (MA and BALLUFFI [1993b]). At last, the magnitude of the correlation factor for the intersticialcy mechanism is found to be roughly equal to that of the vacancy one. Thus, a relatively large correlation factor is no longer the indisputable fingerprint of a vacancy mechanism at work, contrarily to previous findings (ROBINSON and PETERSON [1972]). This last result, together with that concerning the diffusion in a dissociated dislocation, suggests that the vacancy mechanism is not necessarily the dominant mass transport mechanism, as thought before from preliminary simulation work (BALLUFFI *et al.* [1981]; KWOK *et al.* [1981]; CICCOTTI *et al.* [1983]). It is worth mentioning however that the activation volume for self-diffusion in a tilt boundary of Ag bicrystals is consistent with the vacancy mechanism (MARTIN *et al.* [1967]).

7.4. Surface diffusion

Although free surfaces can actually play the role of short-circuits for bulk diffusion (inner surfaces of cavities, surfaces along a crack), they have been mostly studied for their own sakes.

We shall not repeat hereafter the continuous approach which has been already used for interface or grain-boundary diffusion; grain 2 in fig. 16 has only to be replaced by vacuum and the exchanges between the surface and the vacuum suppressed. As in the case of a grain boundary, the characteristic quantity which appears in equations is δD_s, where δ is the "thickness" of the surface layer and D_s the surface diffusion coefficient. We will focus in the following on the atomistic point of view.

7.4.1. Atomic structure and point defects

A surface is essentially made up of terraces which are portions of low-index surfaces; these terraces are separated by ledges of atomic height, along which kinks are present (*TLK* model: fig. 18). Ledges and kinks have a double origin:

– A geometrical one, to provide the misorientation of the actual surface with respect to the dense planes of the terraces (Θ and α angles in fig. 18).

– A thermally activated one for entropy purposes.

Such a description is thought to hold in a range of low temperatures where the formation free energy of ledges is large enough to keep their thermal density at a low level and where reconstruction or faceting are not observed (in practice between 0 K and $0.5T_m$).

As predicted by BURTON *et al.* [1951] a dramatic change in the surface topology occurs at some transition temperature T_R, at which the formation free energy of the ledges vanishes (or becomes very small): as a consequence the surface becomes delocalized (ch. 8, § 5.1). This transition (called *roughness transition*) is due to a large number of steps of increasing height which make the edges of the terraces indistinguishable. This has been clearly illustrated by Monte Carlo simulations on (100) surfaces of a simple cubic lattice (LEAMY and GILMER [1974]; VAN DER EERDEN *et al.* [1978]) Figure 17 of ch. 8 shows examples of LEAMY and GILMER's computations. T_R is roughly

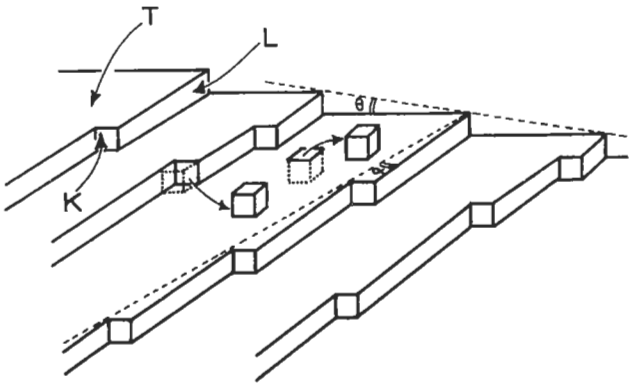

Fig. 18. Terrace–Ledge–Kink (TLK) model for low-index surfaces. The formation of adatoms (the extra atoms bulging out from the plane of a low-index surface) and advacancies (the anti-defects to adatoms) is represented.

given by

$$T_R = 0.5\varepsilon/k,$$

where ε is the strength of the first-neighbour bond. This transition has indeed been observed on several metals using He scattering spectroscopy (for a recent overview, see LAPUJOULADE [1994]). In what follows, we restrict ourselves to surfaces maintained below T_R.

Point defects are also present, namely adatoms and advacancies (see fig. 18); they can be created pairwise at a site of a terrace or separately at a ledge or a kink. The latter case is energetically favoured with respect to the others and is thought to be dominant. Multi-defects can also form by clustering adatoms or advacancies.

Theoretical calculations of point-defect properties on low-index surfaces have so far been performed first with very crude potentials (WYNBLATT and GJOSTEIN [1968]; PERRAILLON *et al.* [1972]; FLAHIVE and GRAHAM [1980a]), and later, refined with atomic potentials derived from the embedded atom method (EAM) (THOMPSON and HUTTINGTON [1982], DESJONQUERES and SPANJAARD [1982], LIU *et al.* [1991], LIU and ADAMS [1992], SANDERS and DE PRISTO [1992]). It is worth noticing that their results do not differ very much, even quantitatively: this is undoubtedly an indication that the formation energies of point defects depend only on very fundamental and simple properties of the surfaces (like the number of lateral neighbours or the packing):

– The formation and migration energies for adatoms and advacancies are found to be highly sensitive to surface orientation.

– The formation energies for both kinds of defect are comparable, except for the (100) surface of an fcc lattice, where the formation energy of the advacancy is significantly smaller than the corresponding energy for the adatom. Therefore, both defects are expected to contribute significantly to matter transport. They will be created in roughly equal amounts, either separately at kinks or pairwise at terrace sites.

– The migration energies have been mainly calculated for adatoms on fcc and bcc

surfaces, and for the vacancy on Cu (PERRAILLON *et al.* [1972]) and Ni (LIU and ADAMS [1992]) surfaces; the advacancy is in most cases the slower-diffusing defect.

For fcc lattices, the migration energies of adatoms increase roughly with increasing surface roughness: $E_m(111) < E_m(113) \sim E_m(331) < E_m(001) < E_m(210)$. For bcc lattices, the migration energies are roughly in the following order: $E_m(110) \sim E_m(211) \sim E_m(321) < E_m(310) < E_m(001) < E_m(111)$. It is worth noticing however that, due to the presence of the defect concentration term, the *surface self-diffusivities* are not necessarily in the same order: a compensation effect occurs, which pairs a low migration to a large defect formation energy (on the (111) surface of fcc lattice, namely). As a result, the surface diffusivity of Ni is expected to be noticeably larger on (113) and (133) surfaces than on any other (LIU and ADAMS [1992]).

A further difficulty stems from the fact that diffusion is expected to be highly anisotropic on non-perfect surfaces: the migration energy along dense rows or in deep channels is usually smaller than the migration energy across these rows or channels. This may obscure the ordering of low-index surfaces with respect to their migrational properties.

Diffusion is thought to take place through individual jumps only at very low temperature and to exhibit a marked anisotropy due to atomic roughness ($T < 0.15T_m$). At higher temperatures, several new mechanisms have been proposed: jumps to more distant neighbours, contribution of multidefects performing collective jumps caused by a strong forward dynamical correlation. Exchange mechanisms involving two or more atoms are believed to play a significant role since they imply a smaller distortion of the surrounding than the hopping of a single atom: after having been observed and simultaneously calculated for the change of channel of the diffusing adatom (BASSETT and WEBBER [1978], HALICIOGLU and POUND [1979]), they have been invoked for the crossing of steps on (111) Al surfaces (STUMPF and SCHEFFLER [1994]), and even recently for the mere migration on (100) Cu (HANSEN *et al.* [1993], BLACK and TIAN [1993]) or the dimer migration on (100), (110) and (111) Ir (SHIANG and TSONG [1994]). Similar mechanisms have also been proposed for bulk or surface diffusion of semi-conductors (PANDEY [1986], FEIBELMAN [1990], KAXIRAS and ERLEBACHER [1994]). All these mechanisms had been previously observed in molecular dynamics calculations on fcc Lennard–Jones crystals (TULLY *et al.* [1979]; DE LORENZI *et al.* [1982]). At last, at still higher temperatures, a delocalization of the adatom is predicted, which spends most of its time in flight rather than on equilibrium sites. The theory of atomic jump at a surface rests on the same model as that for the bulk, namely the reaction rate theory, which considers the saddle point configuration as a possible equilibrium fluctuation; but the dynamical corrections (multiple crossings of the saddle surface, dynamical forward correlation leading to multiple jumps) have been treated slightly differently, starting from the flux–flux correlation function formalism used in the theory of chemical reactions (CHANDLER [1978, 1986, 1988], VOTER and DOLL [1985]). Only recently, a more phenomenological theory has been developed, which covers all the diffusive regimes from the lower temperatures (individual jumps) to the higher ones ((2–D flight of a nearly free adatom over the surface): the particle is described by a continuous equation of motion, including an effective friction term which accounts for the interaction with the

vibrating substrate (ALA–NISSILA and YING [1992]). Quantum effects are easily taken into account and reproduce the diffusion by tunneling expected for very light atoms (H) on metal surfaces (HAUG and METIU [1991], ZHANG *et al.* [1990]).

The next step in the analysis is to deduce a macroscopic *surface diffusion coefficient* D_S as a function of the individual *atomic* jump frequencies (that is, including the defect concentrations) which have been measured or calculated. Following CHOI and SHEWMON [1962], one is intuitively led to write it as:

$$D_S = \frac{1}{4}\sum_{i=1}^{p} \Gamma_i d_i^2$$

where p is the total number of jump types, Γ_i and d_i their frequency and length. However, this expression holds only under restrictive conditions:

– All the diffusion mechanisms must contribute independently to matter transport. At each step, the diffusing atom should be allowed to make a choice between all the p available jump types which are at its disposal.

– All the sites of the surface should be equivalent. The defects should be in equilibrium everywhere and their concentrations should be uniform all over the surface, with no preferential occupancy or trapping sites. This requirement can only be met for close-packed perfect surfaces with no ledges or kinks, e.g., a (111) surface in the fcc lattice.

Real surfaces are not perfect: ledges and kinks are thought to trap the defects. Moreover the jump frequency for the motion along a ledge is different from the frequency for jumping over the ledge. If ledges and kinks could be uniformly distributed over the surface, the equivalence of the surface sites would be maintained and the same expression of D_S could still be used.

As a matter of fact, we know that the misorientation of a real surface from a perfect one is provided by one (or more) periodic array(s) of ledges and kinks. This periodicity (as opposed to uniformity) contradicts the assumption of equivalence between sites, and a new analysis has to be carried out. This has been done only for (310), (h10) and (h11) surfaces (h is any positive integer) of the fcc lattice (COUSTY *et al.* [1981]; COUSTY [1981]), thanks to the atomistic approach which has been already worked out for grain-boundary diffusion (BENOIST and MARTIN [1975a, b]): the method consists of defining a new unit supercell containing all the different types of sites and making up such a basic pattern that it can be used to generate the surface sites by translations in two directions. Effective jump frequencies across this cell, in the direction of the ledges and perpendicularly to them, can be determined by matching the solution of the discrete approach to Suzukoa's solution with the same boundary conditions. The exchanges of matter between bulk and surface are taken into account; but, in its present form, this model requires the knowledge of the atom jump frequencies out of (and into) all the different types of surfaces sites, which is far beyond the scarce experimental information presently available. Careful tracer measurements have been performed on such Cu surfaces, yielding the diffusion coefficients parallel $D_{//}$ and perpendicular $D_{\perp}$ to the steps. The main result is that $D_{\perp}$ is found not to depend on the step density; conversely, $D_{//}$ increases linearly with it, and is thought to decrease with the kink density along the steps.

References: p. 651.

7.4.2. Experimental results

7.4.2.1. Microscopic data. The Field Ion Microscope (FIM) technique (ch. 10, § 5.2.1.) has provided an irreplaceable insight into the migration mechanisms and migration energies of adatoms deposited on low-index surfaces. Table 9 sums up the experimental values (rounded to the nearest tenth of an eV for simplicity) which have been obtained on W (COWAN and TSONG [1975], GRAHAM and EHRLICH [1974, 1975], FLAHIVE and GRAHAM [1980b]), Ni (TUNG and GRAHAM [1980]), Rh (AYRAULT and EHRLICH [1974]) and Pt (BASSETT and WEBBER [1978]). Solute adatoms diffusing on surfaces have been reviewed (EHRLICH and STOLT [1980]), and the modification of self-diffusion on surfaces to which impurities have segregated is treated in ch. 13, § 5.2. An interesting and recently published overview must be quoted (EHRLICH [1994]). Calculated values have not been included since they are intrinsically short-lived and submitted to the fluctuations of the continuous theoretical improvements appearing on the scientific market.

The anisotropy of the adatom jump frequency, which is theoretically expected from the geometrical structure of the surface, is often observed. But it depends on the chemical nature of the diffusing adatom: on the (110) surface of Pt, Au adatoms diffuse only along channels parallel to <110> whereas Pt and Ir adatoms diffuse two-dimensionally with no noticeable anisotropy (BASSETT and WEBBER [1978]).

All the calculations performed so far indicate that diffusion should be very easy on (111) surfaces of fcc metals; this is experimentally observed for Rh but not for Ni, and this difference is not yet understood.

Recent FIM experiments have measured the trapping energy of a self-adatom to a foreign one buried in the first surface layer (KELLOG [1994]); a complex exchange mechanism has also been observed for Re deposited on an (100) Ir surface (CHEN and TSONG [1994]); the trapping energy, when measured, is large and comparable to (or even higher than) the migration energy on the surface.

Remarkable results have been obtained by the promising technique of He scattering spectroscopy, since not only the frequencies but also the jump vectors are measured. The diffusion anisotropy (and, thus, the crystalline character) is maintained on (110) surfaces of Pb close to the melting point: jumps along close-packed rows are more frequent and often multiple, when compared to transverse ones. The resulting diffusion coefficient is larger than that in the bulk liquid phase (FRENKEN *et al.* [1990]); this result is not in agreement with recent simulations on metallic Cu aggregates suggesting that partial surface melting might occur at high temperatures (NIELSEN *et al.* [1994]). The diffusion of isolated Na atoms on (100) Cu surfaces proceeds via a significant fraction of multiple jumps between 200 K and 300 K (ELLIS and TOENNIES [1993]); but the extraction of a migration energy requires a careful separation of the vibrational and of the diffusional component of the observed spectra (CHEN and YING [1993]).

We must remember however that such data, although of importance, cannot be used to deduce straightforwardly an absolute value of the surface diffusion coefficient D_S or any information about its possible anisotropy, for two reasons:

Table 9
Experimental values of migration energies of self-and-solute adatoms on various low-index planes obtained by FIM technique (in eV).

Diffusing adatom	Studied surface (// and ⊥ stand for parallel and perpendicular to dense rows)					
	W (110)	*W* (211)//	*W* (321)//			
W	0.9	0.75	0.85			
Ta	0.75	0.5	0.7			
Re	1.	0.85	0.9			
Ir	0.75	0.6				
Pt	0.65					
Mo		0.55				
	Rh (100)	Rh (110)//	Rh (110)⊥	Rh (111)	Rh (113)//	Rh (133)//
Rh	0.9	0.6	0.9	0.15	0.55	0.65
		Pt (110)//	Pt (110)⊥		Pt (113)//	Pt (133)//
Pt		0.85	0.8		0.7	0.85
Au		0.65			0.55	
Ir		0.8	0.8		0.75	
	Ni (100)	Ni (110)//	Ni (110)⊥	Ni (111)	Ni (113)//	Ni (133)//
Ni	0.65	0.25	0.3	0.35	0.3	0.45

– The surface diffusion coefficient D_S incorporates the concentration of defects, which cannot be reached by the FIM technique since the diffusing atom is deposited from a vapour onto the surface at a temperature where no matter exchange between the bulk and the surface is allowed: the adatom is therefore in high supersaturation and its formation energy cannot be measured with this technique. On the other hand, the formation energy of advacancies has been tentatively measured above room temperature by positron annihilation on copper and silver. The values which are reported are close to 1 eV within experimental uncertainty, that is, only 20% lower than the corresponding energy in the bulk (LYNN and WELCH [1980]). But an appropriate model for the state of a positron at a metallic surface is not presently available and the validity of this technique for probing the advacancies is still questioned (KÖGEL [1992], STEINDL *et al.* [1992]).
– The surface diffusion coefficient D_S is usually measured at a range of much higher temperatures where other diffusion mechanisms may come into play.

7.4.2.2. Macroscopic data. Mass transfer experiments consist in measuring the rate at which a solid changes its shape (at constant volume) in order to minimize its surface free energy. Several techniques can be used: thermal grooving of a grain boundary (MULLINS and SHEWMON [1959]), blunting of a sharp tip observed by conventional transmission electron microscopy (NICHOLS and MULLINS [1965a]) or scanning tunneling microscopy (DRECHSLER *et al.* [1989]), decaying of an isolated (or of a periodic array of) scratch (es) (KING and MULLINS [1962]; NICHOLS and MULLINS [1965b], JAUNET *et al.* [1982]). The possible contributions of bulk diffusion or the evaporation–condensation mechanism must be subtracted to deduce the part due to surface diffusion only. This technique does not yield the surface diffusion coefficient D_S but the product $\gamma_S D_s$ (where γ_S is the surface tension) or, more precisely, some average of this product over the

References: p. 651.

orientation of all the facets making up the macroscopic profile.

A second technique involves the use of a radioactive tracer and consists in measuring the concentration profile of the diffusing species on surfaces of well-defined orientation: it has been used for pure copper (COUSTY *et al.* [1981], GHALEB [1983]). This technique does not yields D_S but the product δD_S where δ is some "thickness" of the surface layer in the continuous approach. For both techniques two crucial points must be checked throughout the diffusion run:

– The absence of any impurity or any two-dimensional superstructure of impurities, both of which might significantly alter the diffusion rate (BONZEL [1976]).

– The absence of any reconstruction of the surface: this point can only be checked for the radiotracer technique, because mass transfer experiments are performed on surfaces, the profile of which evolves in time.

Three points must be noted: (i) The apparent activation energy for self-diffusion is systematically and significantly larger than the migration energy of adatoms which is measured with the FIM technique. The difference is attributed to the energy which is required to form the defects contributing to matter transport. This means physically that the density of defect sources and sinks (steps, kinks) is probably large enough to insure the equilibrium defect concentration throughout the experiment at such temperatures. (ii) The self-diffusion Arrhenius plot is often curved (RHEAD [1975]). If this curvature is not an artefact of the experimental techniques, several explanations can be proposed: contribution of several kinds of defects (advacancies and adatoms, clusters of adatoms, etc.), contribution of multiple jumps, formation of thermal kinks (NEUMAN and HIRSCHWALD [1972]), local melting of the surface (RHEAD [1975]). (iii) Whether the crystallographic structure of the surface induces a marked anisotropy of the surface diffusion coefficient or not is still a matter of controversy: at 0.6 T_m on (110) surfaces of pure nickel, the scratch-decaying technique shows a rather large anisotropy (between one and two orders of magnitude: BONZEL and LATTA [1978], JAUNET *et al.* [1982]), whereas the tracer technique for copper self-diffusion (COUSTY [1981]) or for silver diffusion on copper (ROULET [1973]) exhibits only small differences (at most a factor of 4).

Another route has been followed with diffusion studies at higher coverages ranging from several tenths of a monoatomic layer to several layers (thick deposites) (BUTZ and WAGNER [1979]): these experiments yield a chemical diffusion coefficient, implying the intervention of significant adsorbate–adsorbate interactions. Extensive numerical simulations have been performed to explain how to determine the pronounced maximum of the diffusion at compositions corresponding to ordered structures (BOWKER and KING [1978a, b], UEBING and GOMER [1991], TRINGIDES and GOMER [1992]).

Several points remain somewhat obscure today:

– in the presence of various contaminants (Bi, S, Cl) the surface self-diffusivity can be increased by orders of magnitude and reach much higher values than those typical of bulk liquid state, as high as 10^{-4} m^2/s (RHEAD [1975]). As a rule, chemical interactions of non-metallic character play an important role and give rise to very high surface diffusivities on ionic crystals like alkali-halides for instance (YANG and FLYNN [1989]).

- surface electromigration of metallic adatoms on semi-conductor surfaces differs markedly from the bulk case; the electrostatic field is 10^3 times *larger*, whereas the

current density is 10^3 times *smaller*. As a result, the electrostatic driving force on the solute adatom is much larger than the wind force from the charge carriers, and the metallic ions move in most cases towards the cathode. However, the reversal of the migration direction for Al on (111) Si as a function of the deposited layer thickness is not understood (YASUNAGA [1991]).

– the connection between diffusion and the possible existence of precursor effects in wetting is not understood (ADDA *et al.* [1994]).

8. *Diffusion under non-equilibrium defect concentrations*

Up to now we have discussed diffusion problems involving point defects in thermal equilibrium. In particular, we focused mainly on vacancies; but in some conditions, often of a great technological importance, a high supersaturation of point defects, interstitials and vacancies, can be sustained in steady state. With respect to diffusion, an acceleration of kinetics is the main phenomenon to be observed. Interstitials however have in most cases a high formation enthalpy, and therefore a zero equilibrium concentration. In the case where interstitials are created, apart from an acceleration, new phenomena which are unknown at equilibrium can appear, as we shall see in § 8.3.2.

If point defects are created in a material exceeding their thermal equilibrium concentration, a supersaturation will build up, which results from a competition between creation and elimination, and enhances the diffusion. The new diffusion coefficient can often be written as :

$$D_{acc} = k_v D_v C_v + k_i D_i C_i \tag{74}$$

where k_i, and k_v are coefficients depending on the various jump frequencies of the defects, D_i and D_v are their diffusion coefficients and C_i and C_v their *total* concentrations. The problem of enhanced diffusion is then to calculate the actual C_i and C_v according to the experimental conditions of creation and elimination.

Many situations are now known in materials science where this situation prevails. Without claiming to be exhaustive, we mention the following cases: (i) If vacancy sinks are not very efficient in a sample submitted either to a quench or to a temperature gradient, we can observe a vacancy supersaturation. (ii) Such a supersaturation can also be created in an alloy by vacancy injection from the surface by a Kirkendall mechanism due to preferential depletion of one of the components, by dissolution or oxidation (BURTON [1982], STOLWIJK *et al.* [1994]). (iii) Point defects are also created during plastic deformation. (iv) Under irradiation by energetic particles, a high level of supersaturation can be sustained.

In all these cases the point defect supersaturation is able to accelerate the diffusion and to induce various phase transformations. Let us look first at those cases which involve vacancies only.

8.1. Quenched-in vacancies

Vacancy sinks include free surfaces, dislocations and grain boundaries. Vacancies can

References: p. 651.

also be lost for diffusion by agglomeration as dislocation loops, stacking fault tetrahedra or voids. In some cases (very low dislocation density or surface oxidation for example), the sinks become ineffective, and a supersaturation builds up in the volume which in turn enhances diffusion beyond the thermal equilibrium value. A very important example of the role of quenched-in vacancies is given by the kinetics of age-hardening in alloys displaying precipitation-hardening. We know that GP zone formation is far too rapid to be accounted for by thermal diffusion only: the role of quenched-in vacancies was stressed early (GUINIER [1959]) and later the importance of vacancy-solute complexes (GIRIFALCO and HERMAN [1965]) was recognized in the so-called "vacancy pump" model.

Another very interesting application is the enhancement after a quench of the ordering kinetics in alloys. This phenomenon is at the root of a method for studying defect properties in metals by relaxation measurements (§ 2.2: see also ROBROCK [1981]).

The quenched-in vacancies could also be at work in samples undergoing diffusion under strong thermal gradients (MATLOCK and STARK [1971]). These authors measured the heat of transport of aluminium and found Q^*_{Al} values of 46 kJ/mole in a single crystal and –8.4 kJ/mole in a polycrystalline sample, pointing to the importance of the vacancy formation enthalpy in eq. (72). The same conclusion was drawn from measurements of solute diffusion in a temperature gradient in aluminium or silver (MCKEE and STARK [1975]), SHIH and STARK [1978]). In all these cases, grain boundaries are apparently the only efficient vacancy sinks. The polycrystalline sample is then at equilibrium but not the single crystal. In this last case the hot end imposes its vacancy concentration to the cold one. Therefore the diffusion coefficient is fixed by (i) the hot-end vacancy concentration, (ii) the local vacancy mobility, and is then strongly enhanced in the cold part of the sample. The same effect has been recently observed by HEHENKAMP [1993] in silver using radiotracer measurements and the positron annihilation method. The level of supersaturation observed is of the order of 50 to 100. One can wonder wether at these levels, nucleation of cavities or vacancy clusters should not occur, since they have already been observed in Kirkendall's or electromigration experiments at much lower supersaturations in the same material (MONTY [1972]). Moreover carefully controlled experiments failed to detect such an effect in aluminium, either by measuring the local silver diffusion coefficient at different places along the gradient (BREBEC [1977]), or by measuring the actual vacancy sink activity also all along the gradient by a method using the deplacement of inert markers (LIMOGE [1976a]). Indeed the establishment of a strong enough temperature gradient in a metallic sample is a difficult task, and artefacts are not always avoided, giving rise to an actual gradient much less than expected.

8.2. Cold-work-induced defects

It is now firmly established that during plastic deformation, point defects, probably mainly vacancies, are created by dislocation interactions (WINTENBERGER [1959], FRIEDEL [1964], GONZALES *et al.* [1975a, b]). Two main origins have been proposed. The first one correspond to the annihilation of sufficiently elongated dipoles of edge dislocations which "evaporate" as defects, and the second to non conservative motion of

jogs. The first process is believed to occur mainly in the walls of the dislocation cell structure observed during fatigue experiments or in persistent slip bands (P.S.B.). If we neglect the thermal elimination of defects, a typical concentration could amount to 10^{-3} at. (ESSMAN and MUGHRABI [1979]). However, the very high dislocation density in that case probably prevents such a high supersaturation level (RUOFF and BALLUFFI [1963]). In the second case the production rate could amount to 10^{-6} at. in typical low cycle fatigue experiments, and elimination occurs by diffusion to the walls of the cell or by sweeping by the moving dislocations (TSOU and QUESNEL [1983]). The supersaturation can be quite large at not too high temperatures. Whatever the production mechanism, these excess vacancies have been shown to produce cavity nucleation and growth during fatigue tests in various alloys (ARNAUD *et al.* [1985]). It is then clear that diffusion will be also accelerated, but that any attempt to determine this enhancement by classical *macroscopic* methods (§ 2.1) is hopeless. Artefacts due to surface roughness induced by the slip bands (RUOFF [1967]) or pipe diffusion in dislocation will always screen the actual effect. However, this enhancement can be rendered visible by a local method sensitive to a small number of jumps, such as the Zener effect (NEUMANN *et al.* [1961]) or GP zone formation kinetics (KELLY and CHIOU [1958]). Indeed an acceleration of diffusion has been observed by N.M.R. (see § 2.2.2.1.) in a deformed NaCl crystal (DETEMPLE *et al.* [1991]). The same phenomenon is believed to be at the origin of the dynamic boron segregation at grain boundaries in microalloyed steels: the excess vacancies created during rolling (deformation rates of 1 – 10/sec.) drag the boron atoms to boundaries by a flux coupling mechanism (MILITZER *et al.* [1994]).

8.3. Irradiation-induced defects

The knowledge of the various effects of the irradiation of solids by energetic particles, electrons, neutrons, ions, or photons, is of paramount importance in several domains of materials science: nuclear industry, microelectronics or surface treatment, among others. The topic has been reviewed several times, but not exclusively, by ADDA *et al.* [1975], SIZMAN [1978], ROTHMAN [1981], BREBEC [1990], WOLLENBERGER *et al.* [1992], MARTIN and BARBU [1993]. The domain encompasses three main topics: radiation-enhanced diffusion, segregation and precipitation and phase changes, all of them being generally more or less present simultaneously in any radiation environment.

8.3.1. Irradiation-enhanced diffusion

Fig. 19 shows the result of a diffusion measurement by a tracer method in nickel under self-ion irradiation at an energy of 300 KeV. Three parts can be seen in this graph: thermal diffusion at high temperature; between 1000 K and 700 K, a radiation-enhanced domain corresponding to a thermally activated regime with a lower activation energy; and below 700 K, an athermal part. The efficiency of this last mode is quite high, the resulting squared displacement amounting to 125 A^2/dpa. (MÜLLER *et al.* [1988]). Clearly the origins of the enhancement must be multiple in order to explain this behaviour.

References: p. 651.

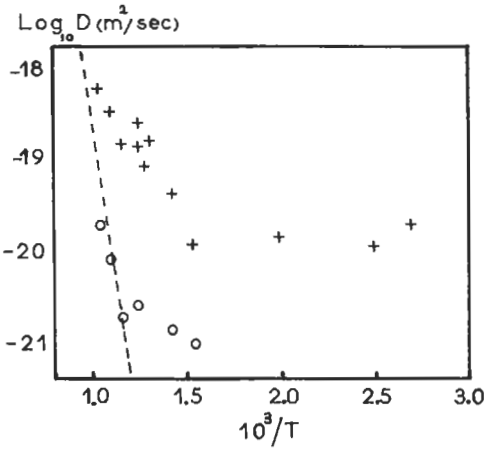

Fig. 19. Self-diffusion coefficient in nickel under self-ion irradiation at 1.2 10^{-2} dpa/s, full symbols, or 1.2 10^{-4} dpa/s, empty dots, dashed line thermal self-diffusion.

8.3.1.1. Defect creation. Under irradiation by energetic particles, the atoms of an alloy suffer elastic and inelastic collisions with the projectiles. Except for very high densities of energy transfer, of the order of several KeV/Angström (BARBU *et al.* [1991]), the electronic excitations are not expected to produce defects. On the contrary the part of the energy which is transfered elastically to a target atom (the primary knocked atom or P.K.A.) will displace it, if the transfer is higher than a threshold E_d of the order of 20 to 50 eV in metals. A Frenkel pair is then created, a lattice vacancy on the initial site and an interstitial on the arrest position. If the energy received by the P.K.A. is high enough, it will in turn act as a projectile and initiate a *cascade of displacements*, also called a *displacement spike*, in the target. The interstitials being created generally at the end of a replacement collision sequence (R.C.S.) will be found at the periphery of the cascade and the vacancies form a dense core at the center. The higher the collisionnal cross section between the moving atoms and the atoms at rest, the more frequent the collisions and the denser the cascade. However a new picture has appeared recently according to which the cascade core is in fact in a molten state, the so-called *thermal spike*, since the mean kinetic energy of the atoms in the cascade core during 10^{-11} sec can amount approximately to 1 eV. This picture is mainly based on Molecular Dynamics simulation results (DIAZ DE LA RUBIA *et al.* [1987]). In this picture the vacancy creation is the result of the ultra fast quench of the molten core, the interstitials are created either by the few R.C.S. escaping from the melt or by a new mechanism of interstitial loops punching from the melt (DIAZ DE LA RUBIA and GUINAN [1992]).

The number of defects created is generally given in the literature with respect to the formula $N_d = KT_D/2E_D$ (TORRENS and ROBINSON [1972]) where T_D is the elastic energy given to the lattice and K an efficiency factor near 0.8. However as soon as the energy of the P.K.A. is higher than a few keV, the vacancy rich core contains too many defects, and collapses more or less into clusters, even at liquid He temperature. The number of

detectable defects is therefore reduced to roughly one third of the above mentioned N_d (AVERBACK *et al.* [1978]). At higher temperatures the defects start to diffuse thermally, and their very inhomogeneous distribution triggers an efficient elimination, either by vacancy-interstitial recombination or by clustering. Finally the fraction of defects able to produce radiation enhanced diffusion is further reduced down to a few percents of N_d in the case of dense cascades. The efficiency of the radiations for producing the so-called freely migrating defects is therefore decreasing from 1 MeV electrons, which are producing only isolated Frenkel pairs with an efficiency of 1, to the heavy ions and even more neutrons which give rise to an efficiency going down to a few 10^{-3} (WIEDERSICH [1990]). (See also ch. 18, § 4.)

8.3.1.2. Collisional diffusion. This effect is also frequently called *Ion-Beam Mixing*, and has been recently reviewed (AVERBACK and SEIDMAN [1987], REHN and OKAMOTO [1989], CHENG [1990]). Indeed, inside a collision cascade the atoms, as a result of the collisions or of the molten state of the matter, will experience an enhanced diffusion not solely due to the presence of point defects. Four origins have been proposed for this new mobility: i) the direct displacement of the knocked atoms, ii) the displacement under subthreshold collisions of the defects already present, iii) the activated jumps of the same defects in the intense thermal field of the spike, iv) the diffusion in the molten core. The first term has been repeatedly shown to give rise to too low a mobility, some A^2/sec at most under heaviest ion irradiations, for explaining the kinetics of ion-beam mixing (LIMOGE *et al.* [1977], SERAN and LIMOGE [1981], BARCZ *et al.* [1984]), despite careful theoretical modeling (LITTMARK and HOFFER [1980]). Nevertheless this negative result has been recently questioned, at least in low Z matrices (KOPONEN [1991]). In the second approach (SERAN and LIMOGE [1981]), the vacancy defects are expected to jump under subtreshold collisions along dense rows ([110] in fcc metals), i. e. involving an energy lower than E_d. Taking into account the actual vacancy concentration in the cascade the above mentioned order of magnitude (fig. 19) is easily explained without any further assumption. The third approach also furnishes the proper order of magnitude provided the migration enthalpy is reduced to roughly one third of the normal value (KIM *et al.* [1988]). The differences between these last two approaches is probably rather small, and they can be viewed as different points of view on the same phenomenon, since each of them rely on a highly idealized description of the state of the matter inside the core, discrete energy transfers in the first case, and equilibrium thermal effects in the second. In the fourth model, atoms are diffusing in the liquid core of the cascade (JOHNSON *et al.* [1985]). Assuming even in the liquid state a thermally activated diffusion scaling with the cohesive energy of the solid, and taking into account the thermodynamical factor in the liquid (see eq. (7)), a qualitative agreement with experimental results can be obtained.

Nevertheless the present authors have the feeling that several well established results (correlation between mixing efficiency and characteristics of diffusion by a *vacancy mechanism in the solid*, no effects of the solute atomic mass on the mixing (KIM *et al.* [1988])), are not well accounted for in this approach. On the one hand the actual mixing is probably the result of the superposition of at least the first three effects; on the other hand we are still lacking of a proper model for the physical structure of the cascade core, for which neither the liquid droplet nor the heavily damaged solid are perfectly adapted concepts.

References: p. 651.

8.3.1.3. Diffusion by thermally activated jumps. This mode of diffusion enhancement, usually called radiation-enhanced diffusion (R.E.D.), can be observed in a medium temperature range, fig. 19, where it is controlled by the thermally activated jumps of the freely migrating defects created by the irradiation. According to the § 8.3.1.2. the denser the cascade, the higher the plateau due to ion-beam mixing, and therefore the narrower the domain of R.E.D. The contribution of the free defects to diffusion is controlled by the equation (74). Two methods have been used for calculating the defect concentrations C_v and C_i. The first is the Monte Carlo simulation method (DORAN [1970], LANORE [1974]). We have no space to discuss it here and refer the reader to the original articles. The other one, a quasi-chemical approach, was initially proposed by LOMER [1954] and progressively refined since. The ingredients of Lomer's model are the following:
– production rate G of spatially uncorrelated point defects (the so called freely migrating ones)
– motion by random walk with coefficients D_i and D_v
– annealing by mutual recombination at a rate K_r, at fixed sinks (supposed to be *uniformly distributed*) at rates K_i and K_v, or at surfaces, generally treated as a boundary condition
– only pure metals where considered in the initial formulation, but now the extension at least to dilute alloys has been done, in the limit of a solution remaining homogeneous.

Since interstitials are present the set of equation (1)–(3) (§ 1.2.2.) has to be completed. The necessary coefficients have been calculated by BARBU [1980] and ALLNATT *et al.* [1983] for fcc dilute solutions (see also § 4.2 and § 5.1.2 for concentrated alloys). It can be shown using a proper thermodynamic model of the solution that the four fluxes can be written:

$$\begin{aligned}
\Omega J_B &= -D_{BI}\nabla C_I - D_{BV}\nabla C_V - \left(M^V_{BB} + M^I_{BB}\right)\nabla C_B \\
\Omega J_V &= -D_{VB}\nabla C_B - D_{VV}\nabla C_V \\
\Omega J_I &= -D_{IB}\nabla C_B - D_{II}\nabla C_I \\
J_A &= -J_B + J_I - J_L
\end{aligned} \tag{75a}$$

These equations define i) in the absence of solute concentration gradients the diffusion coefficient of the defects D_{VV} and D_{II}, written above D_v and D_i for simplicity, ii) in the absence of defect concentration gradients the diffusion coefficient of B, $M^V_{BB} + M^I_{BB}$, which can be put easily in the form (74). If the solute concentration remains homogeneous, the defect concentrations are then solutions of the following equations:

$$\begin{aligned}
\frac{\partial C_V}{\partial t} &= G - \mathrm{Div}\left(\Omega J_V\right) - K_r C_i C_v - K_v\left(C_v - C_v^0\right), \\
\frac{\partial C_i}{\partial t} &= G - \mathrm{Div}\left(\Omega J_I\right) - K_r C_i C_v - K_i C_i
\end{aligned} \tag{75b}$$

where C_V^0 is the concentration of thermal vacancies.

These equations have generally to be solved numerically. Nevertheless, far from the surface, after a very complex transient regime, the duration of which is of the order of

1/K, with K the lower of K_v and K_i, one obtains under the hypothesis of the interstitials being the more mobile defects, a steady-state regime characterized by:
– $D_iC_i = D_v\,(C_v - C_v^0)$ when elimination at sinks prevails
– $C_i = C_v - C_v^0$ when mutual recombinations prevail
– $C_v \sim (G/D_v)^{1/2}$ at low temperatures, i.e., for dominant mutual recombination
– $C_v \sim (G/D_v)\,L$ at high temperatures, i.e., for dominant sink elimination, where L is the mean distance between sinks. At very high temperatures, $T/T_m \geq 0.5$, the defect mobility is sufficient to prevent any noticeable defect supersaturation, and the enhancement is negligible. In table 10 are given the main characteristics of D_{acc} [see eq. (74)] in Lomer's model. To analyze the experiments it must be kept in mind that in most cases they are done near the surface: a correction is then necessary (ERMERT *et al.* [1968]).

In dilute solid solutions we can observe rather severe effects on defect mobility whenever i) a strong defect-solute attractive interaction exists, ii) the pair is immobile (in the case where the pair cannot migrate without dissociating). These two conditions are not linked to one another for the vacancy, but are for the dumbbell interstitial in fcc structures, except may be for very small solutes. In this case the so-called caging effect induces a strong decrease of the mobility of the interstitial defect in the alloy, as long as the concentration is not higher than the percolation limit in the given structure. Beyond this limit the defect can find diffusion paths which do not break the pair (BOCQUET [1986]).

The enhancement being noticeable only at low temperatures, that is at low mobility, D_{acc} will be lower than 10^{-18} m^2/s, and the experiments are very difficult. This fact, as well as the badly known actual level of freely migrating defects, can explain the fairly general discrepancy which has been observed for long between the tracer experiments and the predictions of Lomer's model. The measured values were generally too high, either in self or solute diffusion (ADDA *et al.* [1975], BREBEC [1990]). However, Lomer's model also rests on numerous approximations, for example in the calculations of the various rate terms, K, K_i or K_v, particularly in concentrated alloys [eq. (74)].

Relaxation methods, however, are well suited to this case, owing to their high sensitivity, and their ability to follow all along the kinetics during the complex transient

Table 10
Characteristics of D_{acc} in Lomer's model [eq. (74)]; after ADDA *et al.* [1975]

Régime of elimination	Activation energy of D_{acc}			Dose-rate dependence (G = dose rate)
	Term due to interstitials	Term due to vacancies	Total	
Recombination only in the transient regime	$\frac{1}{2}H_m^i$	$H_m^v - \frac{1}{2}H_m^i$	complex	$G^{1/2}$
Elimination on sinks	0	0	0	G
Elimination both by recombination and on sinks	$\frac{1}{2}H_m^v$	$\frac{1}{2}H_m^v$	$\frac{1}{2}H_m^v$	$G^{1/2}$

H_m^i and H_m^v are the migration enthalpy of, respectively, the interstitial and the vacancy.

References: p. 651.

regime preceding the stationary state. The results of HALBWACHS [1977], HALBWACHS and HILLAIRET [1978] and of HALBWACHS *et al.* [1978a, b] on Ag–Zn alloys by Zener relaxation display a good agreement with the predictions of Lomer's model, if one assumes that, in these alloys, the vacancies are less mobile than interstitials. The use of electron irradiations avoided the ambiguity of the actual level of freely migrating defect production. This result, confirmed by electron-microscopy studies (REGNIER and HALBWACHS [1980]), has given the first evidence of the large pairing effect on the interstitial mobility in solid solutions.

The tracer experiment which has probably for the first time evidenced the R.E.D. in self-diffusion is the one depicted in fig. 19. The authors have been able to adjust in a coherent manner on the experimental results the various parameters entering the model; in particular they invoke a temperature dependent sink density and an efficiency for the production of freely migrating defects amounting to 1.5% only of the Kinchin and Pease value, in agreement with the recent simulation results on defect production in cascades.

8.3.2. Irradiation-induced segregation and precipitation

Irradiation-induced segregation, leading eventually to precipitation in *undersaturated* alloys, is now a well established phenomenon in a large number of systems (for a quite recent review of experimental results see RUSSELL [1985], also ENGLISH *et al.* [1990]). We display in table 11 the characteristics of such precipitation in a few binary alloys. This effect has to be clearly distinguished from a simple radiation-enhanced precipitation in an *oversaturated* alloy.

At a given defect creation rate G, the segregation or the precipitation of a non-equilibrium phase appear in a well defined temperature interval (see figs. 20 and 21). A new variable, or more precisely a new control parameter, has to be added to the classical phase diagram: the defect creation rate (or irradiation flux), in addition to temperature, pressure and composition (ADDA *et al.* [1975]).

Two ways have been explored to explain these results. The first one is a constraint-equilibrium one: the stored energy due to point defects might displace the free enthalpy curves, to such an extent that it renders stable under irradiation a phase which is normally unstable. Careful calculations of this effect have shown that the order of magnitude of the possible displacement is too low to explain the great majority of the results (BOCQUET and MARTIN [1979]). In the second approach, initially proposed by ANTHONY [1972] for vacancies, the elimination of irradiation-created point defects by diffusion to sinks, like surfaces or dislocations, results in defect fluxes which induce, through the flux coupling terms, local solute supersaturations. These supersaturations can grow beyond the solubility limit, resulting in a precipitation. Indeed both terms D_{BV} and D_{BI} (eq. 75a)), if positive, can give rise to such a segregation.

Many authors have developed this idea for dilute alloys and proposed more or less approximate expressions for the coupling terms due to interstitials (OKAMOTO and WIEDERSICH [1974], JOHNSON and LAM [1976], BARBU [1978, 1980]).

As shown in table 11, two forms of segregation or precipitation have been observed, and can be explained in the present framework. The first one is *heterogeneous*, and occurs on sinks, either pre-existing to, or created by, the irradiation. The most elaborate

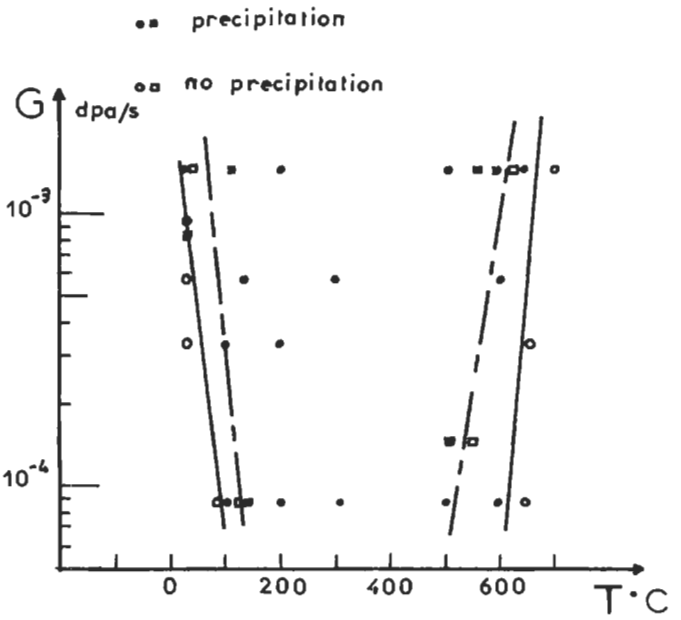

Fig. 20. "Phase diagram", in a flux-temperature section, for the system Ni–Si irradiated by 1 MeV electrons (after BARBU and MARTIN [1977]). Solid line: precipitation borderline for a concentration of 6 at% Si, dashed line idem for 2 at% Si.

numerical solutions of the above set of equations give a fairly good account of experimental results. In particular, the role of sinks, dislocation loops or surfaces is well understood. Nevertheless in this approach the position and the slope of the low-temperature borderline remains to be explained (BARBU [1978]). In all theses models the solute supersaturation results from a balance between the interstitials, which always carry the solute down the gradient and the vacancies, which can act in both directions (BARBU [1980]). At higher temperatures the phenomenon disappears owing to the lowering of the defect supersaturation.

A second kind of precipitation, *the homogeneous precipitation*, was discovered later (table 11), where precipitates are not associated with any pre-existing defect sink. By studying the stability of the set of equations (75) with respect to concentration fluctuations, CAUVIN and MARTIN ([1981], [1982]) have been able to show that, due to the recombination term, the homogeneous solution can become unstable with respect to small concentration fluctuations, giving rise to solute precipitation. Before reaching this instability, the system may become metastable with respect to the growth of large enough precipitates. The analysis of the nucleation problem taking into account the supersaturation of defects, allows to calculate a solubility limit under irradiation. Models have been proposed for incoherent precipitates of oversized solutes (MAYDET and RUSSELL [1977]), or coherent ones, wether over- or under-sized (CAUVIN and MARTIN [1981], [1982]), the latter providing a good agreement with results obtained in Al–Zn

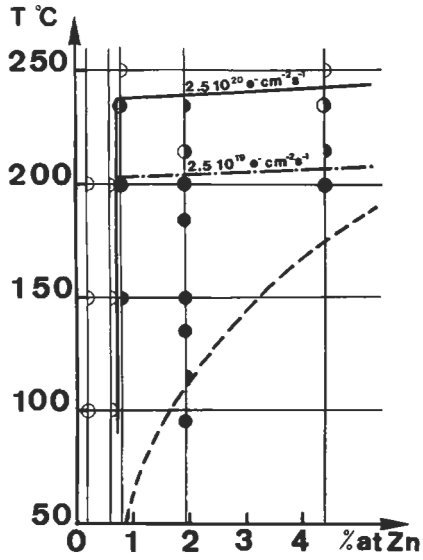

Fig. 21. Solvus line in the Al–Zn system under 1 MeV electron irradiation (after CAUVIN and MARTIN [1981]). Open half-circles: no precipitation; solid half-circles: precipitation at low, or high, flux; dashed line: solvus line without irradiation.

Table 11
Binary alloys where radiation-induced precipitation has been found.

Alloy	Projectile	Precipitate	Morphology
Ni–Be	Ni^+ ions	β-NiBe	at interstitial dislocation loops
Ni–Si	neutrons	γ'-Ni_3Si	at interstitial dislocation loops
	Ni^+ ions	γ'-Ni_3Si	at interstitial dislocation loops
	electrons	γ'-Ni_3Si	at interstitial dislocation loops
	H^+ ions	γ'-Ni_3Si	homogeneous, coherent, in regions of non-uniform defect production
Ni–Ge	electrons	γ'-Ni_3Ge	at cavities or dislocations lines
Al–Zn	neutrons	β-Zn	homogeneous precipitation
	electrons	GP zones + β-Zn	homogeneous precipitation
Al–Ag	electrons	{100} silver-rich platelets	homogeneous precipitation
Pd–W	H^+, N^+ ions	bcc W	at dislocation loops
	electrons	Pd_8 W	homogeneous
W–Re	neutrons	χ-WRe_3	homogeneous
Cu–Be	electrons	G.P. zones + γ	homogeneous
Mg–Cd	electrons	Mg_3Cd	?

alloys under electron irradiations. The origin of this mode of precipitation is to be found in the enhanced recombination probability for the defects in solute rich zones in case of attractive solute-defect interaction.

The theoretical situation is less favourable for concentrated alloys since the available models both for the thermodynamics and for the phenomenological coefficients are much less safe (see § 5.1.2). They are generally based on the random alloy model of MANNING [1971] and discard the specific trapping effects of solutes on the interstitials. As a consequence they do not introduce properly the coupling terms (WIEDERSICH *et al.* [1979]), The more elaborate treatments still suffer from restrictive assumptions (BOCQUET [1987], LIDIARD *et al.* [1990]). The interest of treating the thermodynamics of the alloy and the dynamics at the same level of approximation, has been evidenced by GRANDJEAN *et al.* [1994], who where able to reproduce a whole segregation profile in NiCu alloys.

8.3.3. Irradiation-induced phase transformations

In the two preceding paragraphs we have sketched specific models for irradiation enhanced diffusion and segregation/precipitation phenomena. More generally an alloy under irradiation can be described as a *dissipative dynamical system* which can display a very rich behaviour in response to an irradiation: the system will develop an evolving microstructure with voids, dislocations loops, precipitates, displaying, or not, steady states. The nature and the relative stability of these states can be studied thanks to a whole bunch of methods like deterministic approaches, Langevin equations, Master equation, Monte Carlo simulation, ... which allow to draw dynamical phase diagrams. These topics however are too far from the point of view of the diffusion and the interested reader can found in the specific section of the bibliography the relevant references.

Irradiation-induced segregation and phase transformations are further discussed in ch. 18, § 4.7.

9. *Diffusion in amorphous metallic alloys*

The study of diffusion properties in amorphous metallic alloys (A.M.A.), has been quite active in the past ten years both because these materials have been used as models of disorder for more complex glasses, like oxide ones, but also because they pose an interesting question from the point of view of solid-state physics: what level of structural disorder is sufficient and/or necessary for invalidating the notion of point defect (LIMOGE *et al.* [1982])? The reader is referred to recent reviews (AKTHAR *et al.* [1982], ADDA *et al.* [1987], MEHRER and DÖRNER [1989] and LIMOGE [1992b]), and to the general references on metallic glasses given at the end. The topic is still highly controversial on some points, so the present authors will try, as everybody engaged in the hottest debates, to separate as clearly as possible the established facts from more subjective interpretations.

References: p. 651.

9.1. A primer of metallic glasses

Whatever the preparation mode, vapor condensation, ultrafast quench, it is now recognized that after a proper annealing a unique metastable equilibrium structure is obtained. We have given in fig. 22 a schematic picture of the evolution of the viscosity and self-diffusion in a supercooled liquid during a quench. Two parts are clearly distinguishable. First a high-temperature one, above the so-called glass transition T_g, where the system flows. The diffusion mechanism is of a collective type and, as far as it can be checked, the Stokes–Einstein relationship is obeyed. In this part the well-known WILLIAMS–LANDEL–FERRY [1955] expression works as a mere fit at least as well as any other expression; in particular it describes rather well the near divergence of the viscosity at a finite temperature T_0, which gives rise to the phenomenon of the glass transition. Around T_g a rather abrupt change is observed and a new regime sets in, which has all the characteristics of a mobility in solids. In the following, we will be interested in this latter part, that is, sufficiently below T_g.

As a consequence of these very rapid quenches the glassy alloys are metastable, and as compared to silicate glasses, more "meta" than "stable". As soon as an enhanced temperature allows a sufficient mobility they evolve in a twofold manner. On the one hand they relax towards the (hypothetical) equilibrium liquid structure, probably becoming locally more ordered, and therefore decreasing the mobility. On the other hand if sufficiently large fluctuations of topological and chemical order can form, they will crystallize; the crystallization is controlled by diffusion.

The study of diffusion is thus a quite difficult task. First the allowed (mobility × time) window is very limited by the onset of crystallization: most of the measurements are for example done in a temperature range of less than 100 K, and over two decades of D at most, the total penetration being typically less than 100 nm in tracer experiments. Needless to say, the D values obtained are at the lower limit of the available techniques, imperatively restricting the temperature range where diffusion can be studied. As a second drawback, during this short time the structure itself will evolve: a proper preliminary anneal is generally needed for obtaining a reasonably stabilized structure. This minimum requirement as not been always met in the first studies. Finally, a characteristic feature of the glasses is the wide distribution of physical properties prevailing in non translationally invariant systems. As probed by local methods (see § 2.2) activation energy spectra are frequently found with halfwidth of the order of tenths of an eV.

Glassy alloys have now been discovered in a great number of systems. With respect to diffusion two families only have been studied: the M–Me group where M is a late transition metal or a noble one (or a mixing of them), and Me a metalloid in a concentration between 15% and 25% at.; and the M–M group, alloying an early transition metal (and big) with a late (and small) one in a broader composition range, from 20% to 80% at. approximately. The level of local order is thought to be much more developed in the first class than in the second. As a consequence the properties of the two groups are possibly different. (See also ch. 19, § 4).